Towards neutrally stable compliant shells

Sjaak Kok

TUDelft

Towards neutrally stable compliant shells

by

Sjaak Kok

to obtain the degree of Master of Science
at the Delft University of Technology,
to be defended publicly on Monday September 21, 2020 at 11:00 AM.

ŤUDelft

Preface

During a discussion early on in the project, a seemingly simple structure with interesting but, most importantly, ungraspable behavior caught our attention. At that time, I could not have foreseen that it would lay the foundation of this thesis. The initial stimulus behind the research that followed, was curiosity. What seems to be an ungrounded motivation at first, has repeatedly proven its usefulness throughout history. Some of the greatest inventions of this era, as the first television (and arguably future generations derived from that), we owe to this incentive. The findings presented in this thesis will probably not have such a social impact, but might inspire and lead to ones that do. Evidently, in this case, the observed behavior was of relevance within the research field, but no specific application was thought of and none has been given throughout this thesis. It is left to the curiosity of the reader to find some.

I have enjoyed the freedom that was given to me to direct the focus of the project. There are several things I have learned, that I would never have expected beforehand. Many times I had to remember myself to the exiting, but also immensely humbling fact that doing research is 'exploring the world of the unknown'. And, inevitably, you also encounter less motivating moments wherein you have to deal with setbacks. But this often leads to a creative process that forms the breeding grounds of new insights. It has enabled me to appreciate the experience of learning, even more than I already did. So to all fellow soon-to-be graduate students that find themselves in the middle of this: stay curious and value the process of learning. Do not compare yourself to others but let enthusiasm be the driving force towards your goals. I am sure you will finish with a satisfying result!

For some time, I have been looking forward to the moment of writing this, but I must admit that now I approach the end of this endeavor, the feeling of euphoria simultaneously makes room for a healthy amount of ambivalence. During my years as a student in the vibrant environment of the Technical University of Delft, I have been inspired in many ways. It has been a tremendously valuable experience that I wouldn't have missed for the world. But I am also sure that, with the right amount of curiosity, new and unforeseen challenges lay ahead.

Sjaak Kok
Amsterdam, September 2020

Acknowledgements

It took no more than five minutes of the first lecture of 'Precision mechanism design' before I realized that I had found the research group wherein to look for a master's project. This feeling has only grown stronger over the following years, as it has been reinforced on many occasions and by multiple other inspiring courses. I am very grateful to have been given the opportunity to be guided by and to learn from the people I admire. Therefore, I would like to express my gratitude to those who are all, albeit partially, responsible for finalizing this project.

First and foremost, to Giuseppe and Ali, who have provided excellence guidance and exceptionally useful feedback throughout the project. Giuseppe, your enthusiasm is dangerously contagious and Ali, I admire the effectiveness of your pep talks. I couldn't have wished for a better combination. I have always looked forward to our discussions and I hope we will stay in touch.

To professor Just Herder, who triggered my fascination during the inspiring lectures early on. Thank you for taking the time that was necessary for your valuable, substantive, involvement and the critical, always crucial, comments during the progress meetings.

To fellow (soon-to-become) graduate students, of which some I must call 'friends', for our problem-solving discussions, fruitful conversations and, probably most importantly, the pleasant times. It has been a rewarding experience.

To my friends, who definitely have suffered from my decision to sign up for a master's degree in Delft, but, nonetheless, have always been supportive. I owe you one and I am looking forward to all the catching up we have to do!

And last, but probably the opposite of least, to my family, without whom I would have never been able to achieve my goals. Thank you for supporting me in every way possible.

Summary

Elastic neutral stability involves elastic deformation without stiffness or loads. It is a remarkable appearance, since the deformation of materials is normally associated with an increase of potential energy and a resulting opposing reaction force or moment. Neutrally stable mechanisms can be used to overcome unnecessary actuation which makes them an interesting topic for the aerospace industry, space exploration and the development of wearable assistive devices. This last group benefits from the use of spatially-curved thin-walled elastic structures, called compliant shell mechanisms. A literature review aims to give an overview of occurrences of elastic neutral stability and aims to find methods for creating neutrally stable compliant shell mechanisms. Single element mechanisms are herein further emphasized and a division between the application of pre-stress and the application of geometrical boundary conditions is proposed. So far, all neutrally stable (shell) mechanisms require either of the two conditions to be imposed.

A new type of compliant shell structure, featuring a neutrally stable deformation mode without requiring one of the aforementioned conditions, is presented. The structure is composed of two initially flat compliant facets that are connected via a curved crease. It can be reconfigured into a second zero-energy state without apparent effort via propagation of a transition region. Both the structure's local width and the local crease curvature turn out to be effective parameters for tuning the behavior regarding stability during transition. This structure shows potential for combining geometric simplicity with complex and highly tune-able behavior. However, its discontinuity obstructs physical realization.

Therefore, a monolithic variant of this structure is investigated. The transition of a double-curved distributed compliant shell towards its second equilibrium configuration forms the basis of this investigation. A varying material thickness profile, described by an ideal set of design parameters, is obtained using an optimization procedure. Numerical analysis of the resulting optimized shell structure predicts a significant region of near-constant energy and associated near-zero loads within this unique deformation mode. Prototypes are manufactured using a 3D-printing process and demonstrate the validity of the modelled results by featuring a continuous equilibrium within a significant range of motion. These results lay the foundation for compliant beam elements with an internal statically balanced bending degree of freedom.

Finally, a different deformation mode, involving crease actuation of the same type of structure, is examined. Curved creases are characterized by the coupled facet deformation upon actuation. The forces exerted by the facets can be used to oppose the effects of crease stiffness during actuation to achieve an overall stiffness decrease. An analytical approach, based on a combination of a pseudo-rigid-body model (PRBM) and plate theory, predicts the potential for constant-force actuation around its second stable, or 'inverted' state. The accuracy of the model is validated by numerical simulations. However, due to prototype inaccuracies, the experimental results do not feature the desired constant force behavior. Nevertheless, a stiffness decrease, or 'softening' is experienced, verifying the concept and marking a first step towards statically balanced curved creases.

Samenvatting

Elastische neutraal-stabiele systemen hebben de eigenschap zonder stijfheid of externe belastingen te kunnen vervormen. Het is opmerkelijk gedrag, want elastische vervorming van materialen gaat normaal gesproken gepaard met een toename van potentiële energie en een tegenwerkende reactiekracht of -moment. Neutraal stabiele systemen kunnen worden gebuikt om onnodige actuatie te vermijden, wat het een interessant onderwerp maakt voor de lucht- en ruimtevaartindustrie en voor de ontwikkeling van draagbare ondersteunende hulpmiddelen. Deze laatste groep profiteert van het gebruik van ruimtelijk gekromde dunwandige elastische structuren, zogenaamde (buigzame) schaalstructuren. In een literatuuronderzoek wordt een overzicht van de verschillende verschijningen van elastische neutrale stabiliteit gegeven. Dit dient als doel om methoden te vinden die hieraan ten grondslag liggen. Mechanismen bestaande uit één enkel element worden hierin benadrukt en er wordt een categorisatie op basis van het toepassen van voorspanning en geometrische randvoorwaarden geïntroduceerd. Tot op heden vereisen alle neutraal stabiele schaalstructuren één van deze twee voorwaarden.

In dit onderzoek wordt een nieuw soort schaalstructuur geintroduceerd met een neutraal stabiele vervormingsmodus, zonder dat één van de hiervoor genoemde voorwaarden vereist is. De structuur bestaat uit twee aanvankelijk platte buigzame facetten, die met een gekromde vouwlijn met elkaar zijn verbonden. Een tweede stabiele, geïnverteerde modus kan worden bereikt door de voortstuwing van een transitie gebied, ogenschijnlijk zonder moeite. Zowel de lokale breedte als de lokale kromming van de vouwlijn van de structuur blijken effectieve parameters te zijn om het gedrag omtrent stabiliteit tijdens de transitie te beïnvloeden. Dit toont het potentieel voor het combineren van geometrische eenvoud met complex maar zeer programmeerbaar gedrag. De vervaardiging van prototypes wordt echter belemmerd door de discontinuïteit in de structuur.

Een monolitische variant van deze structuur is daarom aansluitend onderzocht. Hierin wordt de basis gevormd door de transitie van een dubbel-gekromde buigzame schaal naar de tweede, geïnverteerde, evenwichtsconfiguratie. Door middel van een optimalisatieprocedure zijn de ideale parameters voor een variërend dikteprofiel verkregen. Numerieke simulatie van de geoptimaliseerde structuren voorspelt een aanzienlijk gebied van constante energie tijdens de transitie. Prototypes zijn vervaardigd met behulp van een 3D-printprocess en tonen de validiteit van de gemodelleerde resultaten aan. Ze vertonen statisch evenwicht binnen een aanzienlijk gebied van het transitieproces. Deze resultaten leggen de basis voor statisch gebalanceerde buigzame balkelementen.

Ten slotte is er nog een andere vervormingsmodus van dezelfde type structuren onderzocht waarbij de vouwlijn wordt geactueerd vanuit geinverteerde toestand. Gekromde vouwlijnen worden gekenmerkt door de gekoppelde facetvervorming tijdens het actueren. De tegenwerkende krachten die worden uitgeoefend door de facetten kunnen worden benut om de effecten van vouwlijn stijfheid tegen te gaan om zo een algehele afname van stijfheid te bereiken. Een analytische benadering, gebaseerd op een combinatie van een 'pseudo-rigid-body-model' (PRBM) en plaattheorie, toont de mogelijkheid voor actuatie met constante kracht aan. De nauwkeurigheid van het analytische model wordt gevalideerd door de numerieke simulates. Vanwege onnauwkeurigheden in de prototypes vertonen de experimentele resultaten echter niet het gewenste constante-krachtgedrag. Des-alniettemin is er sprake van stijfheidsvermindering, wat het concept valideert en een eerste stap markeert naar statisch gebalanceerde gekromde vouwlijnen.

Contents

1

Introduction

Energy-free systems form a unique group of mechanisms that are in static equilibrium within their range of motion and therefore do not require any operating effort [7]. Not only energy efficiency is improved, also inherent safety is introduced and aspects as force-feedback benefit from more energy-efficient systems [7]. Intersection with the field of *compliant* mechanisms results in statically balanced compliant mechanisms (SBCMs), originally introduced by Herder and Van den Berg [3, 6] and includes the additional advantages of compliant mechanisms, e.g. monolithic fabrication and the absence of backlash. These SBCMs are typically designed for weight balancing and exhibit neutrally stable behavior in presence of an external gravitational force, either distributed in case of the structure's own weight [1, 16], or in the form of a payload [15]. There exists a balance between internal and external forces within the range of motion as gravitational energy is exchanged with elastic energy through deformation of the compliant components [3].

A more specific group of SBCMs operate in the absence of external loads and its state of neutral stability solely relies on the intricate balance between its elastic components. In this case, the *elastic* energy in the compliant mechanism is required to remain constant within the range of motion. This can be considered as a remarkable phenomenon, since deformation of elastic materials is generally accompanied by energy increase and an opposing reaction force or - moment. This state of *elastic neutral stability* was first mentioned in 1867, where the lack of a preferred axial orientation of an initially straight broomstick under a bending load is described [11]. The focus of recent research is directed towards neutrally stable *compliant shell mechanisms*, i.e. thin-walled structures capable of undergoing large elastic deformation, with applications in the context of space exploration, where lightweight and compact deployable booms are currently being developed [13, 14, 17, 19]. However, a recurring property of these neutrally stable shells is the need for pre-stress, either in the form of pre-stressed assembly [4, 5, 12, 18, 22] or boundary conditions imposed during operation [2, 11, 20, 21]. These requirements cause performance loss over time [9] and obstruct the potential applicability respectively [8]. A more comprehensive overview of occurrences and working principles of elastic neutral stability is given in chapter two: A literature review.

The research in this thesis aims to contribute to the library of neutrally stable mechanisms, by development of compliant shells that feature neutral stability *without* having to rely on pre-stressed assembly or externally applied boundary conditions. Throughout this thesis, variations to a specific, double-curved, shell geometry are investigated, whereby two very different deformation modes are brought to the attention.

The first part is based around a unique deformation mode that emerges while connecting the curved inner edges of two arch-shaped flat elastic plates in a hinged fashion. Because of their curved nature, a *curved crease* is created and actuation is accompanied by plate deformation. Neutral stability seems to occur after the initially opposing faces are inverted at one of the ends and the resulting *transition region* is propagated through the structure. Its simplicity in combination with this neutral stability differentiate the structure from existing neutrally stable examples and motivate further investigations. Its behavior is characterized in chapter three, as the suspicion of a neutrally stable deformation mode is confirmed.

However, material discontinuity and fabrication challenges limit the applicability. Therefore, the succeeding part describes the design process towards a continuous, monolithic and distributed compliant variant of

the curved-crease shell structure, with the goal to omit the aforementioned limitations. This paper, which forms the core of this thesis, is presented in chapter four and is to be submitted to the Journal of Extreme Mechanics Letters (EML).

Along the way, another interesting potential of the investigated structure stood out: its capability of balancing out elastic crease forces, with relevance for e.g. origami mechanisms. Despite its different deformation mode and the seemingly absent relationship to the main thesis subject, this behavior is further analysed and described in the form of a short paper in chapter five.

It is followed by a finalizing conclusion in chapter six, wherein the overall contributions of this thesis are discussed. The appendices contain supplementary information of the last three papers, in which, among other things, details on the modelling procedure, the fabrication of prototypes and suggestions for future work are set forth.

The main body of this thesis is presented in the form of scientific papers, often with more than one author. In all cases, the first author is responsible for the content, whereby the subsequent authors fulfilled the role of reviewers and provided the indispensable feedback during the process.

2

Paper I: A literature review

Literature review of occurrences and working principles of elastic neutral stability

Sjaak Kok, Giuseppe Radaelli and Ali Amoozandeh Nobaveh

Abstract— **Zero-stiffness systems are widely discussed in the field of mechanics. Elastic neutral stability also requires the external loads to be zero over a finite deformation path. It is a remarkable appearance, since the deformation of materials is normally associated with an increase of potential energy and a resulting opposing reaction force or moment. Neutrally stable mechanisms can be used to overcome unnecessary actuation which makes them an interesting topic for the aerospace industry, space exploration and the development of wearable assistive devices. This last group benefits from the use of spatially-curved thin-walled elastic structures, called compliant shell mechanisms. Work has been done on characterizing their behavior by creating a library of building blocks. So far, no building blocks that show neutrally stable behavior have been discussed. Therefore, this paper aims to give an overview of occurrences of elastic neutral stability and aims to find methods for creating neutrally stable compliant shell mechanisms. Examples consisting of single and multiple elements have been found in literature. In addition, several examples with their origin in nature are mentioned, some of which functional, others mere incidental occurrences. Mechanisms containing multiple components obtain their neutrally stable properties by modifying the constitutive components individually. Single element mechanisms are further emphasized and a division between the application of pre-stress and the application of geometrical boundary conditions is proposed. While both are methods for retaining the elastic potential energy, the applied method has implications for the practical feasibility and design freedom of the resulting mechanism.**

I. Introduction

When, in general, a system is in equilibrium, a system is in balance and forward and reverse actions occur with the same equal but opposite magnitude. This can create the illusion of no activity while many hidden processes take place. When equilibrium occurs in mechanical systems, all forces and moments are balanced out within the system. When the sum of the loads on a body is zero, it is said to be in *static* equilibrium. When the state of equilibrium persists while a mechanism is deformed, it is said to have a *continuous* equilibrium. As a net result, no potential energy is added to or withdrawn from the system. In literature, this mechanism is said to be in neutral equilibrium and is often referred to as 'neutrally stable'. While in this case, 'stable' actually describes the nature of the equilibrium point.

The reaction force or moment of a mechanism is defined as the first derivative of the potential energy with respect to a spatial degree of freedom. The stiffness of a mechanism, being the second derivative of the potential energy with respect to a spatial degree of freedom, is a measure of how the reaction forces and moments change during displacement. Both properties are instantaneous, meaning they provide information about

a single configuration of the mechanism. However, in literature, 'zero-stiffness' often refers to mechanisms with constant reaction forces and moments over a certain displacement path. Figure 1 shows a classification of zero-stiffness mechanisms. When a gravitational force is part of the system, the elastic energy has to be exchanged with gravitational potential energy. These 'gravity balancers' or 'gravity equilibrators' are only in neutral equilibrium with a constant gravitational load. When the required reaction forces and moments are not only constant, but also equal to zero, the total *elastic* potential energy remains constant upon deformation. Internal elastic loads are balanced out by other elastic loads and no reaction forces or moments are required to maintain the state of equilibrium: the mechanism has a neutrally stable elastic deformation mode. Tarnai [1] and Schenk [2] give intuitive examples and discuss the difference between occurrences of zero-stiffness and neutral stability.

Elastic neutral stability is a remarkable appearance since, normally, the deformation of materials with a positive modulus of elasticity is associated with an increase of potential energy and a resulting opposing reaction force or moment. An elastic mechanism in neutral equilibrium can only deform without load if the necessary energy is already stored inside the system and redistributed upon deformation. Because of this unique property, the focus in this report will be on this specific group of neutrally stable mechanisms. Neutrally stable elastic mechanisms can either consist of multiple constitutive elastic components [3] or only one single elastic component [4]. This division forms the first step in the classification process discussed further in this paper.
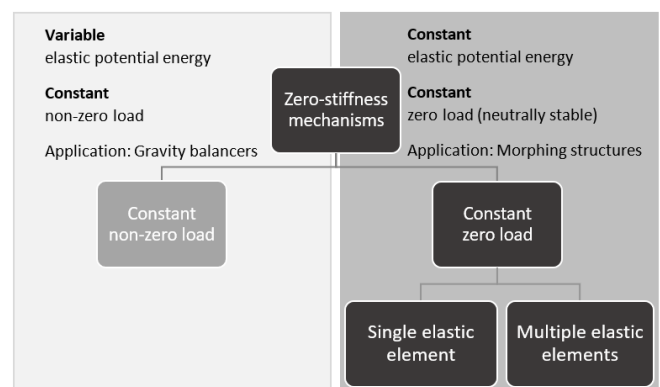

Fig. 1. The tree captures an important division within zero-stiffness mechanisms. Situations with zero external load and non-zero external load can be distinguished.

Compliant shell mechanisms form a group within compliant mechanisms and have become an interesting research topic over the last years. Because of their versatile potential, they are recently circumstantially investigated in the aerospace industry and in the field of assistive devices [5] [6] [7]. They can be described as spatially curved thin-walled structures able to transfer or transmit force, motion or energy through elastic deflection. In contrast to classical compliant elements, these three-dimensional shaped compliant shells allow for large deformations and have potential to be tuned through shape optimization to achieve any desired load path [8]. Work has been done on characterizing their behavior by creating a library of building blocks [9]. So far, no building blocks that show neutrally stable behavior have been discussed.

This paper aims to give an overview of the occurrences of elastic neutral stability and categorize examples, with the goal to find methods for creating neutral stability in compliant shell mechanisms.

Emphasis in this paper will be on single element shell mechanisms, but other examples will be discussed for better understanding and to expose the working principles of their behavior.

The approach to the literature review will first be discussed in the method section of this paper. Several results of examples will then be reviewed and a categorization structure is formed in the third chapter. Examples belonging to each class are then reviewed in detail in chapter four, where an effort is made to categorize their working principles. In the discussion, methods for creating neutrally stable mechanisms are qualitatively compared and an attempt is made to give an integral explanation of their working principles.

II. METHOD: A LITERATURE SURVEY

In literature, neutrally stable mechanisms are often hidden within the broader term 'zero-stiffness'. Therefore, the term zero-stiffness is also included in the search query and examples without neutral stability are excluded manually. In order to find results in other disciplines, an iterative search process was used, where synonyms originating from other fields where added to the query.

TABLE I
SEARCH QUERY USED TO SEARCH IN THE MECHANICAL DOMAIN.
VERTICAL TERMS IN EACH COLUMN ARE COMBINED WITH 'OR'.

Aspects combined with AND	
Neutral* stable	Mechanism
Neutral stability	Shell
Neutral equilibrium	Structure
Neutral* elastic	Tape spring
Continuous equilibrium	Tape loop
Static* balanc*	
Zero-stiffness	
Zero W/5 stiffness	
Zero W/5 elastic	

Next to the expected results within the mechanical discipline, examples of neutral stability were also discovered in biology. Two separate search queries are used to find relevant results. Table I and table II present the queries that focus on the mechanical and the biological domain respectively.

TABLE II
SEARCH QUERY USED TO SEARCH IN THE BIOLOGICAL DOMAIN.
VERTICAL TERMS IN EACH COLUMN ARE COMBINED WITH 'OR'.

Aspects combined with AND		
Growing	Leaf*	Pre-stress*
Growth	Shell*	Prestress*
Morphing	Birod*	Self-stress*
Wrinkling		Selfstress*
		Buckling

III. RESULTS: OCCURRENCES AND CLASSIFICATION

A division within the group of neutrally stable elastic mechanisms, based on the amount of constitutive elastic components, was proposed in the introduction. In this chapter, two cases are discussed: systems containing multiple and systems containing one single elastic element. A complete overview of the classification can be found in figure 2.

A. Mechanisms of multiple elastic elements

The constitutive components of neutrally stable elastic systems are often connected at the end effector. They co-operate in parallel, so they all share the same degree of freedom. The majority of the examples found in literature consist of only two elements with two separate functionalities. An elegant example is given by Herder [10], where two of the most simple spring elements are used to create a statically balanced mechanism (fig. 3(a)). This results in a system with constant elastic energy, independent of the configuration of the degree of freedom. This behavior can be explained intuitively by imagining two 'basic' gravity balancers as building blocks that are tilted on their sides and connected through their end effector. By adjusting their design parameters, they both deliver the same, but opposite horizontal force and cancel each other out.

A different example is described by Tolou [11], where a micro mechanism is statically balanced by adding a pre-stressed buckled beam. Multiple leaf spring flexures provide the positive stiffness and positive force part of the mechanism. A buckled beam is then designed to exactly match the mirrored behavior of the leaf spring flexures, all within a certain range of motion (fig. 3(b)). Within that region, forces cancel each other out and neutrally stable behavior can be observed.

Elastic mechanisms that deform with positive stiffness can be balanced by adding a second elastic element in parallel that behaves in an exact opposite way. Addition of an element with solely opposite stiffness is not sufficient for the neutrally stable requirement. Also, the loads needs to be balanced out to zero, meaning that the load-displacement curve needs to be mirrored in the displacement axis, corresponding to zero
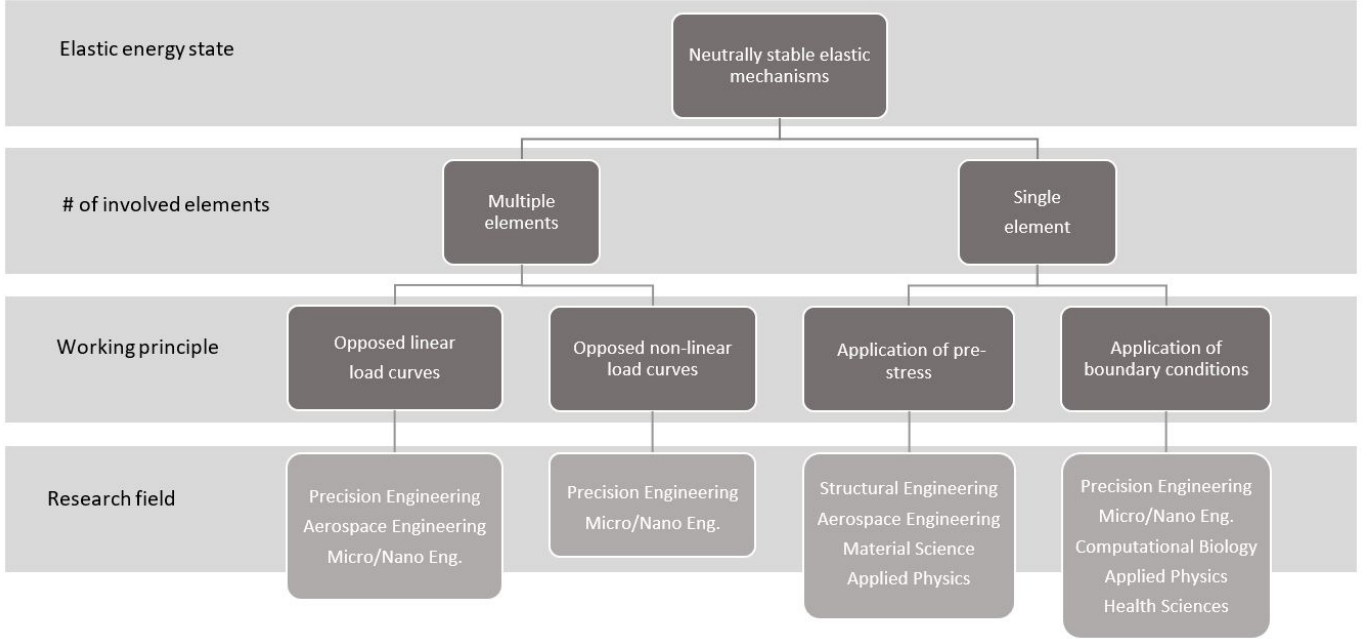
Fig. 2. A tree that captures the classification of all neutrally stable mechanisms found in literature. A first division is based on the number of involved elements, a second is based on the working principle. The research fields and origin of the examples are finally provided in the last layer.

force or moment. Herein, the two given examples differ and, in general, two different situations can be distinguished: neutral stability by (1) opposed linear portions of load curves and (2) opposed non-linear load curves. Mechanisms with a positive linear load-displacement relationship are most common since most materials deform according to Hooke's law, resulting in true linear or affine functions. A true negative linear load-displacement relationship is not possible, as this would imply an infinite source of elastic energy. Instead, this behavior can be observed in a certain finite range of motion. Non-linear relationships exist in the form of constant load curves, higher-order curves or hybrid curves, constructed from the aforementioned.
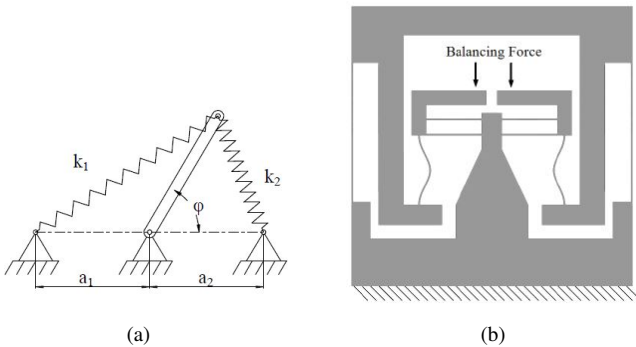

Fig. 3. Two neutrally stable mechanisms are shown. (a) shows a spring-to-spring balancer by Herder [10] and (b) shows a balanced micro mechanism based on buckled beam flexures by Tolou [11].

B. Single element mechanisms

The occurrence of neutrally stable elastic behavior of systems containing only a single element is even more interesting.

In contrast to systems where the behavior of the constitutive independent elements can individually be tuned and added up, their behavior is more complex and their working principles can not easily be explained. By comparing examples from multiple disciplines, an effort is made to categorize these and clarify the explanation behind their existence.

During research on bi-stability of shell elements, Guest [12] developed pre-stressing conditions for a cylindrically curved rectangular plate that shows neutrally stable behavior when rotating the axis of curvature. This was achieved by two consecutive same-sense pre-stressing steps. The initially flat rectangular strip was first cylindrically deformed around its longitudinal axis and later around its (perpendicular) transverse axis. With the correct amount of pre-curvature and resulting residual stress, this resulted in bi-stable behavior with the energy barrier in between reduced to zero. In other words, a continuous equilibrium where all bending axis-orientations in between longitudinal and transverse were energetically equally preferable (fig. 4(a)).

An other interesting neutrally stable element arises when the two ends of a carpenters tape spring are connected into a closed-loop structure, creating a so-called tape loop. Vehar [13] showed that a tape loop can potentially be used as a linear guide, where the two parallel portions of the loop can be translated alongside each other without any force. Relative translation of the parallel portions of the tape spring results merely in shifting of the deformed regions, but no change in overall geometry (fig. 4(b)). Although the elastic energy associated with deformation is difficult to model, it remains constant during deformation in its neutrally stable mode and no load is required. The cylindrically single-curved cross-section
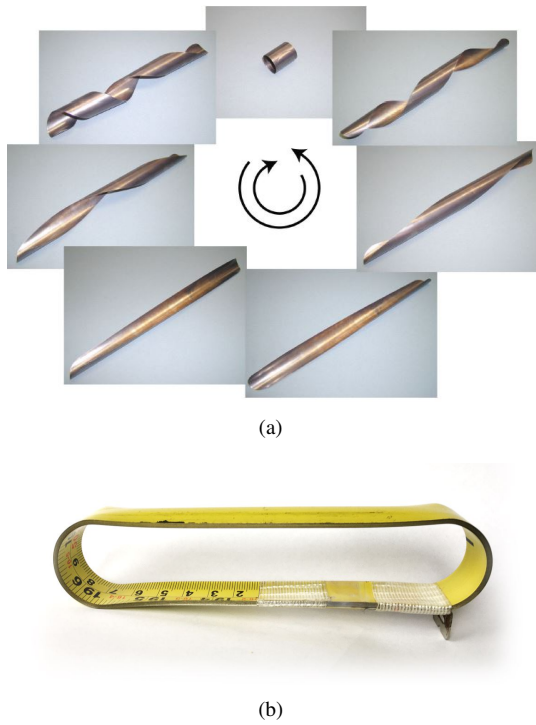
(a)

(b)

Fig. 4. Two neutrally stable single-element mechanisms are depicted. (a) The neutrally stable cylindrical shell by Guest [12] and (b) a tape loop: an endless configuration of a tape spring where the two ends are connected.

of the tape spring results in a tape loop that has significant stiffness in other degrees of freedom and therefore has the potential to bear loads. The striking ease of manufacturing contrasts the relatively complex and sensitive pre-stressing method discussed by Guest.

Residual stress in the equilibrium state of a system supplies the necessary energy for that equilibrium state to be potentially neutrally stable. This self-stress can be imposed during a controlled pre-stressing action. The system is then in equilibrium but also in a state of geometric frustration, where it can not meet the resolving deformations corresponding to all imposed stresses simultaneously [14]. When truly balanced, these systems exhibit neutrally stable behavior in a degree of freedom the pre-stress was optimized for [12] [15]. Alternatively, the application of boundary conditions can be the used to generate self-stress. When the tape spring is elastically deformed and thereby closed in on itself, the resulting continuous loop is already in a state of self-stress that can not be resolved by any deformation [16] [4]. Based on this inherent difference, two groups within the single element category can be distinguished: (1) self-stress by the application of boundary conditions and (2) self-stress by a controlled pre-stressing step. These two methods can be used to create mechanisms with a finite or an infinite range of motion in their neutrally stable degree of freedom, as will be discussed next.

IV. NEUTRAL STABILITY PER CATEGORY

A. Mechanisms composed of multiple elements

1) Opposed linear load curves: In linear elastic mechanisms, the load increases linearly with deformation. They are naturally most common since most involve a Hookean material that, without transmissions or geometrical aspects, deforms accordingly. Examples are torsion bars and leaf springs that are used sufficiently close around their equilibrium. Hoetmer [17] analyses the use of negative-stiffness building blocks to compensate for linear elastic behavior. As a design case, buckled beams with rectangular cross-section are used to statically balance a compliant gripper (fig. 6(a)). The buckled beams show bi-stable behavior, but only the linear region with negative slope within the force-deflection curve is used for this application. The working principle is similar to that of Tolou. Morsch [18] proposes a method for statically balancing a cross-flexure hinge that normally shows positive stiffness behavior. The additional leaf springs provide a counteracting moment with negative stiffness in the degree of freedom of the mechanism (fig. 6(b)). Torsional stiffness is compensated in the work of Lachenal [19] and Daynes [20], where the constant positive stiffness of an airfoil skin and airfoil construction members respectively is balanced out (fig. 5(a) and 5(b)). Both provide a moment-free pitch adjustment method suitable for airplane wings and wind turbine blades.
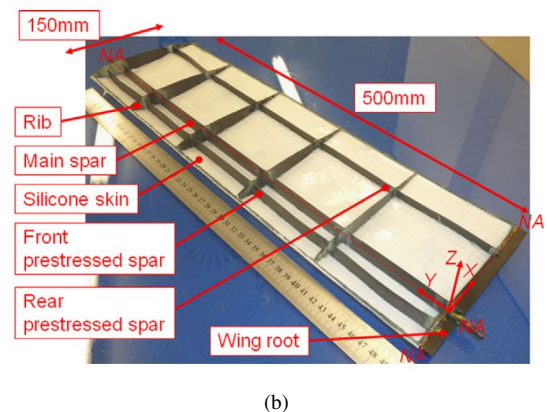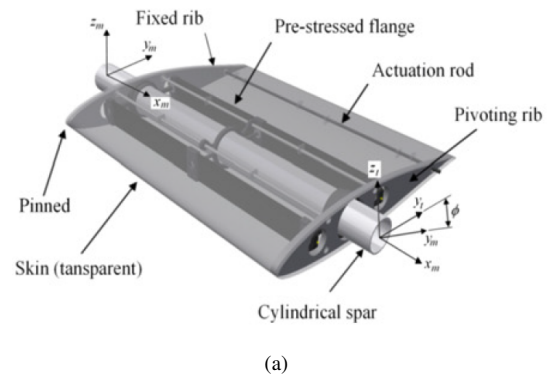

(a)

(b)

Fig. 5. Two mechanisms are shown to compensate for the torsional stiffness of (a) the airfoil's skin by Lachenal [19] and (b) the structural frame members of the wing by Daynes [20].

2) Opposed non-linear load curves: Constant force curves are considered as non-linear curves because of the existence of a zero-load resting state. A comprehensive overview of spring-to-spring balancing mechanisms is given by Herder [10]. Figure 3(a) shows an example of the simplest of mechanisms that involves two linear zero-free-length springs. Mechanisms that consist of more than two spring elements are also discussed. The working principle of the majority of these, sometimes multiple degrees-of-freedom, balancers can be explained by intricate compositions of the fundamental single spring constant-force balancer. Neutral stability of the end effector is then achieved by a summation of all constant force curves that add up to zero. It should be mentioned that the constant force assumption depends on the degree of freedom that is considered. Spring-to-spring balancing mechanisms that also involve higher-order springs (i.e. springs wherein the force is proportional to a positive integer power of its length) are discussed in the work of Soethoudt [21]. The performance of this group of balancers can be evaluated analytically, while assuming springs that meet the zero-free-length condition.
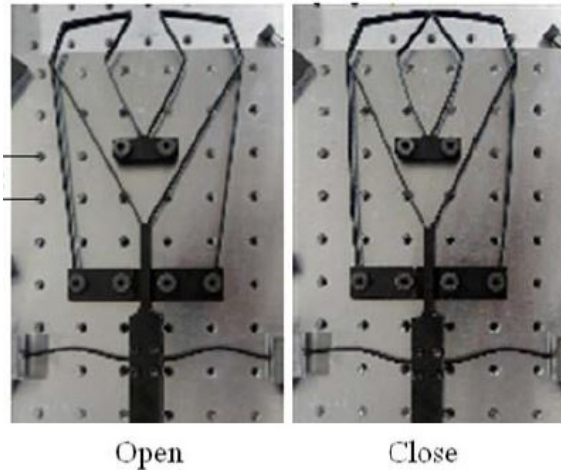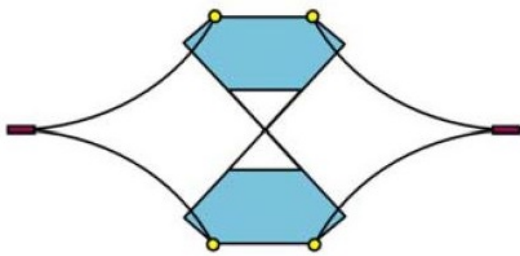
A potential energy field approach to the design of a statically balanced straight-line mechanism is proposed by Radaelli [22]. Four identical shape-optimized leaf springs co-operate to provide sufficient stiffness to the end-effector in all directions, except for the direction of the linear degree of freedom (fig. 7(a)). During that motion, two groups of two flexures contribute each in an opposite way to the overall stiffness and force in that direction. Figure 7(b) shows the two components, each consisting of a pair of flexures, that result in zero stiffness and zero force [1]. Both components have a non-constant stiffness, resulting in a non-linear, roughly quadratic force increase or decrease as their separate contribution.
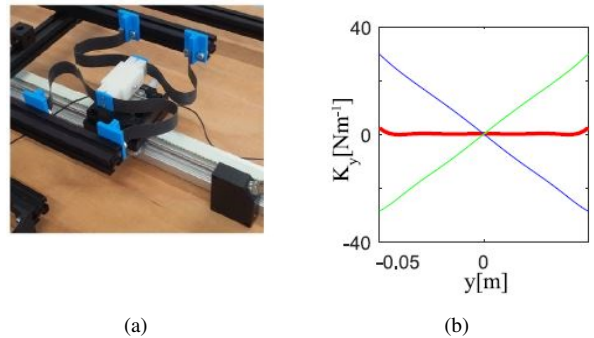
(a)   (b)

Fig. 7. The statically balanced straight-line mechanism by Radaelli [22] uses four identically shaped leaf spring flexures. The mechanism is shown in (a) and the resulting stiffness in its neutrally stable degree of freedom is shown in (b).

B. Single element mechanisms

1) Application of pre-stress: Finite range of motion
An example of a neutrally stable deployable rectangular strip is given by Murphey [23]. In contrast to the method used by Guest, two cylindrical shells with opposite curvature senses and perpendicular curvature directions are bonded together. The separate shell elements can either be constructed from initially flat, plastically deformed sheet metal or from fiber reinforced plastic composite, molded around a cylindrical surface. The result is a single element with the same mechanical characteristics as the shell produced by Guest (fig. 8(a) and 8(b)). Murphey also described the possibility of other pre-stressing techniques as, for example, extensional fiber pre-stressing. When anisotropic materials are used, their anisotropic properties can be exploited for creating pre-stress. Doornebal [24] and Stacey [25] describe a method based on the difference in thermal expansion coefficients of the components and stresses that remain after curing.

So far, neutrally stable behavior had occurred as a consequence of present pre-stress. The energy level is kept constant, but non-zero when compared to the undeformed geometry as reference. Schultz and Liuyi handle the following less rigorous definition of neutral stability in the context of deployable


Open   Close

(a)

(b)

Fig. 6. Two mechanisms are shown where an element with positive constant stiffness is combined with an element with negative constant stiffness. (a) shows statically balanced grippers by Hoetmer [17] and (b) shows a statically balanced compliant cross-flexure by Morsch [18].

[1]The zero force condition can not be confirmed based on the information given in this figure. The reader is referred to the work of Radaelli for more details.
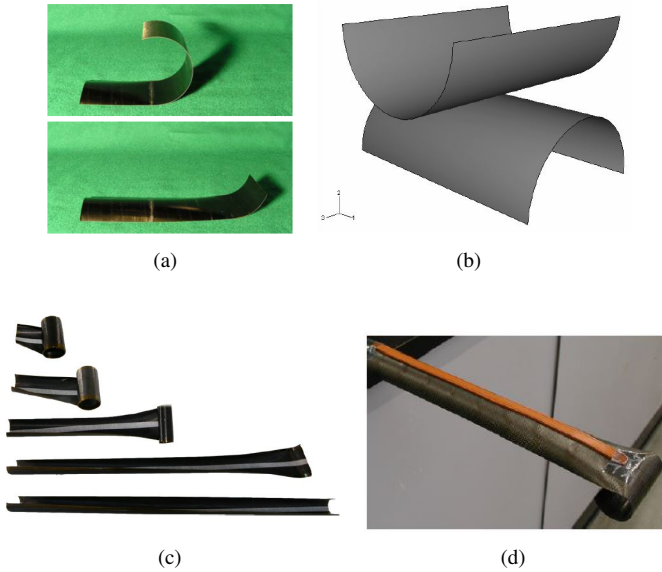
Fig. 8. Neutrally stable deployable shell structures are shown in the form of (a) a rectangular plate that consists of (b) two bonded pre-stressed layers by Murphey [23], (c) a neutrally stable deployable boom by Liuyi [26] and (d) Schultz [5].

booms for space exploration: 'a structure that will show neither an inclination to spring out nor to roll up when partially rolled to any position [5] [26].' Here, a fiber reinforced laminate is used in combination with carefully chosen matrix material. The specific Poisson ratio of the matrix in combination with the layup sequence, results in zero bending stiffness. In practice, little stiffness is present but is shadowed by internal damping, rendering the structure effectively neutrally stable (fig. 8(c) and 8(d)). Another example where neutrally stable elastic behavior is achieved via constitutive relations is given by Kumar [27]. He describes self-propagating edge dislocations in the crystal structure of materials during bending as the 'materials analogue of zero-stiffness structures'. Bending a plate that contains an edge dislocation results in a constant level of stored elastic energy throughout the deformation process for a finite, but significant range of motion.

2) Application of pre-stress: Infinite range of motion

The pre-stressed neutrally stable shell that was investigated by Guest showed neutrally stable behavior because of accurately designed levels of pre-stress. No configuration exists wherein relaxation of all stresses occurs. As a result, every configuration is associated with the same non-zero elastic stain energy (fig. 4(a)). Guest discussed the similarities with a bimetallic flat disk and found a 'hidden symmetry'. Upon heating, the difference in expansion coefficient results in a dome-shaped structure. At some point, a bifurcation takes place in order to reduce in-plane stretching, associated with high energy costs. A cylindrical shape is adopted that requires the storing of less elastic potential energy. The axis of bifurcation is arbitrary and deformation on a continuous path with varying direction does not change the stored energy. Deformation along this path is thus a neutrally stable mode (fig. 9(c)).

Expansion of a bimetallic disk, in combination with the arbitrary axes of bifurcation, was first mentioned by Wittrick in the year 1953 [28] and recently investigated by Seffen [29]. Lamacchia [30] mentioned an annular plate with circumferentially distributed moments and suggested symmetry breaking bifurcation as an explanation for the emerging neutrally stable mode. Hamouche [31] utilized the neutrally stable precession path of the axis of principal curvature of a pre-stressed circular plate for generating an infinite motion of a propagating wave, shown in figure 9(b). The working principle is identical to the neutrally stable shell described by Guest. The disk is pre-stressed by plastic deformation into a cylindrical shape, with two perpendicular curvature directions. All axes with curvature directions in between require equal amounts of elastic bending energy. But, in contrast to Guest's shell, the axially symmetric circular undeformed geometry results in a deformed geometry that remains invariant when the axis of curvature is rotated.

Similarities can be found when circular disks are stretched or compressed along radial curves. Klein [32] investigates the result of lateral nonuniform shrinkage of flat elastic sheets. When compression stresses dominate along the perimeter of the disk, wavy patterns emerge. The locations of the peaks and valleys is arbitrary and can be moved along the edge without the need to change the elastic energy potential of the system [32]. This state of self-stress also occurs in the context of origami, where curved creases cause the outer perimeters to experience compression stresses [14] (fig. 9(a)). Holmes [33] and Pezulla [34] utilize swelling of compliant disks in the context of soft actuation. They describe the emergence of 3D-shaped objects from initially 2D-shaped flat disks. Again, due to the symmetry of the initial circular shape, no single buckled orientation is preferred: a neutrally stable mode exists.

3) Application of boundary conditions: Finite range of motion

Equivalent to the tape loop is a Rolamite mechanism [35]. This concept consists of a thin flat strip that is enclosed by a set of rollers and two rolling surfaces (fig. 11(c)). The additional elements constrain the strip to follow a certain path that remains invariant upon deformation of the mechanism. Actuation of the rollers in other degrees of freedom always load the strip in tension, its stiffest direction. Similar to the tape loop, the region of deformation propagates through the mechanism, without change in the resulting geometry, thus keeping the amount of deformation and associated elastic energy constant. While the geometry of the tape loop is determined by a single contact constraint at the endpoints, this geometry is determined by contact constraints along the complete length of the curved strip. But in contrast to the always-in-tension-loaded strip in the Rolamite mechanism, the tape loop is relatively compliant when actuated in other deformation modes due to the lack of additional supporting constraints.

The unstressed cylindrically-shaped cross-section of the tape spring causes it to buckle when subjected to the boundary
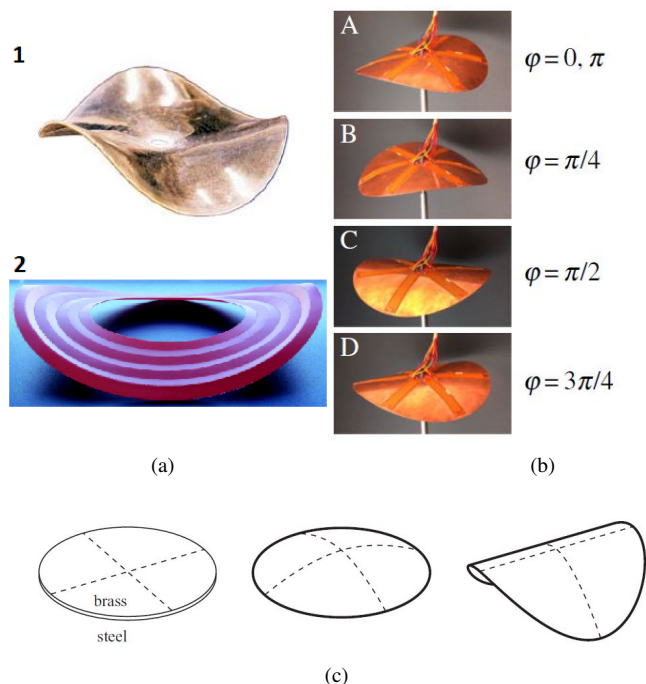
Fig. 9. Several occurrences of neutrally stable deformation are shown. (a) depicts the wave pattern result of compression in the outer perimeter of a flat disk, either by (1) swelling [32] or (2) curved crease paper folding [14]. (b) shows the neutrally stable precession of the bending axis by Hamouche [31] and (c) illustrates the under laying principle of the occurrence of a neutrally stable deformation mode of an initially flat disk.

Fig. 10. When a initially straight flexure is compressed between to surfaces (a), deformation is located in a finite region that can be shifted without adding energy to the system (b). Similarly, reverse rotating an elastic helicoid (c) results in a inverted region that can be shifted around energy free.

condition and forms two opposed regions with defined perpendicular curvature. Figure 10(b) and 10(a) show a theoretical example where this geometry is forced by an extra constraint. A leaf spring flexure with non-curved cross-section and pivoting ends is compressed between two parallel surfaces. In this case, this extra constraint forces the deformation to be localized in a specific region and excludes the ends from the elastic deformation process. Relative translation of the plates results in propagation of the deformed region, without changing the elastic energy of the system. Similarly, an *infinite* range of motion emerges when the two ends of the leaf spring are connected. This is an intermediate example wherein more than a single constraint at the end points determines the equilibrium geometry, without constraining contact over the complete length.

A comparable rotational example is given by reverse-rotating an elastic helicoid, as depicted in figure 10(c) and 10(d). The structure is initially free of stress and first twisted opposite to the direction of its pitch. After initial buckling, a portion of the structure will obtain an inverse twist in order to meet the applied boundary condition. The length of this portion will then increase linearly with the rotation, resulting in a constant moment throughout the deformation. Moreover, when after rotation both sides are fixed, the location of this region with inverse pitch can be shifted through the structure without applying a moment or adding energy to the system.
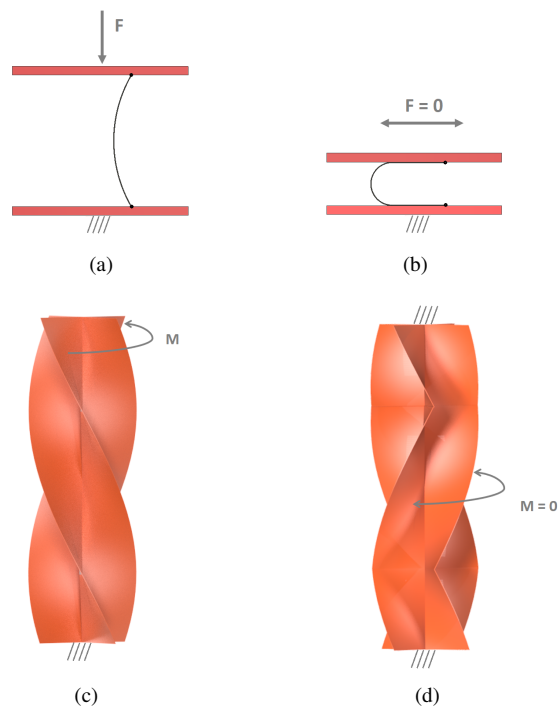
4) Application of boundary conditions: Infinite range of motion

Elastic neutral stability was probably first mentioned by Thomson and Tait [16] in the book 'Treatise on natural philosophy', that was published in 1867. There, an initially straight rod is described that exhibits a state of neutral equilibrium around its centroidal axis when bent into a circle and connecting the ends. Rotation can occur without the need to introduce a load or to add energy to the system. This concept is exploited by Baumann [36] to drive circular rings of pre-stressed polymer fibers that are exposed to a temperature gradient. The temperature difference between the top and bottom of the ring causes a stress gradient similar but perpendicular to the already present stress-gradient as a result of the pre-stressing step. The ring restores its lowest energy potential by rotating its cross-section so that it coincides with the geometrically imposed pre-stress gradient (fig. 11(a)). These simple motorized mechanisms are potentially suitable for small-scale applications [36].

In fact, a similar motorized machine on DNA level is described by Kulic [37]. There, a ring of DNA, called a miniplasmid, is formed out of an unstressed straight DNA chain, bending it into a circle and connecting the ends. By selective heating of the ring, rotation around the centroidal axis occurs and the 'twirling' ring generates a hydrodynamic flow field. Small, deliberate differences in bending stiffness of the straight DNA chain are used to create the 'ratchet effect' to boost the efficiency of the propulsion, but these can be avoided creating a truly neutrally stable deformation mode.
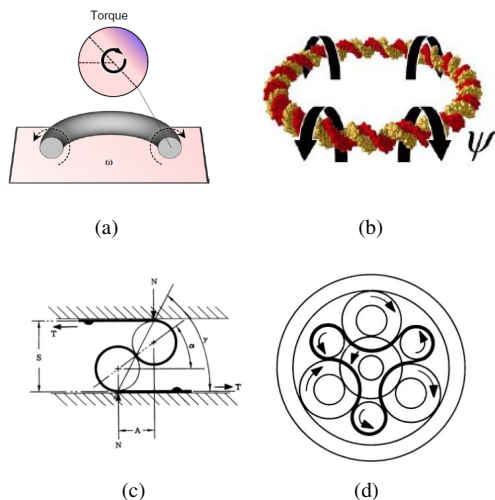
Fig. 11. Multiple axial symmetric variants of neutrally stable mechanisms are shown. (a) depicts the fiberdrive mechanisms by Baumann [36], (b) a similar molecular motor composed of DNA molecules by Kulic [37]. The basic concept and a rotational infinte variant of the Rolamite mechanism is illustrated in (c) and (d) respectively.

The Rolamite concept can also be used for creating mechanisms with an infinite range of motion, as depicted in figure 11(d). By connecting the ends of the strip, a continuous and neutrally stable rotational deformation mode exists where contact constraints cause the geometry to remain invariant. However, the cross-section of the strip does not need to be constant to create a force generator, as analysed by Cadman in the year 1969 [38] and recently in the context of a modified version of a tape spring by De Jong [39].

Several occurrences of neutrally stable elastic behavior in nature can also be found in literature. Marko [40] describes the internal 'slithering' of supercoiled DNA as an elastic deformation with no energy costs. When DNA strands are translated, the double helix is cut, untwisted and later sealed up. Residual twist causes DNA to become supercoiled (fig. 12(a)). Many examples are known where two distant portions of DNA need to be brought into physical contact in order for the gene to be expressed. Molecules connected to the DNA strand inside the supercoil help the DNA strand 'slither' without resulting energy costs until the required contact has taken place.

For a more intuitive understanding of this phenomenon, an example is given in the book 'mathematics and mechanics of biological growth' by Alain Goriely [41]. He describes the twisting of an initially straight wire of isotropic section. When after a finite amount of twist, the ends are connected, the resulting equilibrium geometry depends on the amount of applied twist. After the critical twist is reached, the ring buckles into a figure-eight-shape. But the locations where bending occur are arbitrary and the location of intersection can be 'slithered' through the structure (fig. 12(c)). A neutrally stable mode has emerged. This phenomenon can be experienced when coiling up an electrical cord or garden hose.

Another example of a neutrally stable twisted ring is a Mobius band, where an initially flat unstressed ribbon undergoes a twist of half a rotation, after which the two ends are connected. In the translation of a paper by Wunderlich, first published 1962 [42], the equilibrium geometry of a Mobius strip is analyzed using both geometrical and mechanical models by considering differential geometry and strain energy (fig. 12(b)). It is mentioned that the location of the concentrated deformations is entirely arbitrary and could be relocated with no energy penalty. In fact, the Mobius ring is an example of a whole family of twisted rings of which the supercoiled DNA geometry is part of. Herein, the deformations can be relocated without adding energy to the system.
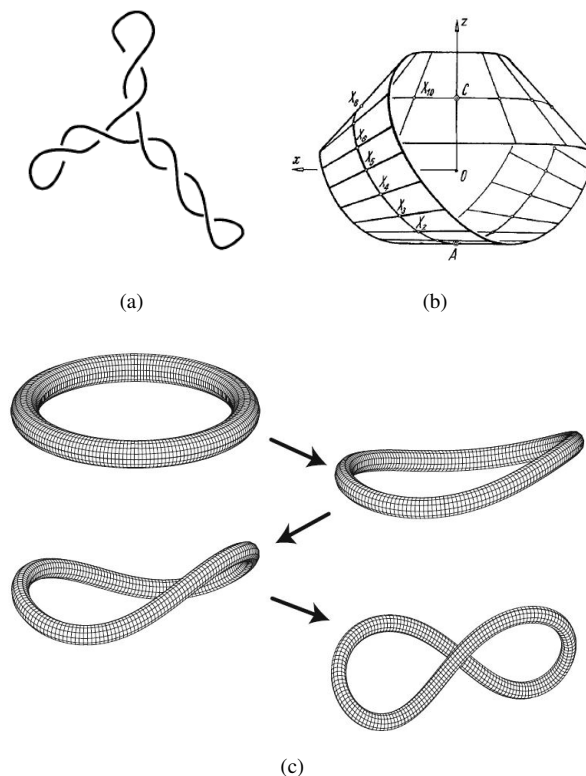

Fig. 12. The formation of neutrally stable shapes in twisted loops is shown by (a) Marko [40] in the 'slithering' motion of DNA strands that can be explained by (c) increasing torsion in a endless ring from the book of Goriely [41]. Such a twisted configuration can also be found in (b) Mobius strips [42].

Active propulsion in organisms is often achieved by propagation of a wave along the edge of the body's structure. When a viscous medium is introduced, the resultant thrust propels the organism. This mechanism is used in biology on both micro- and macro scales and is referred to as 'Taylor's swimming sheet' [43]. Similar to the propagation of the waves on the perimeter of an edge-stretched disk, this wave continuously redistributes the elastic energy along the edge. During research on the optimal shape of an elastic flagellum, Spagnolie [43] mentioned the ability to pass through the elastic energy between portions contributing on the propagation of the wave. In practice, the open ends of the finite structure provides a location where the stored elastic energy can flow out. The previously discussed actuated 'gear-less motor' developed by

Hamouche [15] (fig. 9(b)) can be considered as the rotational equivalent of Taylor's swimming sheet with an infinite range of motion.

Although not as salient, neutrally stable structures also arise in biology in the form of growing structures, but no further functions are mentioned in literature. Growing organisms undergo bending and wrinkling due to inhomogeneous growth. When two connected rods (birods) grow with unequal rates, the resulting stresses can be relaxed by bending in the direction that results in extension of the rod under compression. This mechanical system provides the basis for directional growing of plants under influence of sunlight [44] . Changing to an axisymmetric variant of the situation, where the complete outer mantle is under tension and inner fiber under compression, a preferred bending direction no longer exists and bending around any axis is equally favorable. The structure can be brought into a different equilibrium state by precession of the bending axis while maintaining minimal potential energy. In a planar growing case, leaves undergo geometric frustration by inhomogeneous growth. In order to grow a stress-free planar surface, cell multiplication should meet the quadratic requirement for area increase, while cell multiplication occurs exponentially naturally. Promotion and inhibiting of growth is regulated through the endocrine system and determines the appearance of the leaf on macro scale [45].

When tension dominates in the outer perimeters, the leaf becomes dome shaped. Compression in outer rings, however, creates out of plane wrinkling to resolve the compression stresses. But the location of the peaks and valleys is without preference. The associated non-zero bending energy is less than the energy associated with in-plane stresses and does not change upon propagation of the deformation wave.

Nath [45] discussed the relation between growth hormone, the presence of stresses and the spatial geometry of growing leaves. Audoly [46] [47] created the first model of the formation of ripples in plant leaves that was based on elasticity. In a subsequent paper, he discussed the occurrence of self-similar structures near the boundaries of stretched edges. This research links to the paper by Klein (fig. 9(a)), discussing the formation of waves upon waves on edge-stressed disks. Wave pattern-formation was also investigated by Sharon [48] [49], who emphasized the similarities between occurrences in biology and man-made structures, as for example ripples in torn garbage bags (fig. 13(c)). Figure 13(a) and 13(b) show the wrinkled edge of a leaf that forms curved strips when flattened. Liang [50] investigated the relation between in-plane stresses and resulting geometry of long leaves and Rudraraju [51] researched the wavy pattern formation in growing sea shells (fig. 13(d)). These can be considered as the biological examples of the edge-stressed neutrally stable geometries discussed earlier. Although, it is worth saying that the examples mentioned above are approached theoretically to illustrate the relation between self-stress and energy-free deformation. Processes as lignification and stress relaxation probably prevent the neutrally stable propagation of the wave to be ever experienced.
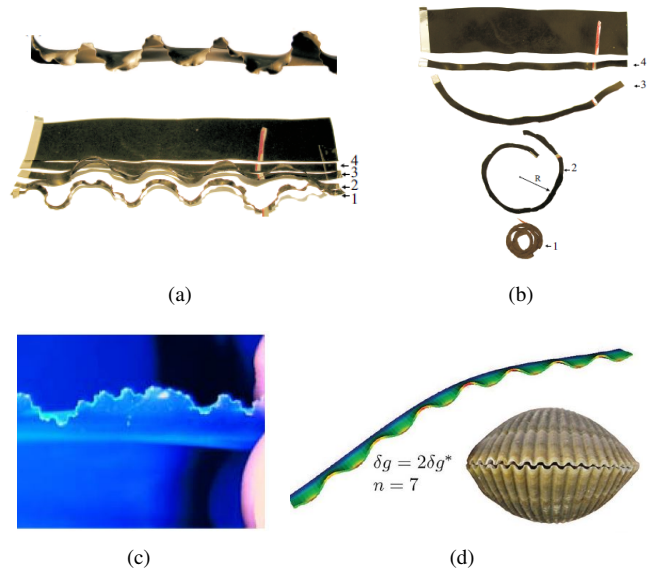

Fig. 13. The (a) winkled edge of a leaf forms (b) circular strips when flattened as analysed by Sharon [48]. Also garbage bags form wrinkles on the edge due to compression stresses after tearing [49] and sea shells grow wrinkled because of inhomogenous growth, explained by Rudraraju [51].

V. DISCUSSION

An important distinction between the application of geometrical boundary conditions and the application of pre-stress can be made based on practical feasibility. The manufacturing process of pre-stressed structures was described as 'difficult' and 'sensitive' by Guest and Murphey whereas the application of boundary conditions seems to be less of a challenge. This can be explained by the fact that control over internal stress is indirect. When the application of boundary conditions is considered, accurate control over dimensions and material continuity is required which is direct and therefore more easy to achieve. A disadvantage of the application of boundary conditions is the necessity of constraining reaction forces and moments. This problem is bypassed by the creation of a looped geometry, where the reaction forces and moments are applied to itself. However, the geometry will always be restricted to a loop. Shape-freedom is obtained by accurate pre-stressing, resulting in neutrally stable mechanisms that can be optimized for their application.

The occurrence of a neutrally stable closed-loop mechanism can be explained intuitively. If an initially unstressed elastic system is subjected to a boundary condition, a neutrally stable deformation mode is present when infinitely many energetically equally preferred solutions for the equilibrium geometries exist. This is often the case when the initial geometry shows axial symmetry. Two examples are used to demonstrate this intuitive explanation. After that, a theoretical mechanism showing two neutrally stable deformation modes is synthesised.

Consider the bent rod described by Thomson and Tait. A full rotation is applied at the endpoints of the rod with finite length that brings them together. Because of the rod's

initial axial symmetry, the rotational orientation of the rod does not matter: the rod is free to rotate around its centroidal axis throughout the deformation process. A different, non-axisymmetric example is given by the tape loop. A full rotation is applied to the endpoints of a tape spring with finite length and the ends are connected. Two half-turn folds are energetically more favorable than a continuous loop or three folds, so a flat loop with two parallel contours and two localized bending regions emerges. However, the locations of these folds is arbitrary due to the initial constant cylindrically-shaped cross-section and can be moved with no energy penalty.

Consider the situation where the two deterministic properties are combined into an initial geometry with axial symmetry that shows softening upon bending. Similar to the tape loop, a non-circular shape results when the two ends are connected. The localized regions of accumulated deformation form as a result of the minimal potential energy condition. Similar to the tape loop, the locations of the localized regions of deformation are arbitrary. But because of the isotropic nature of the initial bending stiffness, this non-circular structure also features a second neutrally stable deformation mode. There exists no preferred bending direction, resulting in an energetically allowed rotation around the centroidal axis that is also neutrally stable.

VI. Conclusion

The goal of this literature survey is to give an overview of the occurrences of elastic neutral stability, categorize examples and find methods for creating neutral stability in compliant shell mechanisms. Examples of neutrally stable elastic systems have been found in both mechanical and biological disciplines. In mechanical systems, they overcome the need for additional 'parasitic' actuation. The occurrence of neutrally stable structures in biology is not unexpected, since also organisms would benefit from efficient actuation. However, only a few with a defined purpose have been identified in literature, others are mere incidental occurrences where theory predicts the presence of a neutrally stable deformation mode.

Mechanisms consisting of multiple separate components can obtain their neutrally stable properties by modifying the constitutive components individually. Neutral stability in single element mechanisms seems to originate from different mechanisms for maintaining a constant energy level. However, similarities between methods for retaining the elastic energy were found. Therefore, as the main contribution of this paper, a division between the application of pre-stress and the application of geometrical boundary conditions as an approach for creating neutral stability is proposed.

When pre-stress is applied, the potential energy remains within the mechanism by a phenomenon called geometric frustration: no deformation mode exists that relaxes all present stresses simultaneously. The directions and magnitude of the pre-stress can then be optimized for the required neutrally stable deformation path. When, on the other hand, boundary conditions associated with an increase in potential energy are imposed, energy remains stored in the system because no deformation mode that does not meet the boundary conditions is allowed to exist. For a neutrally stable deformation mode to arise, infinitely many equally favorable solutions to that boundary condition should exist. The neutrally stable deformation mode is then defined by the continuous path that contains all solutions. Looped geometries are a special case and result from an angular boundary condition that involves a full rotation.

In this paper, effort is made to explain the occurrence of elastic neutral stability on a practical level. New insight into their working principles was obtained and often involved geometric symmetry. Future work can be done to reveal the influence of the presence of symmetry in the initial geometry on the resulting neutrally stable geometry and associated deformation path.

References

[1] T. Tarnai, "Zero stiffness elastic structures," *International Journal of Mechanical Sciences*, vol. 45, no. 3, pp. 425–431, 2003.

[2] M. Schenk and S. D. Guest, "On zero stiffness," *Proceedings of the Institution of Mechanical Engineers, Part C: Journal of Mechanical Engineering Science*, vol. 228, no. 10, pp. 1701–1714, 2014.

[3] M. Schenk, S. D. Guest, and J. L. Herder, "Zero stiffness tensegrity structures," *International Journal of Solids and Structures*, vol. 44, no. 20, pp. 6569–6583, 2007.

[4] H. W. R. Houwers, "Closed-loop two-fold tape spring transmissions," Delft University of Technology, Tech. Rep., 2016.

[5] M. R. Schultz, M. J. Hulse, P. N. Keller, and D. Turse, "Neutrally stable behavior in fiber-reinforced composite tape springs," *Composites Part A: Applied Science and Manufacturing*, vol. 39, no. 6, pp. 1012–1017, 2008.

[6] J. Geerts, "Towards compliant and compact arm supports," Delft University of Technology, Tech. Rep., 2017.

[7] S. van der Kemp, "Design of a compact wearable arm support utilizing shape optimized compliant shell mechanisms," Delft University of Technology, Tech. Rep. September, 2018.

[8] G. Radaelli and J. L. Herder, "Gravity balanced compliant shell mechanisms," *International Journal of Solids and Structures*, vol. 118-119, pp. 1339–1351, 2017. [Online]. Available: http://dx.doi.org/10.1016/j.ijsolstr.2017.04.021

[9] J. R. Leemans, "Characterization of non-linear compliant shell mechanisms compliant scoliosis brace," Delft University of Technology, Tech. Rep., 2018.

[10] J. L. Herder, "Energy-free Systems. Theory, conception and design of statically," Ph.D. dissertation, 2001.

[11] N. Tolou, V. A. Henneken, and J. L. Herder, "Statically balanced compliant micro-mechanisms," pp. 1–8, 2010.

[12] S. Guest, "Zero stiffness elastic shell structures," vol. 6, no. 7, 2011.

[13] C. Vehar, S. Kota, and R. Dennis, "Closed-loop tape springs as fully compliant mechanisms -preliminary investigations," in *Proceedings of the ASME Design Engineering Technical Conference*, vol. 2 B, 2004, pp. 1023–1032.

[14] M. A. Dias, L. H. Dudte, L. Mahadevan, and C. D. Santangelo, "Geometric mechanics of curved crease origami," *Physical Review Letters*, vol. 109, no. 11, pp. 1–5, 2012.

[15] W. Hamouche, C. Maurini, A. Vincenti, and S. Vidoli, "Basic criteria to design and produce multistable shells," *Meccanica*, vol. 51, no. 10, pp. 2305–2320, 2016.

[16] W. T. B. Kelvin and P. G. Tait, *Treatise on natural philosophy*. Claredon Press, 1867, vol. 1.

[17] Hoetmer, "Negative stiffness building blocks for statically balanced compliant mechanisms," vol. 6, no. 7, 2010.

[18] F. M. Morsch and J. L. Herder, "Design of a generic zero-stiffness compliant joint," pp. 1–9, 2010.

[19] X. Lachenal, S. Daynes, and P. M. Weaver, "A zero torsional stiffness twist morphing blade as a wind turbine load alleviation device," *Smart Materials and Structures*, vol. 22, no. 6, 2013.

[20] S. Daynes, X. Lachenal, and P. M. Weaver, "Concept for morphing airfoil with zero torsional stiffness," *Thin-Walled Structures*, vol. 94, pp. 129–134, 2015. [Online]. Available: http://dx.doi.org/10.1016/j.tws.2015.04.017

[21] B. Soethoudt and J. L. Herder, "Synthesis of perfect spring balancers with higher-order zero-free-length springs," *2007 Proceedings of the ASME International Design Engineering Technical Conferences and Computers and Information in Engineering Conference, DETC2007*, vol. 8 PART B, pp. 751–762, 2008.

[22] G. Radaelli and J. L. Herder, "A potential energy field (PEF) approach to the design of a compliant self-guiding statically-balanced straight-line mechanism," *Mechanism and Machine Theory*, vol. 114, pp. 141–155, 2017. [Online]. Available: http://dx.doi.org/10.1016/j.mechmachtheory.2017.04.007

[23] T. W. Murphey and S. Pellegrino, "A novel actuated composite tape-spring for deployable structures," *Collection of Technical Papers - AIAA/ASME/ASCE/AHS/ASC Structures, Structural Dynamics and Materials Conference*, vol. 1, pp. 260–270, 2004.

[24] B. Doornenbal, "Zero stiffness composite shells: Using thermal pre-stress," Delft University of Technology, Tech. Rep. September, 2018.

[25] J. P. Stacey, M. P. O'Donnell, and M. Schenk, "Thermal Prestress in Composite Compliant Shell Mechanisms," *Journal of Mechanisms and Robotics*, vol. 11, no. 2, pp. 1–10, 2019.

[26] Y. Liuyi, T. Huifeng, and C. Zongsheng, "Thin-Walled Neutrally Stable Deployable Composite," no. July, pp. 19–24, 2015.

[27] A. Kumar and A. Subramaniam, "Materials analogue of zero-stiffness structures," *Philosophical Magazine Letters*, vol. 91, no. 4, pp. 272–279, 2011.

[28] W. H. Wittrick, W. H. Wittrick, D. M. Myers, and W. R. Blunden, "Stability of a bimetallic disk," *Quarterly Journal of Mechanics and Applied Mathematics*, vol. 6, no. 1, pp. 15–31, 1953.

[29] K. A. Seffen and R. A. McMahon, "Heating of a uniform wafer disk," *International Journal of Mechanical Sciences*, vol. 49, no. 2, pp. 230–238, 2007.

[30] E. Lamacchia, A. Pirrera, I. V. Chenchiah, and P. M. Weaver, "Non-axisymmetric bending of thin annular plates due to circumferentially distributed moments," *International Journal of Solids and Structures*, vol. 51, no. 3-4, pp. 622–632, 2014.

[31] W. Hamouche, C. Maurini, S. Vidoli, and A. Vincenti, "Multi-parameter actuation of a neutrally stable shell: A flexible gear-less motor," *Proceedings of the Royal Society A: Mathematical, Physical and Engineering Sciences*, vol. 473, no. 2204, 2017.

[32] Y. Klein, "Shaping of Elastic Sheets by," *Science (New York, N.Y.)*, vol. 9, no. February, pp. 1116–1120, 2007.

[33] D. P. Holmes, M. Roché, T. Sinha, and H. A. Stone, "Bending and twisting of soft materials by non-homogenous swelling," *Soft Matter*, vol. 7, no. 11, pp. 5188–5193, 2011.

[34] M. Pezzulla, S. A. Shillig, P. Nardinocchi, and D. P. Holmes, "Morphing of geometric composites via residual swelling," *Soft Matter*, vol. 11, no. 29, pp. 5812–5820, 2015.

[35] D. F. Wilkes, "Rolamite-a new mechanical design concept," 1967.

[36] A. Baumann, A. Sánchez-Ferrer, L. Jacomine, P. Martinoty, V. Le Houerou, F. Ziebert, and I. M. Kulić, "Motorizing fibres with geometric zero-energy modes," *Nature Materials*, vol. 17, no. 6, pp. 523–527, 2018.

[37] I. M. Kulić, R. Thaokar, and H. Schiessel, "Twirling DNA rings - Swimming nanomotors ready for a kickstart," *Europhysics Letters*, vol. 72, no. 4, pp. 527–533, 2005.

[38] R. Cadman, "Rolamite-Geometry and Force analysis," 1969.

[39] M. G. De Jong, W. W. Van De Sande, and J. L. Herder, "Properties of twofold tape loops: The influence of the subtended angle," *Journal of Mechanisms and Robotics*, vol. 11, no. 2, pp. 1–7, 2019.

[40] J. F. Marko, "The internal 'slithering' dynamics of supercoiled DNA," *Physica A: Statistical Mechanics and its Applications*, vol. 244, no. 1-4, pp. 263–277, 1997.

[41] A. Goriely, *Interdisciplinary Applied Mathematics 45 The Mathematics and Mechanics of Biological Growth*.

[42] T. Todres, "On a developable mobius band," *The Mechanics of Ribbons and Möbius Bands*, pp. 351–352, 2016.

[43] S. E. Spagnolie and E. Lauga, "The optimal elastic flagellum," *Physics of Fluids*, vol. 22, no. 3, pp. 1–15, 2010.

[44] T. Lessinnes, D. E. Moulton, and A. Goriely, "Morphoelastic rods Part II: Growing birods," *Journal of the Mechanics and Physics of Solids*, vol. 100, no. September 2014, pp. 147–196, 2017. [Online]. Available: http://dx.doi.org/10.1016/j.jmps.2015.07.008

[45] U. Nath, B. C. Crawford, R. Carpenter, and E. Coen, "Genetic control of surface curvature," *Science*, vol. 299, no. 5611, pp. 1404–1407, 2003.

[46] B. Audoly and A. Boudaoud, "'Ruban à godets': An elastic model for ripples in plant leaves," *Comptes Rendus - Mecanique*, vol. 330, no. 12, pp. 831–836, 2002.

[47] Me, B. Audoly, and A. Boudaoud, "Self-Similar Structures near Boundaries in Strained Systems," *Physical Review Letters*, vol. 91, no. 8, pp. 3–6, 2003.

[48] E. Sharon, M. Marder, and H. Swinney, "Leaves, Flowers and Garbage Bags: Making Waves," *American Scientist*, vol. 92, no. 3, p. 254, 2004.

[49] E. Sharon, B. Roman, and H. L. Swinney, "Geometrically driven wrinkling observed in free plastic sheets and leaves," *Physical Review E - Statistical, Nonlinear, and Soft Matter Physics*, vol. 75, no. 4, 2007.

[50] H. Liang and L. Mahadevan, "The shape of a long leaf," *Proceedings of the National Academy of Sciences of the United States of America*, vol. 106, no. 52, pp. 22 049–22 054, 2009.

[51] S. Rudraraju, D. E. Moulton, R. Chirat, A. Goriely, and K. Garikipati, "A computational framework for the morpho-elastic development of molluskan shells by surface and volume growth," *PLoS Computational Biology*, vol. 15, no. 7, pp. 1–28, 2019.

3

Paper II: An idealized crease

Neutrally stable transition of a curved-crease planar shell structure

Sjaak Kok, Giuseppe Radaelli, Ali Amoozandeh Nobaveh and Just Herder

Abstract—**Elastic neutral stability in compliant mechanisms is a remarkable appearance since it requires the energetic state of the structure to remain unchanged during deformation. Several examples in literature require either plastic deformation or external constraints to be enforced for obtaining a state of pre-stress and often require the use of anisotropic materials. This paper presents a new type of compliant shell structure featuring a neutrally stable deformation mode without requiring one of the aforementioned conditions. The structure is composed of two initially flat compliant facets that are connected via a curved crease. It can be reconfigured into a second zero-energy state via propagation of a transition region, without any apparent effort. Both the structure's local width and local crease curvature turn out to be effective parameters for tuning the behavior regarding stability during transition. The modelled results are verified by several prototypes that match the modelled predictions qualitatively, as well as by measurement results that show quantitative agreement. The new type of structure introduced here features neutral stability without relying on the application of pre-stress during manufacturing or externally applied boundary conditions. Moreover, it shows potential for combining geometric simplicity with complex and highly tune-able behavior.**

I. Introduction

A surprisingly simple yet intriguing structure arises when two flat arched-shaped compliant sheets are stacked and connected in a hinged fashion along their shortest curved edges. The resulting mechanism features two obvious stable zero-energy equilibrium configurations: as-fabricated and inverted, with either the top sides or the bottom sides of the arches facing each other. However, *transition* between the stable states is not straightforward since the curved nature of the hinge does not allow energy-free operation. This type of hinge can be considered a curved crease and based on the presence of it, the structure can be classified as curved-crease origami, where actuation of the curved crease is coupled to inherent deformation of the facets [1]. The structure can then arguably be classified as a compliant facet origami mechanism (COFOM), an origami mechanism wherein compliance of the facets is used to incorporate energy storage [2].

The transition is initiated when the edges at an arbitrary end are flipped with respect to each other (figure 1). As the *transition region* is propagated through, it progressively inverts the structure until it has been completely flipped over. A significant part of this transition appears to be an energy-free process since the transition region merely shifts through the structure. The mechanism then features a continuous equilibrium as its behavior resembles the fascinating class of statically balanced structures. In that particular situation, it is said to be 'neutrally stable'.

Elastic neutral stability is a remarkable appearance since, normally, the deformation of materials is associated with increasing potential energy and a resulting opposing force or moment. An elastic mechanism in neutral equilibrium can only

deform without load if the necessary energy is already stored in the system and redistributed upon deformation [3]. This unique property is investigated by Guest et al. [4], who utilize plastic deformation of an initially flat rectangular plate as a source for pre-stress and describe the behavior of the resulting neutrally stable cylindrically curved shell. Because of residual stresses, rotation of the axis of curvature does not change the strain energy, thereby rendering all possible curvature-axes configurations equally preferable. Schultz et al. [5] describe a neutrally stable deployable composite boom that is stable in both the coiled and extended state and every configuration in between.

Elastic neutral stability was probably first mentioned by Thomson and Tait [6] in the book 'Treatise on natural philosophy' (published in 1867). There, an initially straight rod is described that exhibits a state of neutral stability around its centroidal axis when the ends are connected to form a circular, pre-stressed, geometry. Rotation can occur without
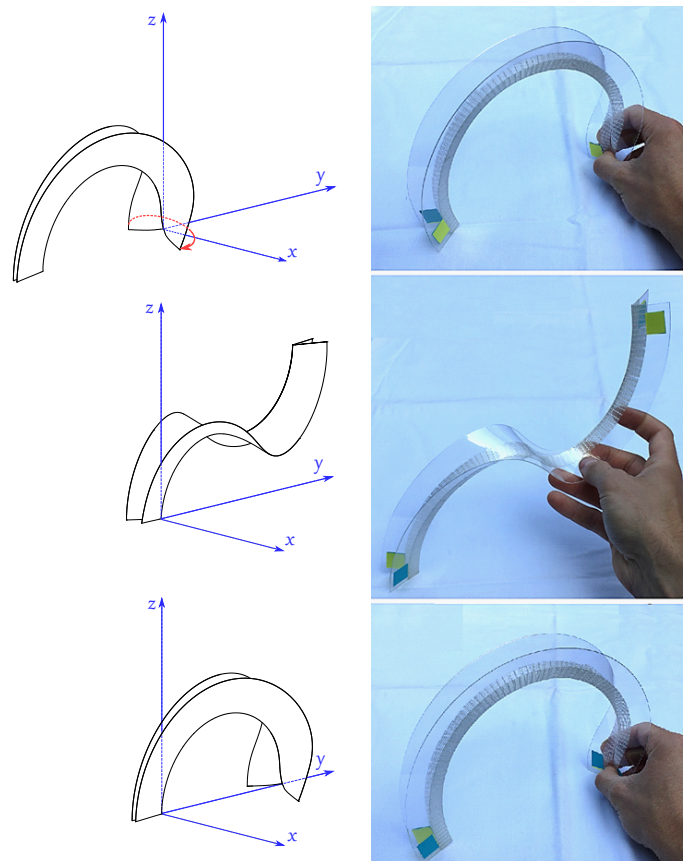

Fig. 1. The transition between the two stable zero-energy states is depicted both schematic (left) and using a physical prototype (right). After the transition is initiated (top), the transition region propagates through the structure (middle) until it reaches the opposite end (bottom).

the need to introduce a load or to add energy to the system. The tape loop, first thoroughly investigated by Vehar et al. [7], is a more recent example where boundary conditions applied to a compliant shell structure result in a neutrally stable deformation mode. When the two ends of a tape spring are connected into a loop, the equilibrium configuration associated with minimal potential energy consists of two localized folds. Because of the invariant cross-section, the location of these folds is arbitrary and can be propagated collectively through the structure without energetic costs. The structure presented here closely resembles the tape loop, apart from the notable difference that no loop formation is required, resulting in an open-ended structure with beam-like properties.

Until now, all neutrally stable shell structures described in literature require either plastic deformation [4], [8]–[11], the use of anisotropic materials [5], [12]–[14] or external constraints to be enforced (e.g. form a loop) [6], [7], [15], [16] to create the desired state of pre-stress. The first two result in a complex and sensitive manufacturing process and the latter limits design freedom, thereby narrowing down the potential applications. The structure presented here requires neither of the aforementioned conditions. In order to be considered a new class of neutrally stable structures, its neutrally stable properties need to be verified. Therefore, this study aims to characterize the unique deformation mode of this structure by examining the influence of the design parameters on its stability.

The method section of this paper addresses the approach taken to investigate the behavior during transition, as well as the influence of two design parameters hereon. The numerical IGA-based model setup is discussed, together with a unique choice for controlling the state of transition by manipulating the geometry of the transition region locally. The results of the numerical analysis are presented in the results section and illustrated by physical realisation of several variants of the mechanism that show different behavior. The results are quantitatively validated by measurements taken in an experimental setup. All findings are further discussed and concluded in the subsequent discussion and conclusion.

II. MECHANICS OF TRANSITION

The stability of the mechanism can be determined by the potential energy stored in the form of material strain. The energetic state during propagation of the transition region is a measure for the stability and existence of equilibria throughout the deformation path. The location of the transition region can be described by the location of the *inflection point* along the crease line. Here, the curvature of the crease line changes sign. The *inflection axis* is the material axis perpendicular to the crease line at the inflection point (figure 2). It is the infinitesimal location within the transition region that tends to neither of the flat equilibrium configurations and is therefore assumed to be locally undeformed.

The structure consists of two identical sandwiched shells that, when assumed to be inextensible, are only subjected to bending [17]. Each can be considered a *developable ruled surface* (i.e. the mid-plane resembles a ruled surface with
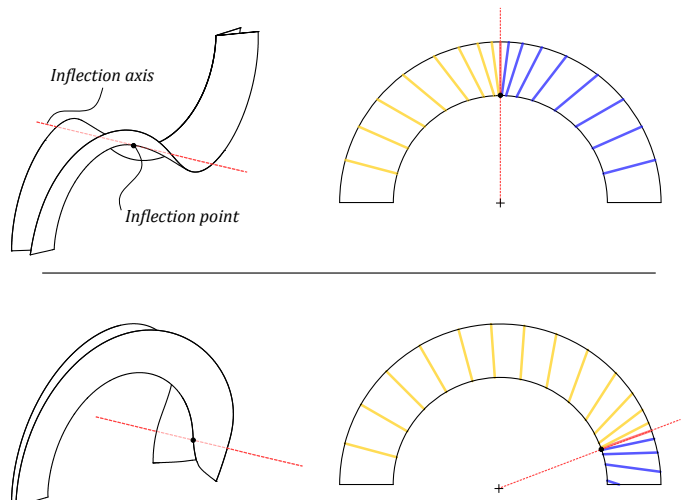

Fig. 2. The inflection point and associated inflection axis is depicted for two states during transition (left). The inflection axis is locally undeformed and directed perpendicular to the inner perimeter at the inflection point. A schematic representation of the deformation projected on the undeformed geometry is depicted (right), where the yellow and blue lines represent the generators with positive and negative curvature respectively.

zero Gaussian curvature), where the local bending axes form the *generators* (figure 2). Everywhere on the surface one of the two principal curvatures equals zero, relating the local curvature directly to the bending magnitude around the local bending axis. However, it should be mentioned that the generators' directions are not invariant but are determined by the current location of the transition region. It can be observed that the transition region is consistently subjected to relatively high strains, suggesting that the total energy is predominantly determined by the energy stored around the inflection point (figure 3(a)).

The course of the energy curve during propagation of the transition region can be manipulated by design parameters of the undeformed geometry. Energy storage around the inflection point can locally be influenced by changing the amount of material (figure 3(b)). The local width of the arch-shaped geometry is directly proportional to the amount of material and will therefore be used as the first design variable (figure 4(a)). The local curvature of the crease at the location of the inflection point also influences the required material deformation (figure 4(b)). For instance, the limit case of a crease with zero curvature (i.e. a straight folding line) would be able to operate without deforming the material. In this work, the effect of introducing variable arch width and variable crease curvature on the behavior of the structure during transition is further investigated.

III. METHOD

In order to investigate the complex geometrical configurations that occur during transition, a numerical approach is substantiated. In this section, expressions for the variable geometry are defined and modelling details are discussed.
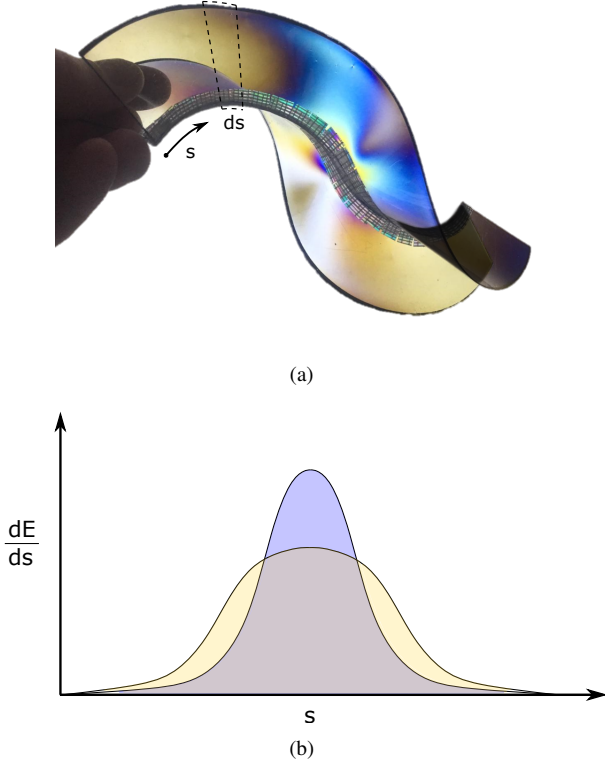
(a)

(b)

Fig. 3. (The stress distribution within the structure is visualised using a phenomenon called photoelasticity where color gradients in the material represent stress gradients (a). A schematic representation of the energy distribution as a function of the material coordinate s is also depicted (b). The two curves each represent a possible distribution for certain design parameters where the surface area equals the total elastic potential energy within the system.

A. Numerical model setup

An isogeometric framework (IGA) [18] forms the basis of the numerical analysis. A shell model based on the Kirchhoff-Love plate theorem is used and a linear isotropic elastic constitutive law is applied. The geometry is modelled as the mid-plane surface of a shell of uniform thickness and described by B-splines. These are defined by a set of control points and make up a planar grid, with the primary and secondary material directions perpendicular to and along with the curved crease line respectively (denoted with d_1 and d_2 respectively in figure 5). The boundaries of the surface are given by the inner and outer perimeter, r_{in} and r_{out} and a subtended angle, θ. The local width of the structure is defined as the distance between r_{in} and r_{out} perpendicular to r_{in}. The control points are placed along the inner perimeter with equal angular intervals ($n = 60$) and spaced linearly along the width ($m = 10$). Because of symmetry, only a single half of the structure is modelled. The effect of the interaction between the two halves is replaced with a geometrical constraint, enforcing the control points that describe the crease line to live on the symmetry plane.

The effects of variations in local width and curvature are investigated separately. The local width is varied by altering the geometry of the outer perimeter while maintaining a

crease of constant curvature. The addition of a sine-function of parameterized amplitude p is chosen to perturb the outer perimeter, creating a smooth transition through the structure. A parameterization of the investigated curves is given as:

$$r_{\mathrm{w,in}}(\theta) = r_0 \tag{1}$$

$$r_{\mathrm{w,out}}(\theta) = (1 + p\sin\theta)\, w_0 + r_0, \tag{2}$$

with

$$0 < \theta < \pi,$$

where $r_{\mathrm{w,in}}$ describes the inner perimeter, or crease line, of constant curvature and $r_{\mathrm{w,out}}$ describes the perturbed circular outer perimeter. r_0 is the standard radius of curvature, w_0 is the standard width (table I) and θ is the angular coordinate with respect to the positive x-axis. The period is chosen so that the width at the boundaries equals w_0. The amplitude p is used to produce geometries of different width profiles with $-0.4 < p < 0.4$ with equal intervals of $\Delta p = 0.1$, resulting in geometries with both narrower and wider middle sections.

An elliptical geometry is used to study the effect of local curvature. A parameterization of the investigated inner curve is given as:

$$r_{\mathrm{c,in}}(\theta) = \frac{a_1 b_1}{\sqrt{(b_1 \cos\theta)^2 + (a_1 \sin\theta)^2}}, \tag{3}$$

with

$$a_1 = r_0$$
$$b_1 = r_0\, q$$

and

$$0 < \theta < \pi.$$

Variables a_1, b_1 are the semi-minor and semi-major axis of the inner and outer part of the perimeter respectively. The ratio between the semi-minor axis and semi-major axis is represented by the factor q, with $0.8 < q < 1.2$ with equal intervals of $\Delta q = 0.05$. A value of $q = 1$ results in a circular segment and a ratio $q > 1$ results in a geometry with higher curvature towards the boundaries. The outer perimeter $r_{\mathrm{c,out}}$ is traced out by the last control points in the d_1-direction, defined as the normal to the inner perimeter $r_{\mathrm{c,in}}$ (figure 5). The width of the curve, measured in the direction of d_1, is kept constant and equal to w_0. Values for other design parameters are denoted in table I.

B. A moving constraint

The control points on the inner perimeter r_{in} of the modelled half of the shell structure are constrained to live on the symmetry (xy-) plane, i.e. $z = 0$. One (arbitrary) control point along r_{in} is fixed in space. The local geometry of the inflection axis can be considered as a straight line and invariant throughout the deformation process. Propagation of the transition region is therefore modelled by locally aligning the structure perpendicular to the symmetry plane (figure 6).
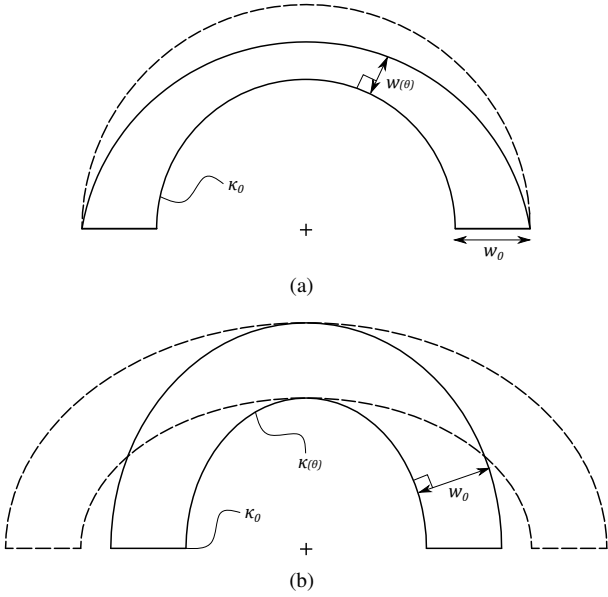
Fig. 4. A graphical representation of the design variables used to control the behavior of the transition. Either (a) the local width is varied while maintaining a constant crease curvature or (b) the local curvature is varied while maintaining a constant width.

The direction from control point (1) to (2) is aligned with the x-axis. Control point (3) is constrained to share its y-coordinate with point (1), such that control points (1), (2) and (3) span the xz-plane. This condition is consecutively imposed on all control points along the curved crease. The resulting moving constraint affects the geometry locally, thereby omitting parasitic deformations resulting from a more general clamped loading condition. The elastic potential energy during propagation is investigated as a measure for the stability of all encountered intermediate configurations.

C. Experimental validation

Validation of the modelled results is achieved by reproducing the constraint conditions in an experimental setup. The setup, depicted in figure 7, is based on a three-point bending framework that constrains three symmetrically oriented material points to be aligned over a distance d_c at a specific location along the curved crease. A $9N$ miniature S-beam load cell (Futek LSB200) is used together with a signal conditioner (Scaime CPJ2S) and a data acquisition module (NI USB-6008) to measure the reaction force on the middle contact point. Due to symmetry and static equilibrium conditions, the remaining two opposing reaction forces can be derived. The reaction force is a measure for the tendency of the structure to reconfigure towards an equilibrium configuration. Measurements are taken at discrete intervals of $\frac{\pi}{20}$rad along the crease line.

Prototypes are constructed from 0.5mm polycarbonate (PC) sheet with a Young's modulus of 2.5GPa. Designs are modelled in CAD-CAM software and a CNC-operated drag knife is used to accurately reconstruct the modelled geometries. The curved crease is realised using glass fiber reinforced adhesive tape (3M 8959) on both sides of the PC sheets. Since a fixed distance d_c between the contact points is imposed in this setup, only geometries featuring a constant width, i.e. elliptical variations, are used for quantitative analysis. Prototypes with varying width are used to validate the modelled results qualitatively.
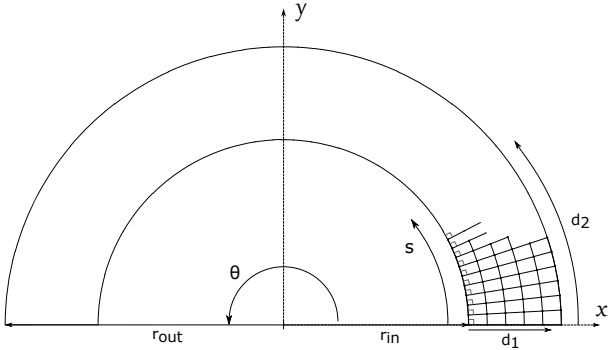

Fig. 5. The parameters used to describe the undeformed geometry are depicted in both the Cartesian and polar coordinate system. The design variables (r_{in}, r_{out}, θ), material directions used to define the control points (d_1, d_2) and the curvelinear material coordinate s are denoted.

IV. RESULTS

A. Modelling results

Figure 8 and 9 show the elastic energy during transition of the structure with varying local width and varying local curvature respectively. In both figures, a schematic graphical representation of the state of the structure is depicted. Every
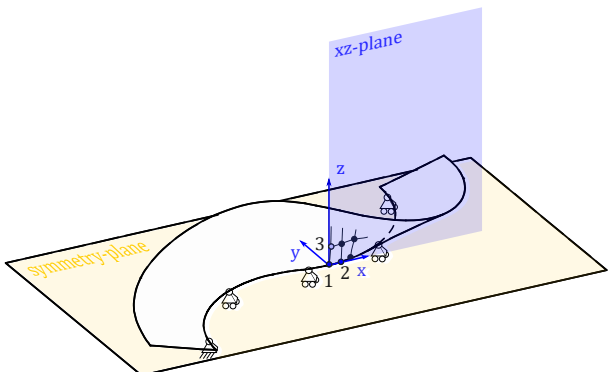

Fig. 6. The constraints used to model the propagation of the transition region. Only one half of the shell is modelled, whereby the inner perimeter r_{in} lives on the symmetry plane. Control point 1,2 and 3 are subjected to angular constraints.
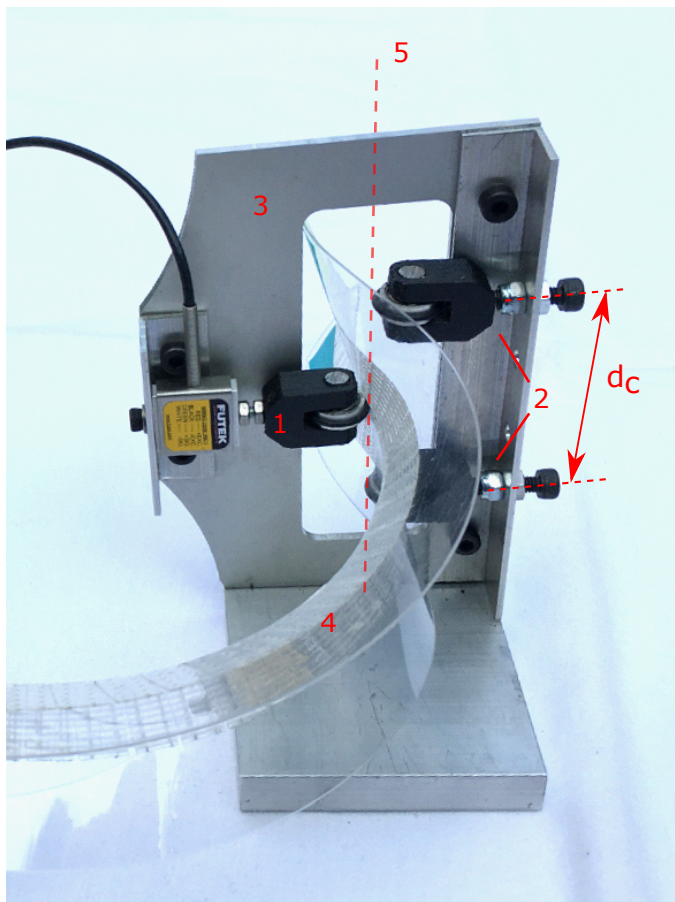
Fig. 7. The measurement setup based on a three-point bending framework. Reaction forces are measured by the middle contact point that is connected to a force transducer (1), while opposing forces are provided by two adjustable contact points (2) connected to the frame (3). Three material points are aligned on the structure to be analysed (4), representing the inflection axis (5).

through the transition ($p = -0.4$ and $q = 1.2$) also show this behavior in practice. Structures with a predicted unstable equilibrium ($p = 0.4$ and $q = 0.9$) always showed a tendency towards their flat configurations. Finally, prototypes with a predicted region of near-constant energy ($p = -0.1$ and $q = 1.05$) have been constructed and showed no tendency towards any configuration. Within that region, no external loads were required in order to maintain static balance. Prototypes of the elliptical extremes are depicted in figure 11.

V. DISCUSSION

A. Results of the numerical analysis

A local energy maximum represents an unstable equilibrium, while a local energy minimum predicts the existence of a stable equilibrium. It can be seen that both geometric groups feature stable and unstable equilibria.

A circular geometry of constant width (corresponding to $p = 0$ and $q = 1$ and the interupted curves in figure 8 and figure 9 respectively) does not show stable behavior. When the structure is symmetric with respect to the inflection point and both sides are equal in size, a local maximum exists. This effect is amplified when the middle of the structure either features higher width or higher curvature with respect to the ends (corresponding to values of $p > 0$ and $q < 1$). For values of $p < -0.05$ and $q > 1.05$, the structure exhibits a third stable, albeit non-zero-energy equilibrium. The local energy minimum implies a tendency of the mechanism to maintain this symmetric configuration. For values of p around $p = -0.05$ and $q = 1.05$, the potential elastic energy curve neither shows local maxima nor local minima around this symmetric configuration, extending the state of equilibrium over a significant portion of the investigated range of motion. This shows that compensation for the edge-effects of the open ended structure is possible, by geometrical variations to the standard circular structure of constant width. Note that this unique property is not a result of a specific optimization procedure but arises simply due to the variation of either of two principal design parameters. This aspect could be generalized by stating that the behavior is tune-able to a high extend, creating the potential to be optimized for customized behavior.

curve represents unique behavior, where the geometry is determined by a certain value of the the parameters p and q. The dashed curve represents the same, circular, geometry with constant width in both figures. Note that the zero-energy states are not depicted here since they do not feature an inflection axis and fall therefore outside the analysis window.

B. Experimental results

Figure 10 shows the reaction forces on the static contact points of four variations to the elliptical geometry. A geometry with a third equilibrium ($q = 1.2$), a constant energy region ($q = 1.05$), a circular geometry ($q = 1$) and an unstable geometry ($q = 0.9$) are investigated. The dashed lines represent the boundaries of the discrete measurement results and the markers denote the discrete measurement locations. Locations where contact was barely present are denoted with zero. The shaded area illustrates the variance in the measurement results. A change of sign of the measurement signal required a physical flip of the analysed structure to ensure continuous contact with the contact points.

Prototypes that represent the most extreme variations to the elliptical and the circular geometries have been constructed. The two variations with a predicted stable equilibrium halfway

B. Results of the experimental analysis

Measurement results show similar behavior when compared to the modelled predictions. However, measured forces are notably lower then predicted, which could be due to several discrepancies between simulations and the physical realisation of the structure. The crease is modelled to have zero stiffness, while this is evidently not achievable in practice. Crease forces could have opposed the reaction forces of the shell elements, thereby affecting the measurements. Also, visco-elasticity of the prototype material was not taken into account in the numerical simulations. Moreover, the finite width of the crease allowed for some relative motion between the structure's components, resulting in another mismatch with the modelled conditions. Finally, the manual operations allowed for some inconsistency regarding positioning and propagation velocity and left some room for interpretation of the measured forces.
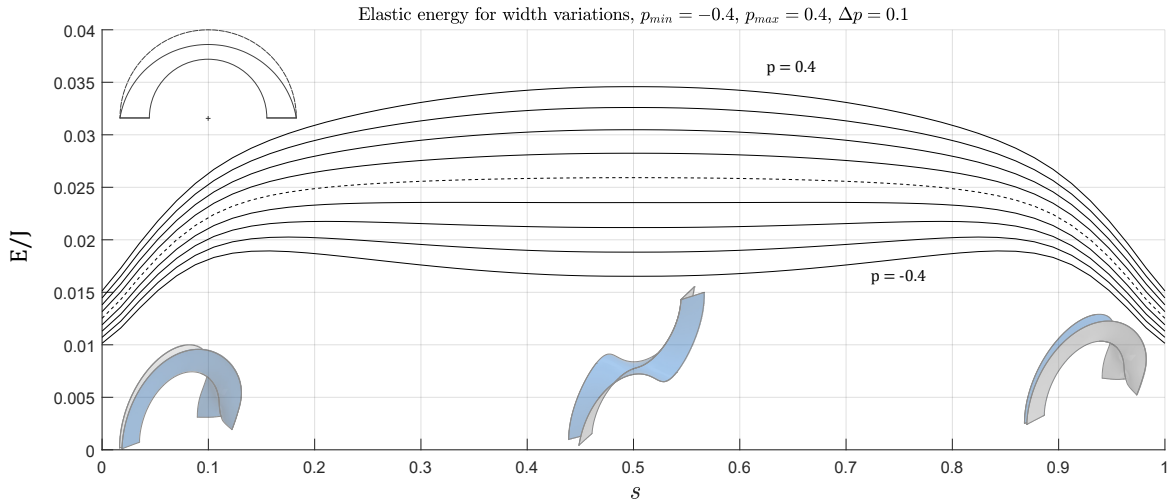
Fig. 8. The energetic paths for different values of the design parameter p, associated with a varying local width are depicted. The curves show the elastic energy during transition between the two stable zero-energy states. The dashed curve represents a structure of constant width.
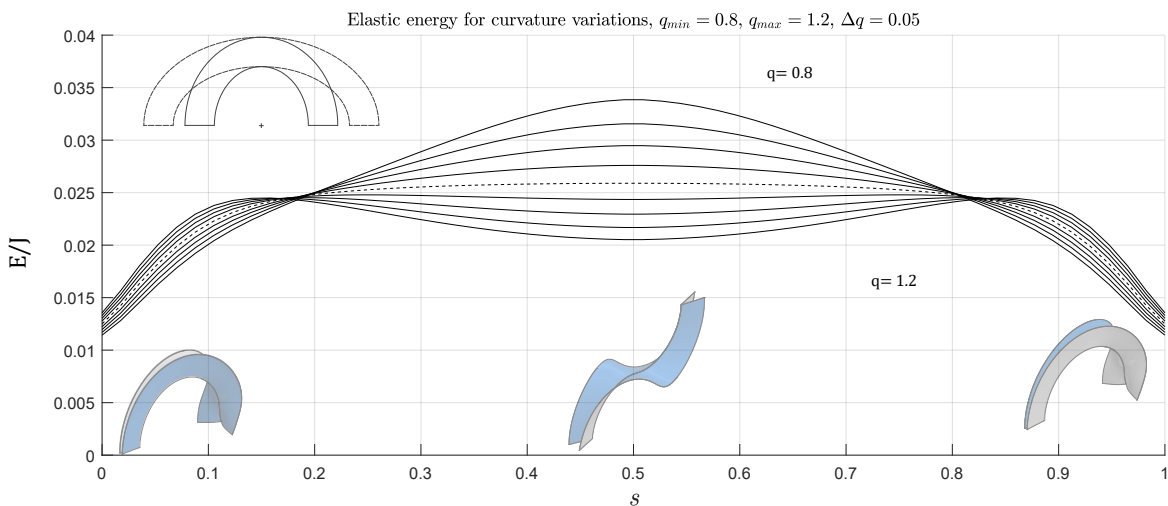

Fig. 9. The energetic paths for different values of the design parameter q, associated with a varying local curvature are depicted. The curves show the elastic energy during transition between the two stable zero-energy states. The dashed curve represents a structure of constant curvature.

Qualitative analysis showed stable or un-stable behavior as predicted and confirmed the existence of a neutrally stable geometry in between.

VI. CONCLUSION

In this paper, a new type of compliant shell structure featuring a curved crease is presented. Transition between two stable zero-energy states occurs by propagating a transition region through the structure without apparent effort. This unique behavior is characterized by analyzing the influence of two principal design parameters on the stability of the encountered configurations.

It has been shown that the energetic path during transition can be manipulated by both the structure's local width and local crease curvature. For a unique set of design parameters, a third prolonged equilibrium exists within a significant range of motion, rendering the structure neutrally stable and verifying its potential to be optimized for specific behavior. The modelled results are substantiated qualitatively by constructing several prototypes that show behavior in agreement with the modelled predictions. Moreover, measurement results of pronounced stable and unstable geometries show quantitative agreement with the modelled results. This verifies the validity of the modelling approach.

In contrast to existing neutrally stable compliant structures, operation of the structure presented here neither requires material anisotropy, nor taylored plastic deformation nor boundary conditions to be enforced. Therefore, we present a new type of neutrally stable compliant structure that does not rely on the application of pre-stress during manufacturing and therefore allows an unstressed configuration to exist. Moreover, isotropic material is allowed and no external constraints are required during operation. This type of structure allows geometric simplicity to be combined with behavior that is generally considered complex.
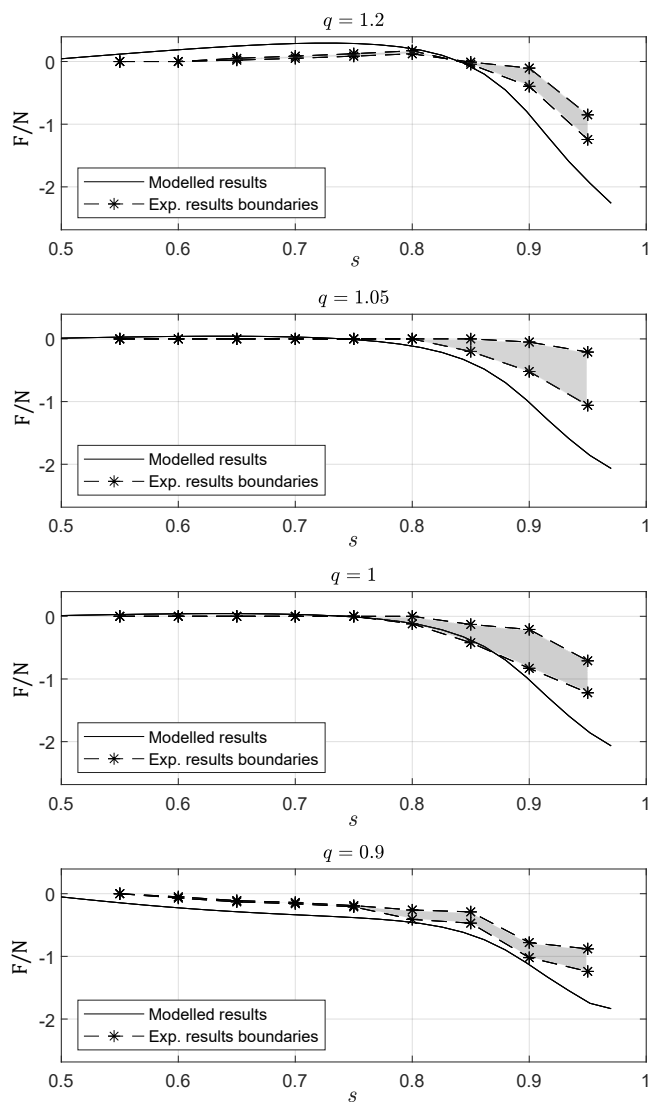
Fig. 10. The modelled and measured reaction forces depicted for an elliptic geometry for various values of the design parameter q. The solid line represents the modelled results while the shaded area depicts the spread of measurement results.
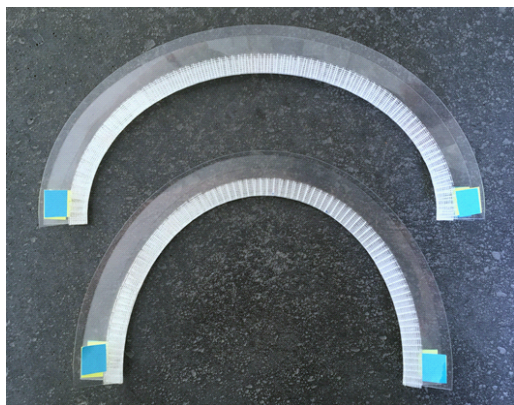

Fig. 11. Prototypes are constructed for qualitative comparison to the modelled results. Here, the two most extreme variations to the elliptical geometries, corresponding to $q = 1.2$ (top) and $q = 0.9$ (bottom) are shown.

REFERENCES

[1] M. A. Dias, L. H. Dudte, L. Mahadevan, and C. D. Santangelo, "Geometric mechanics of curved crease origami," *Physical Review Letters*, vol. 109, no. 11, pp. 1–5, 2012.

[2] J. Rommers, G. Radaelli, and J. Herder, "A Pseudo Rigid Body model of a Single Vertex Compliant-Facet Origami Mechanism (SV-COFOM)," *Proceedings of the ASME Design Engineering Technical Conference*, vol. 5B-2016, pp. 1–10, 2016.

[3] S. Kok, "Literature review of occurrences and working principles of elastic neutral stability," Tech. Rep., 2020.

[4] S. Guest, "Zero stiffness elastic shell structures," vol. 6, no. 7, 2011.

[5] M. R. Schultz, M. J. Hulse, P. N. Keller, and D. Turse, "Neutrally stable behavior in fiber-reinforced composite tape springs," *Composites Part A: Applied Science and Manufacturing*, vol. 39, no. 6, pp. 1012–1017, 2008.

[6] W. T. B. Kelvin and P. G. Tait, *Treatise on natural philosophy*. Claredon Press, 1867, vol. 1.

[7] C. Vehar, S. Kota, and R. Dennis, "Closed-loop tape springs as fully compliant mechanisms -preliminary investigations," in *Proceedings of the ASME Design Engineering Technical Conference*, vol. 2 B, 2004, pp. 1023–1032.

[8] W. H. Wittrick, W. H. Wittrick, D. M. Myers, and W. R. Blunden, "Stability of a bimetallic disk," *Quarterly Journal of Mechanics and Applied Mathematics*, vol. 6, no. 1, pp. 15–31, 1953.

[9] E. Lamacchia, A. Pirrera, I. V. Chenchiah, and P. M. Weaver, "Non-axisymmetric bending of thin annular plates due to circumferentially distributed moments," *International Journal of Solids and Structures*, vol. 51, no. 3-4, pp. 622–632, 2014.

[10] K. A. Seffen and R. A. McMahon, "Heating of a uniform wafer disk," *International Journal of Mechanical Sciences*, vol. 49, no. 2, pp. 230–238, 2007.

[11] W. Hamouche, C. Maurini, S. Vidoli, and A. Vincenti, "Multi-parameter actuation of a neutrally stable shell: A flexible gear-less motor," *Proceedings of the Royal Society A: Mathematical, Physical and Engineering Sciences*, vol. 473, no. 2204, 2017.

[12] J. P. Stacey, M. P. O'Donnell, and M. Schenk, "Thermal Prestress in Composite Compliant Shell Mechanisms," *Journal of Mechanisms and Robotics*, vol. 11, no. 2, pp. 1–10, 2019.

[13] T. W. Murphey and S. Pellegrino, "A novel actuated composite tape-spring for deployable structures," *Collection of Technical Papers - AIAA/ASME/ASCE/AHS/ASC Structures, Structural Dynamics and Materials Conference*, vol. 1, pp. 260–270, 2004.

[14] Y. Liuyi, T. Huifeng, and C. Zongsheng, "Thin-Walled Neutrally Stable Deployable Composite," no. July, pp. 19–24, 2015.

[15] D. F. Wilkes, "Rolamite-a new mechanical design concept," 1967.

[16] A. Baumann, A. Sánchez-Ferrer, L. Jacomine, P. Martinoty, V. Le Houerou, F. Ziebert, and I. M. Kulić, "Motorizing fibres with geometric zero-energy modes," *Nature Materials*, vol. 17, no. 6, pp. 523–527, 2018.

[17] E. Kebadze, S. D. Guest, and S. Pellegrino, "Bistable prestressed shell structures," *International Journal of Solids and Structures*, vol. 41, no. 11-12, pp. 2801–2820, 2004.

[18] T. J. Hughes, J. A. Cottrell, and Y. Bazilevs, "Isogeometric analysis: CAD, finite elements, NURBS, exact geometry and mesh refinement," *Computer Methods in Applied Mechanics and Engineering*, vol. 194, no. 39-41, pp. 4135–4195, 2005.

4

Paper III: A continuous shell

Neutrally stable double-curved shells by inflection point propagation

Sjaak Kok, Giuseppe Radaelli, Ali Amoozandeh Nobaveh and Just Herder

Abstract—**Compliant mechanisms that can deflect without effort form a remarkable group within their field, since it requires the energetic state to remain unchanged during elastic deformation. Several examples in literature obtain this state of neutral stability by the application of pre-stress, either as a result of manufacturing processes or the application of imposed boundary conditions. In this paper, we present a new type of statically balanced compliant mechanism that exhibits neutral stability as part of a continuous deformation process, while allowing a stress-free configuration to exist. The transition of a double-curved compliant shell towards its second equilibrium configuration forms the basis of this investigation. A varying material thickness profile, described by an ideal set of design parameters, is obtained using an optimization procedure. Numerical analysis of the resulting optimized shell structure predicts a significant region of near-constant energy and associated near-zero loads within this unique deformation mode. 3D-printed prototypes demonstrate the validity of the modelled results by featuring a continuous equilibrium within a significant range of motion. These results lay the foundation for compliant beam elements with an internal statically balanced bending degree of freedom.**

I. INTRODUCTION

Compliant shell mechanisms have become an interesting research topic over the last years and are recently circumstantially investigated. Relevant applications can be found in e.g. the aerospace industry and wearable devices, where the potential arises for organically-shaped functional structures that fit close to the human body. As a group within the increasingly popular research area of compliant mechanisms, compliant shells can be described as 'spatially curved thin-walled structures able to transfer or transmit force, motion or energy through elastic deflection' [1]. A high degree of design freedom allows for development of compliant mechanisms with non-linear force-deflection behavior, e.g. weight balancing mechanisms. As a design tool, shape optimization can be used to develop complex shell geometries that follow a desired load-displacement path [1].

Compliant shell mechanisms that are in static equilibrium throughout their range of motion belong to the group of statically balanced compliant mechanisms (SBCMs) [2], [3]. SBCMs are typically designed for weight balancing and exhibit neutral stability in presence of an external, gravitational force [1], [4], [5]. Other applications require this state of neutral stability to occur in absence of external loads [6], [7]. In the last case, the *elastic* energy in the compliant shell is required to remain constant within the range of motion. Energy is stored in the form of pre-stress and redistributed within the structure itself to allow deformation to occur.

Pre-stress can be the result of an assembly process wherein multiple elastic elements are connected in such a way that no zero-energy configuration exists. Lachenal and Daynes describe a moment-free pitch adjustment in airplane wings,

realized by adding a compliant shell structure that provides negative stiffness [8]–[11]. Likewise, the composition of two cylindrical shells with opposite curvature senses and perpendicular directions can result in neutral stability, with applications such as deployable booms for space exploration [7]. Shell mechanisms containing only a single element obtain their state of pre-stress via various processes, as shown by the authors in [12]. For example, Guest describes a cylindrically curved compliant shell that shows neutral stability after introducing pre-stress by plastic deformation [13]. Also, the curing process of anisotropic laminates leaves residual thermal stresses behind and can be used to generate the required pre-stress. This has been successfully implemented as a method for reducing stiffness of compliant shells, as described by Doornenbal [14] and Stacey [15]. The tape loop, first thoroughly investigated by Vehar, is an example of pre-stress resulting from boundary conditions [16]. The location of the folds, which arise when connecting the ends of a standard tape spring into a loop, is arbitrary due to its constant cross-section. The folded regions can be propagated through the structure without energetic costs, creating a neutrally stable deformation mode.

Until recently, all neutrally stable shell structures described in literature required either the introduction of pre-stress during the manufacturing process or external constraints to be enforced during neutrally stable operation [12]. Combining multiple components in a pre-stressed assembly (1), plastically deforming material to obtain a state of self-stress (2) and introducing residual thermal stresses during the curing process of laminates (3), all result in a complex and sensitive manufacturing process. In addition, a structure that is pre-stressed during fabrication may suffer from deteriorating performance over time because of creep and relaxation [17]. The required presence of boundary conditions, either in the form of external - or internal constraints, e.g. a looped geometry, limits design freedom, thereby narrowing down the potential applications. Prior work by the authors [18] resolves these issues by introducing a neutrally stable compliant shell structure that does not rely on pre-stressed fabrication. Similar to the tape loop, it involves the propagation of a region of localized strains, though it omits the requirement of a looped geometry, resulting in an open-ended structure with beam-like properties. However, an idealized zero-stiffness crease is assumed, causing a discontinuity in the structure that complicates physical realization and obstructs its potential applications.

The goal of this research is to develop a monolithic compliant shell mechanism that features a neutrally stable deformation mode without the need for pre-stressed manufacturing and boundary conditions to be applied. A unique and promising deformation mode of a double-curved compliant shell structure will be investigated. It features the transition between two naturally occurring stable configurations via elastic, ideally

energy-conserving, deformation. Interplay occurs between the so-called 'flange' - and 'crease' sections. The influence of the geometric design parameters on its neutrally stable potential is therefore examined.

In the next section, the shell structure with its intended deformation mode is introduced. The geometrical aspects and the mechanics of the transition are illustrated and its natural bi-stable behavior is explained by derivation of an analytical approximation of the kinematics. In the methods section, a design approach is substantiated and the modelling setup and optimization procedure are described. The design of an experimental setup and practical considerations for manufacturing prototypes are also discussed. The last part of this section will focus on modelling of the transition using an IGA-based approach and the optimization of design parameters to obtain the desired neutrally stable behavior. The results section presents both the modelled and the experimental results, followed by a discussion and a conclusion.

II. MECHANICS OF TRANSITION

This section serves to introduce the shell structure by describing its features and design parameters and to give the reader an intuitive understanding of its mechanical behavior. Aspects around the intended deformation mode, featuring a transition region, are first elucidated and illustrated by a schematic representation of the expected energy-deflection behavior. This is further substantiated by an attempt to analytically derive the mechanics of an alternative deformation mode that predicts the same bi-stable behavior. The reader is free of choice to skip this last section, as it merely serves a supportive purpose.

A. Geometry description and design parameters

This investigation is based on a compliant shell structure with specific geometrical features, wherein two parts with different functionalities can be distinguished. The base of the mechanism resembles the surface section of a torus with negative Gaussian curvature, effectively forming a curved crease. Its two principal curvatures are perpendicular in direction and opposite in sign (figure 1). The two longitudinal edges are tangentially extended to create two symmetric ruled surface sections, from now on referred to as the 'flanges'.

The undeformed geometry is parameterized by the width of the flanges, w, the longitudinal - and transverse radius, $r_{l,0}$ and $r_{t,0}$ and the associated longitudinal - and transverse subtended angles, $\theta_{l,0}$ and $\theta_{t,0}$, that determine the overall length of the structure and the initial angle between the flanges respectively. Variables t_c and t_f denote the crease - and flange thickness respectively. The radius of the circular boundary between the crease - and flange sections is assumed to be equal to $r_{l,0}$ since $\frac{r_{t,0}}{r_{l,0}}$ is designed to be small.

B. Deformation process: initiating a transition region

A characteristic property of this group of shell structures is the existence of a second stable, though non-zero energy, configuration, from hereon referred to as the 'inverted state'.
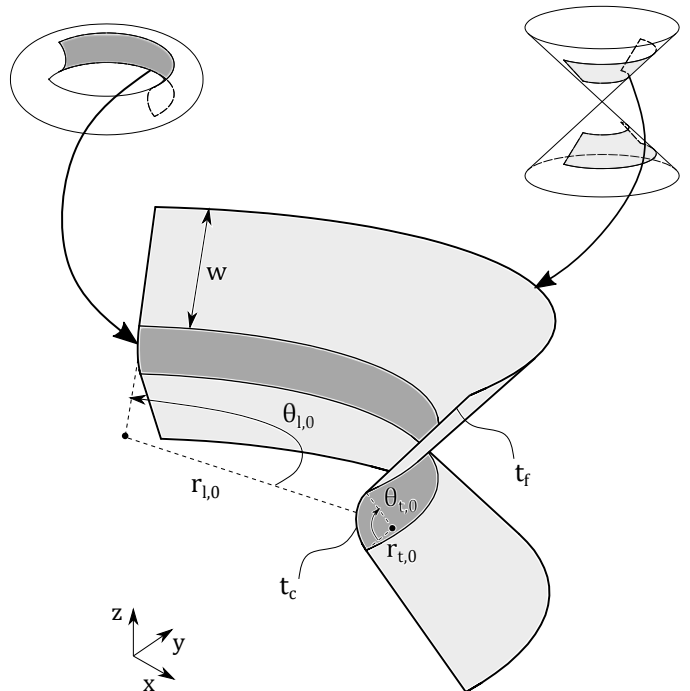

Fig. 1. The geometry of the shell structure is composed of a torus surface section with negative Gaussian curvature and two developable cone surface sections with zero Gaussian curvature. The design parameters that define the undeformed geometry are depicted.

Bi-stable behavior of similar compliant shells, both with and without Gaussian curvature, is discussed in the context of laminated composites [19]–[22]. In this research, so-called 'slit tubes' form either positive - or negative barrel-shaped coils at their second equilibrium configuration when a positive - or negative longitudinal curvature is applied respectively. The shell structure that forms the basis of this research differentiates itself by its material isotropy, yet shows resemblance regarding its mechanical behavior.

A practically feasible method to obtain the second stable configuration involves the introduction and propagation of a *transition region* (figure 2, top). It is initiated when the flanges at one end of the structure are rotated with respect to each other until the previously opposing faces point away from each other (1). A comprehensive description of this process is given in prior research by the authors [18]. The emerging transition region is characterized by high localized strains, predominantly present in the flanges. Its location s is defined as the normalized location of the inflection point along the symmetry line, or 'spine'. Its formation can be considered as the required pre-stressing part of the deformation process or, analogue to chemical reactions, as the activation energy required to initiate a sequence of events. The associated energy is referred to as the 'transition energy' and characterized by a steep energy increase with respect to variable s. Preliminary numerical analysis resulted in the schematic plots of figure 2.

As the transition region is propagated in the longitudinal direction, the structure is progressively inverted (2). With resemblance to tape loop behavior, the transition region geometry and associated transition energy are roughly preserved
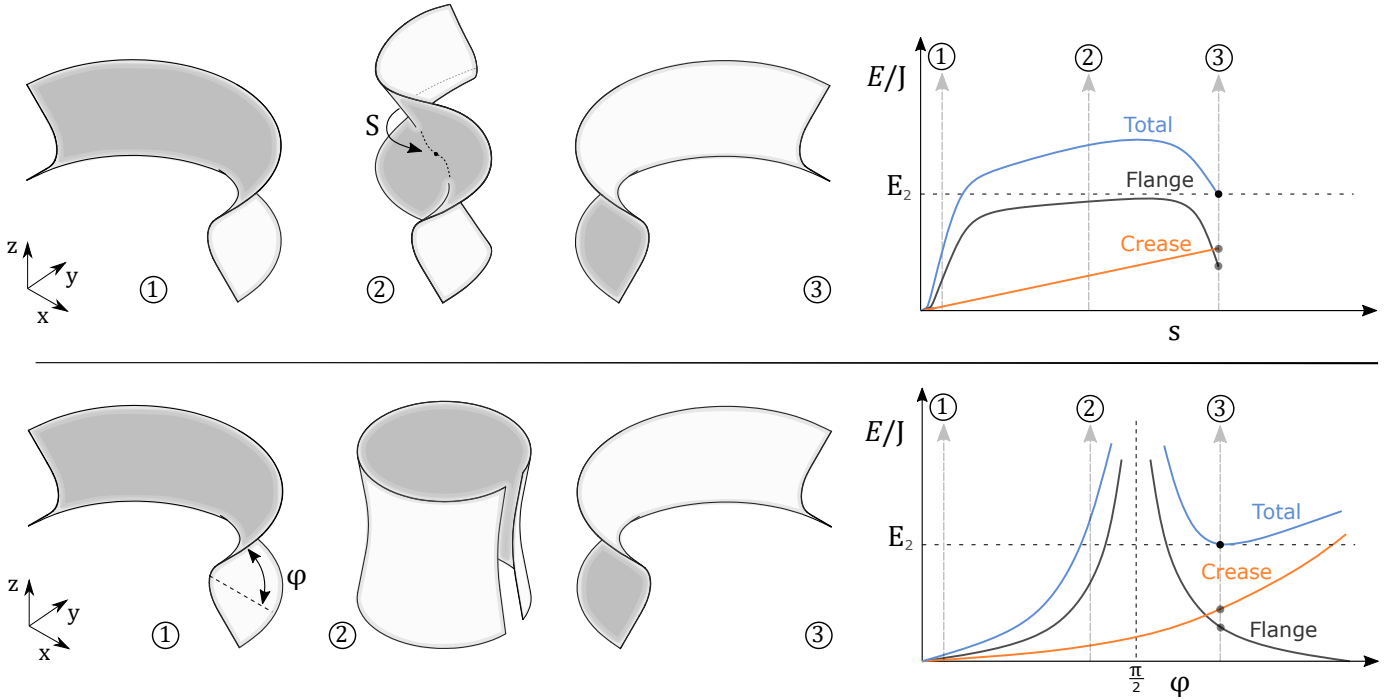
Fig. 2. The inverted state can be obtained in practice by initiation of a transition region (top). Its location is defined as the location of the inflection point of the spine, annotated by the normalized dimensionless distance s along the spine of the shell structure. The deformation process is depicted in step (1)-(3) and a schematic energy plot gives an impression of the energetic state throughout transition. The existence of an inverted stable equilibrium can also be shown by relating the elastic energy to the inclination angle φ of the flanges (bottom) where the energetic paths are plotted based on the analytical expressions from eq. 15-17. Note that, although the deformation paths are fundamentally different, the end states (3) and associated energy levels E_2 can not be distinguished.

along its way. However, an increasing part of the crease section is deformed, accounting for an approximately linear energy increase in the succeeding part of the transition. Edge effects allow the transition energy to gradually decrease to zero towards the end (elaborated in prior research by the authors [18]), leaving behind the structure in its inverted, non-zero energy state (3).

C. An analytical approach

1) Inextensibility and shell assumptions: In this section, the geometry is assumed to be inextensional, which is valid for thin shells whereby the energy required for in-plane stretching is orders of magnitude higher then for bending [23]. As a result of this assumption, Gaussian curvature remains invariant upon deformation and kinematic relations can be approximated. A second assumption is that circular cross-sections remain circular during the application of a load. Both these conditions enable an analytical approach to the mechanics of the shell structure. As an attempt to give the reader a natural understanding of its mechanical properties, an alternative deformation process is described that predicts the same bi-stable behavior.

2) Kinematic coupling: The flanges can be considered as surface segments of a cone and are therefore developable, meaning one of the two principal curvatures equals zero, i.e. they have zero Gaussian curvature. The toroidal section that connects the flanges can be regarded as a curved crease of circular cross-section. Because of its curved nature, actuation

by varying the angle φ also results in deformation of the compliant flanges. Following the inextensibility assumptions, the kinematic relationship between the constitutive elements can be approximated.

Variation of the generalized coordinate φ results in a geometric change of both the crease and the flanges (figure 3(a) and 3(b)), where the following relation applies to the undeformed geometry:

$$\varphi_0 = \frac{\pi - \theta_{t,0}}{2}. \tag{1}$$

The transverse radius and associated curvature of the crease are directly linked to the angular deflection between the flanges via conservation of the arc length, according to:

$$r_t = \frac{\theta_{t,0}\, r_{t,0}}{\pi - 2\varphi} \tag{2}$$

$$\kappa_t = \frac{1}{r_t} = \frac{\pi - 2\varphi}{\theta_{t,0}\, r_{t,0}}. \tag{3}$$

Substitution of eq. 1 in eq. 2 results in the initial transverse radius $r_{t,0}$.

The longitudinal radius of curvature r_l follows from the inextensibility assumption and can be analytically derived by projecting the flange geometry on a cone with variable pitch (figure 3(b)). The kinematic relation between the flange angle φ and longitudinal radius of the crease r_l is calculated via the invariant distance r_i:

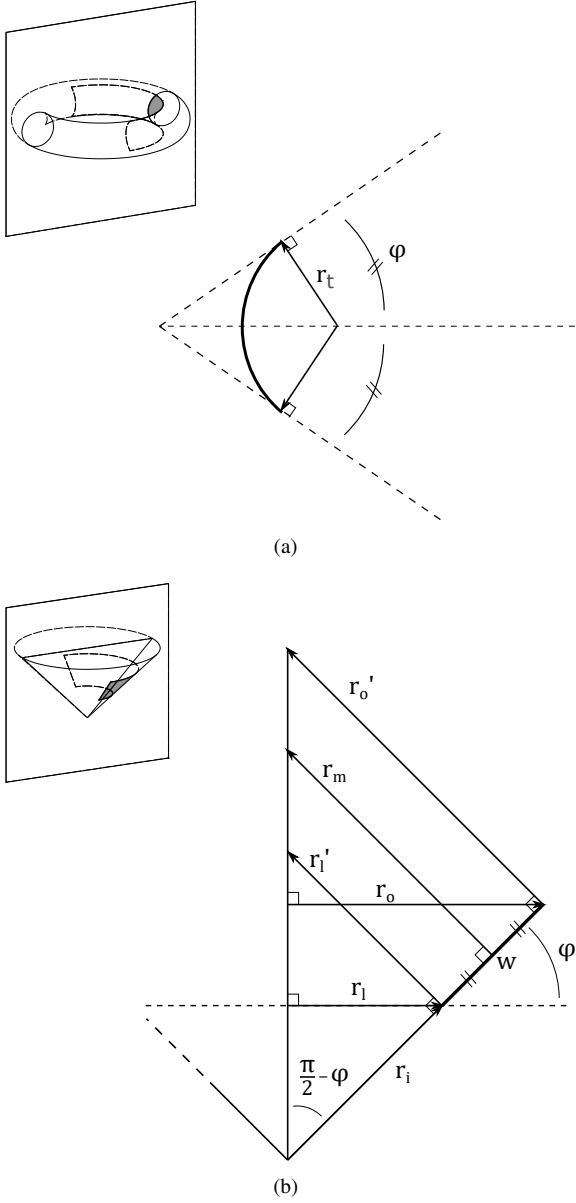$$r_i = \frac{r_{l,0}}{\cos\left(\frac{\pi - \theta_{t,0}}{2}\right)} \tag{4}$$

(a)

(b)

Fig. 3. A cross-section of the torus (a) and cone (b) shows the kinematic relationship between the crease and flange geometry. The flange angle φ is considered as the generalized coordinate.

$$r_1 = r_i \cos(\varphi), \tag{5}$$

where substitution of eq. 1 in eq. 5 results in the initial longitudinal radius $r_{1,0}$. The longitudinal curvature change of the crease section is omitted for simplicity, since it is designed to be small compared to κ_t.

The curvature of the cone-shaped flanges is approximated as the average of the surface curvature along the most inner - and outer perimeter with radius r_1 and r_o respectively, via calculation of their local radius of *surface* curvature, according to:

$$r_1' = \frac{r_1}{\sin(\varphi)} \tag{6}$$

$$r_o' = r_1' + \frac{w}{\tan(\varphi)} \tag{7}$$

$$r_m = \frac{r_1' + r_o'}{2} \tag{8}$$

$$\kappa_m = \frac{1}{r_m}. \tag{9}$$

The curvature change of all elements is then given by the difference between the curvature of the undeformed and the deformed geometry, as:

$$\Delta\kappa_t = \kappa_t(\varphi) - \kappa_t(\varphi_0) \tag{10}$$

$$\Delta\kappa_m = \kappa_m(\varphi) - \kappa_m(\varphi_0). \tag{11}$$

3) Elastic energy relations: The energy associated with elastic deformation that follows a linear material law is given by [23]:

$$\mathcal{E} = \frac{1}{2} \int_A \begin{bmatrix} \boldsymbol{\gamma} \\ \Delta\boldsymbol{\kappa} \end{bmatrix}^{\mathrm{T}} \begin{bmatrix} \mathbf{A} & \mathbf{B} \\ \mathbf{B} & \mathbf{D} \end{bmatrix} \begin{bmatrix} \boldsymbol{\gamma} \\ \Delta\boldsymbol{\kappa} \end{bmatrix} dA, \tag{12}$$

where $\boldsymbol{\gamma}$ and $\Delta\boldsymbol{\kappa}$ denote the membrane stretch and curvature *change* vectors respectively that are related to the energy $\mathcal{E}$ via the ABD-matrix and surface area A. For thin shells that meet the inextensibility condition, no stretching of the mid-plane is assumed, i.e. $\boldsymbol{\gamma} = 0$. Evaluating the elastic energy per longitudinal radial unit length of shells with initial curvature, this simplifies to:

$$\frac{\mathcal{E}}{\theta_{l,0}} = \mathcal{E}' = \frac{1}{2} \int_S \Delta\boldsymbol{\kappa}^{\mathrm{T}} \mathbf{D} \Delta\boldsymbol{\kappa} \, dS, \tag{13}$$

where length unit S denotes either the arc length of the circular crease cross-section or the width w of the flanges. Matrix $\boldsymbol{D}$ contains the local material properties in accordance with [23]:

$$\boldsymbol{D} = \frac{Et^3}{12(1-v^2)} \begin{bmatrix} 1 & v & 0 \\ v & 1 & 0 \\ 0 & 0 & \frac{1-v}{2} \end{bmatrix}. \tag{14}$$

When the elastic energy of the curved crease section is superimposed on the elastic energy of the flanges, the total energy follows from the sum of its individual components:

$$\mathcal{E}_c' = \frac{1}{2} \mathbf{D}_{c,(1,1)} \, \Delta\kappa_t^2 \, \theta_{t,0} \, r_{t,0} \, r_{1,0} \tag{15}$$

$$\mathcal{E}_f' = \frac{1}{2} \mathbf{D}_{f,(1,1)} \, \Delta\kappa_m^2 \, (wr_{1,0} + \frac{1}{2}w^2) \tag{16}$$

$$\mathcal{E}_{\mathrm{tot}}' = \mathcal{E}_c' + 2 \, \mathcal{E}_f', \tag{17}$$

with subscript 'c' and 'f' denoting the (material) properties of the crease and the flanges respectively. The bottom right of figure 2 shows a schematic plot of the energy paths, described by equation 15, 16 and 17 for a geometry with initially parallel flanges (i.e. $\varphi_0 = 0$). According to equation 4, 5, 7-10 and 16, the flange energy follows a $\tan(\varphi)^2$ trajectory and shows

symmetric behavior around the asymptote $\varphi = \pi/2$. Energy approaches infinity when $\varphi = \pi/2$, before showing a decrease in energy for values of $\varphi > \pi/2$. The transverse component of the crease energy follows a quadratic increase (equation 3, 10 and 15). Together, this predicts the theoretical existence of a second stable, though non-zero energy configuration: the inverted state. At this local energy minimum, the tendency of the flanges to flatten opposes the tendency of the crease towards its as-fabricated state, resulting in static balance. However, approaching the inverted state by this deformation process is not possible in practice since it requires a configuration with infinite strain energy.

The two discussed energetic paths required to obtain the second stable state (figure 2) are fundamentally different, yet the final configurations (3) can not be distinguished from each other.

III. METHODS

A. Conceptual approach

The energetic path obtained during propagation of the transition region is the result of a complex interplay between the various elements in the structure and is ultimately determined by the design parameters. A stiff crease, either caused by a small transverse radius or relatively large thickness, results in a more pronounced energy increase during propagation of the transition region, as illustrated in figure 2. Since this effect negatively influences neutrally stable transition, a logical approach would be to minimize the crease stiffness.

Figure 4 shows the schematic energy profile (blue) of a standard (dashed) and a desired geometry (solid). Both cases feature a loading region that can be considered as the pre-stressing action, which is required for neutral stability to occur [12]. In case of the standard geometry, it is followed by a significant region dominated by crease energy increase and ends with an unloading region, that leaves the structure in its inverted state. Prior research by the authors [18] has shown that the energetic contribution of the flanges (black) during propagation of the transition region is tune-able to a high extend. This gives rise to the possibility to compensate for the increasing crease energy (orange) during transition by manipulation of the local properties of the flanges. Specifically, it requires an approximately linear decrease of the flange energy component with equal slope of opposite sign.

Several methods have shown to be effective for manipulating the local energy storage in the flanges [18]. In this investigation, a material thickness variation in longitudinal direction is applied to the flanges, while maintaining a constant, sufficiently small, material thickness of the crease. The rationale behind this choice will be elucidated in the subsequent sections.

B. Numerical simulation

1) Model setup:
The shell structure is modelled according to the Kirchhoff-Love plate theorem and a linear isotropic elastic constitutive law is applied to describe its elastic behavior. An isogeometric framework forms the basis of the numerical analysis, whereby the geometry is described using B-splines
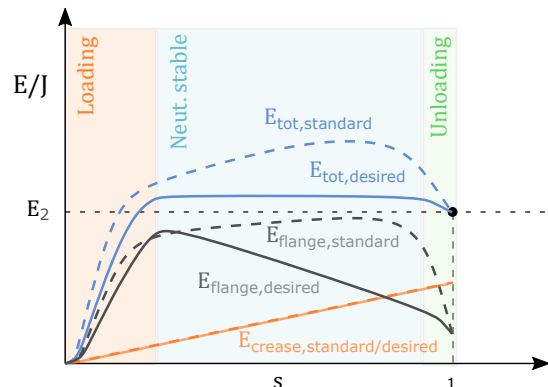

Fig. 4. A schematic representation of the energy curves belonging to the constitutive parts during transition. The dashed and solid lines represent the standard and desired, i.e. neutrally stable, geometry respectively.

[24]. A Newton-Raphson numerical integration scheme is used to solve for the static equilibrium configurations.

The control points that define the B-splines are placed in the transverse (u)- and longitudinal (v) direction of the shell structure to create a two-dimensional grid of control points (figure 5). Unequal spacing is used in the u-direction, where a higher model accuracy is obtained in the curved-crease region. The geometry is defined by $m = 35$ control points in the u-direction (of which 17 to describe the curved crease region) and $n = 56$ equally spaced control points in the v-direction.

Two geometric variants of the structure are chosen for investigation by setting either a small or a large crease radius $r_{t,0}$, resulting in lumped compliance with a distinctive crease (e.g. an origami mechanism) or distributed compliance respectively. Other design variables and material properties used for modelling are denoted in table I. Note that not all design parameters are constant throughout the structure, since the flange thickness is allowed to vary in the longitudinal direction, as $t_f = t_f(v)$.

2) Modelling the transition:
The transition is initiated when a transition region forms and an inflection point develops along the spine curve. An effective way to achieve this involved modelling the inverted state by estimating its inverted-state geometry and numerically solving for its closest equilibrium configuration. From here, two opposing flange ends are rotated back to their original configuration, while constraining the *opposing* half of the control points on the edge the in vertical(z)-direction (detailed description in supplementary material, B.1). Finally, equilibrium is maintained by releasing all but one set of edge constraints that imposes a fixed constraint distance d_c between two symmetrically located control points on opposite edges, denoted as the ith set of control points in v-direction (figure 5). It is located sufficiently close but behind the inflection point expressed as its location s along the spine.

The location of the transition region can indirectly be controlled by imposing the constraint to subsequent sets of control points along the edge in positive v-direction towards the opposite end. To ensure effective propagation, d_c is chosen to be equal to the maximum distance between the control points on opposite edges of the inverted state (elucidated in
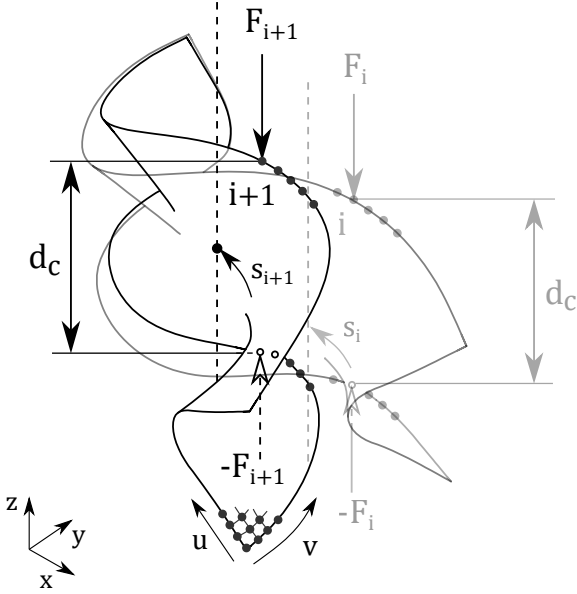
Fig. 5. Material directions u and v generate the two dimensional grid of control points. The transition is modelled by the application of a constraint on the distance d_c between the ith set of two opposing control points on the edges of the shell. F_i and F_{i+1} represent the reaction forces that belong to two consecutive steps. Distance d_c remains constant throughout the transition.

Parameter	Value	Unit
Geometry		
$r_{t,0}$	$0.01, 0.035$	m
$r_{l,0}$	0.1	m
$\theta_{t,0}$	$\frac{\pi}{2}$	rad
$\theta_{l,0}$	π	rad
w	0.4	m
t_c	$4e^{-4}$	m
t_f	$(a\frac{v}{n} + t_{f,0})$	m
m	35	-
n	56	-
Material		
E	$1.8e^9$	$\frac{\text{N}}{\text{m}^2}$
ν	0.4	-
Optimization		
$\boldsymbol{x}$	$[a \quad t_{f,0}]$	m
$\boldsymbol{x}_{0, r_{t_0}=0.01}$	$[0 \quad 1.6e^{-3}]$	m
$\boldsymbol{x}_{0, r_{t_0}=0.035}$	$[0 \quad 8e^{-4}]$	m
$\boldsymbol{x}_{\min}$	$[0 \quad 3e^{-4}]$	m
x_{tol}	$1e^{-6}$	m
i	$\frac{n}{4} < i < \frac{3n}{4}$	-
d_c	$0.045, 0.060$	m

supplementary material, B.1). The location of the transition region can be controlled as long as its tendency exists to return to its original position, which is characterized by a positive constraining force F_i. Consequently, when the force required to maintain equilibrium equals zero, neutrally stable transition is obtained.

Apart from spatial fixation to prevent rigid body translation and - rotation, no clamped boundary conditions are applied during the modelling of the structure. This enables the analysis of a free shell and allows for the edge effects to be studied.

3) Optimization procedure: During optimization, the geometry is varied in the search for a unique combination of design parameters, i.e. the optimization variables, that minimizes the effort required for transition, i.e. the objective function.

Implementing a thickness variation over the flanges as a variable design parameter allows for fixed coordinates of the control points during variation of the optimization variables. This ensures consistent results from the constraint choice and decreases computing time (detailed description in supplementary material, B.1). The simplest continuous thickness variation can be described by a constant gradient and is chosen as initial strategy, according to:

$$t_f(v) = a\,\frac{v}{n} + t_{f,0}, \tag{18}$$

where v is a discrete value that denotes the vth set of m control points. This choice requires only two optimization variables:

$$\boldsymbol{x} = [a \quad t_{f,0}]. \tag{19}$$

To promote the existence of a transition region, the optimization window is chosen such that the transition region is located sufficiently far away from the edges, while still

including a significant part of the transition. It is achieved by application of the constraint within boundaries that span the middle half of the structure, given by the interval:

$$\frac{n}{4} < i < \frac{3n}{4}. \tag{20}$$

The objective function in this optimization problem is defined as the sum of all encountered constraining forces, as:

$$f(\boldsymbol{x}) = \sum_{i=\frac{n}{4}}^{\frac{3n}{4}} |F_i|. \tag{21}$$

Note that this value is no measure for the amount of work done since the movement direction of the constraint is perpendicular to its reaction force. Though, it becomes zero when neutral stability is obtained.

Minimizing the value of the objective function is the goal of the optimization procedure. The function *fmincon* from the Matlab®*Optimization toolbox* is employed. The optimization procedure is interrupted when the difference between two consecutive steps of either of the two objective variables is within the predetermined tolerance $x_{\text{tol}} \leq 1e^{-6}$. To ensure a material thickness above a feasible limit, a lower bound is set on the objective variables, defined by $x_{\min}$. Two optimization runs are performed, i.e. one for each variation of $r_{t,0}$. The initial values for the optimization variables, $\boldsymbol{x}_0$, are denoted in table I.

4) Prototype fabrication: An accessible manufacturing method, able to deal with the double-curved geometry and variable shell thickness, is 3D-printing. Multi jet fusion is a suitable printing technique that provides respectable material homogeneity, enables material thickness down to the tenth-of-a-millimeter scale and allows for processing of materials with

TABLE II
DETAILS ON THE 3D-PRINTING PROCESS

Parameter	Value	Unit
Material (PA-12)		
Tensile strength (XY)	$48e^6$	$\frac{N}{m^2}$
Tensile strength (Z)	$48e^6$	$\frac{N}{m^2}$
E (XY)	$1.7e^9$	$\frac{N}{m^2}$
E (Z)	$1.8e^9$	$\frac{N}{m^2}$
Process		
Accuracy	0.3	%
Layer thickness	0.08	mm

TABLE III
OPTIMIZED RESULTS FOR THE OPTIMIZATION VARIABLES

| Parameter	Value	Unit
$x_{r_{t_0}=0.01}$	$[1.3411e^{-3} \quad 8.3703e^{-4}]$	m
$x_{r_{t_0}=0.035}$	$[9.5574e^{-4} \quad 3.1856e^{-4}]$	m

Fig. 6. The experimental setup used to mimic the simulated conditions during transition of the shell. The measurement frame (1) holds the force sensor (2) with primary contact point (3) and the secondary contact point (4). The prototype is clamped between the contact points at a known distance d_c, thereby mimicking the simulations.

sufficient elasticity (i.e. high yield strength with respect to E-modulus). The prototypes were constructed out of PA-12 with material properties denoted in table II.

Printing orientation determines material homogeneity to a large extent, especially in regions of low thickness. To mitigate the resulting effects, printing orientation is chosen such that the printing layers are oriented parallel to the horizontal construction(xy)-plane, ensuring layer cross-sections with a consistent line-like appearance.

C. Experimental validation

1) Measurement setup: To verify the simulated results, a measurement setup is designed that mimics the modelled conditions (figure 6). A measurement frame (1) with two contact points formed by grooved rollers (3,4) serves as the constraint. Rolling is prevented by brake screws and position is maintained by friction between the prototype's edges and the roller surfaces. The distance d_c between the contact points is adjustable and chosen to match the simulated conditions corresponding to each prototype. A $9N$ miniature S-beam load cell (Futek LSB200) is connected to the upper contact point with its measurement axis in line with the direction of the two contact points. Vertical orientation of this axis enables elastic reaction forces to be measured while excluding gravitational forces. The force signal is processed by a signal conditioner (Scaime CPJ2S) before fed into a acquisition module (NI USB-6008).

After manual initiation of a transition region, the specimen is clamped between the contact points at a discrete location x_c along the edge with intervals of $l_{edge}/10$ and moved manually through the measurement setup. Sliding motion as a result of the parallel component of the reaction force is prevented by friction. The measured force can be directly compared to the constraint force obtained from the model.
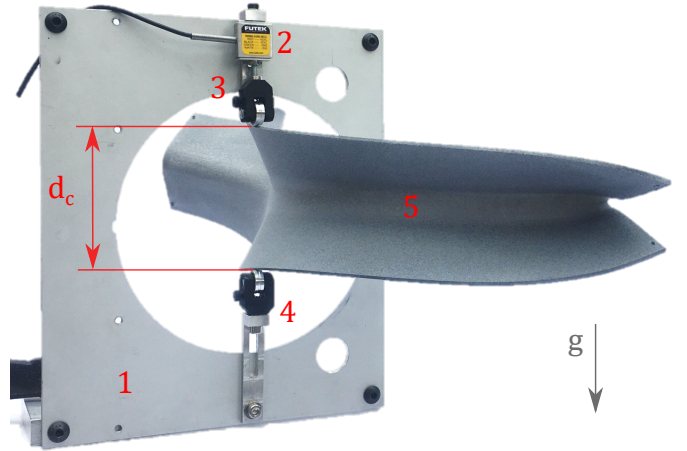
IV. RESULTS

A. Simulation results

This section presents the results of two successful optimization runs that were limited by the convergence criterion of $x_{tol} = 1e^{-6}$m on the optimization variables. Figure 7 shows the energetic paths of the two optimized geometries during transition on the beginning and end of the optimization window, denoted with (1) and (2) respectively. Values are plotted with respect to the location of the inflection point s (not to be mistaken with the constraint location x_c). The separate energy contributions of the flange - and crease sections (distinguished by shading in figure 1) are indicated by the intermittent lines. Only data points are plotted for configurations that featured an inflection point along the spine, accounting for the abrupt ends.

The optimization procedure resulted in an energy variation of less than 4% and 2% of its average within the optimization window for $r_{t_0=0.01}$ and $r_{t_0=0.035}$ respectively. The optimized design variables are presented in table III and the resulting optimized flange thickness gradient t_f along the v-direction is depicted in figure 8. The deformation process is shown in figure 9, where also the volumetric strains are indicated.

Figure 10 shows the reaction forces required to maintain equilibrium during transition. Results for $x = x_0$ (i.e. prior to optimization) are represented for comparison by the dashed lines while the solid lines denote the optimized results. Data points are solely available for configurations where an inflection point on the spine could be localized, resulting in the seemingly abrupt beginning and ending of the plots.

B. Experimental results

Measurements on the dimensions revealed a disparity between the digital models and the physical, 3D-printed prototypes. Because of the small dimensions on material thickness, deviations easily cause large relative differences. In combination with the cubic relation between material thickness
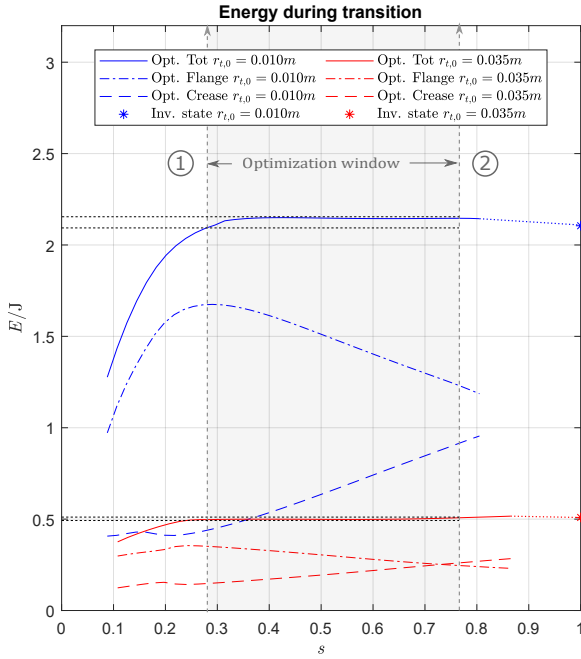
Fig. 7. The resulting energy paths of the two optimization runs, with respect to the location of the inflection point, s, during propagation of the transition region are depicted. The vertical dashed lines, denoted with (1) and (2) represent the optimization window, i.e. the interval wherein the objective function (eq. 21) is defined. The horizontal dashed lines illustrate the energy variation and the markers denote the energy level of the fully inverted state. Individual flange - and crease components are plotted by the intermittent lines.
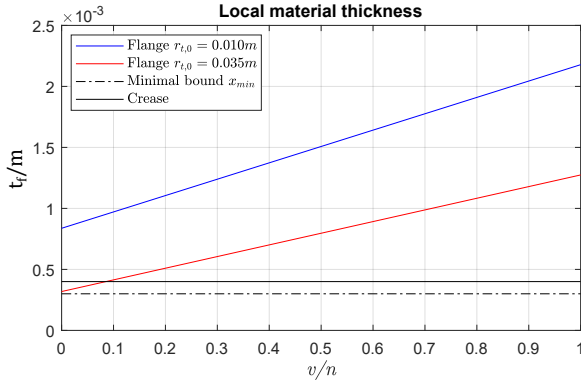
Fig. 8. The optimized local thickness variation $t_f(v)$ of both structures. The crease thickness t_c is constant and equal in both variants. The dash-dotted line represents the optimization minimal bound.
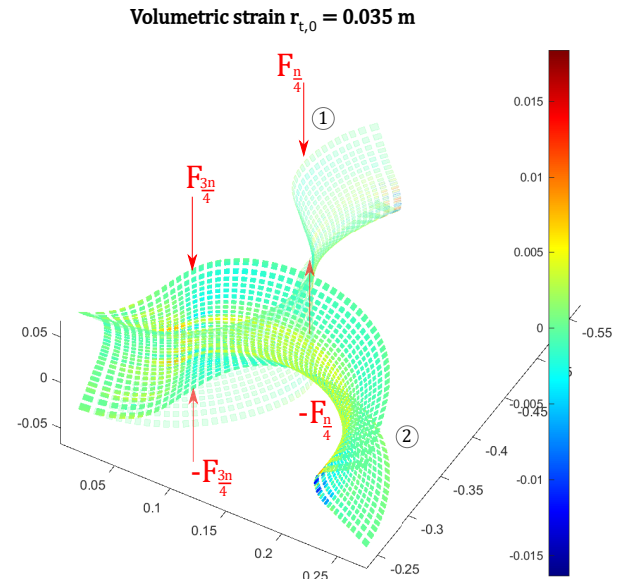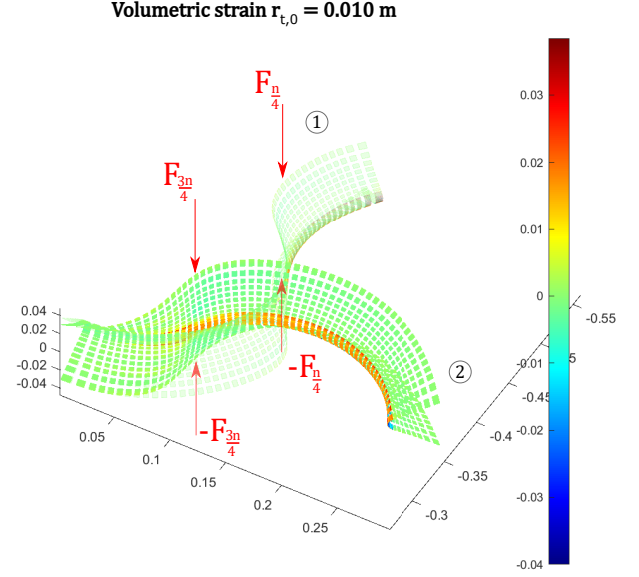

Fig. 9. The deformation process during transition and associated volumetric strains, belonging to configurations at the beginning (opaque) and end (translucent) of the optimization window, denoted with (1) and (2) in figure 7 respectively.

and associated elastic energy, behavior is expected to be most sensitive to this metric. Measurements taken along the circumference of both prototypes show that differences as high as 50% occurred (figure 11).

Figure 10 also shows the measurement results of the reaction forces of both prototypes, required to maintain equilibrium throughout the transition process. For comparison, simulated results that are corrected for measured thickness are presented as dashed-dotted lines. Measurement range was limited by the force transducer, causing reaction forces above $20N$ not to be measured with the current setup. The markers represent

the upper and lower measurement bounds, following from measurements taken in a loading or unloading direction respectively. Zero force measurements (i.e. when contact loss occurred) are denoted with circles. The gray area contains all possible encountered measurements, independent of approach direction and indicates the visco-elastic behavior and hysteresis of the material. Measurements from where 'self propagation' occurred correspond to a negative constraining force and are therefore discarded.

Reaction force $r_{t,0} = 0.010m$

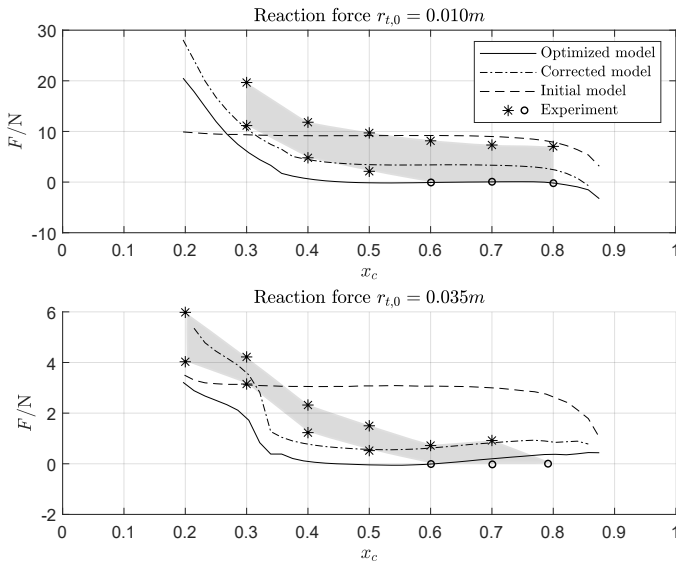
Reaction force $r_{t,0} = 0.035m$

Fig. 10. Experimental results of the reaction forces required to maintain equilibrium are depicted by their upper and lower boundaries (markers), corresponding to the loading and unloading directions respectively. Optimized modelled results are presented by the solid lines and the modelled results, compensated for the prototype thickness, are depicted as dashed-dotted lines. The reaction forces that belong to the starting parameters of the optimization procedure x_0 are represented by the dashed lines.
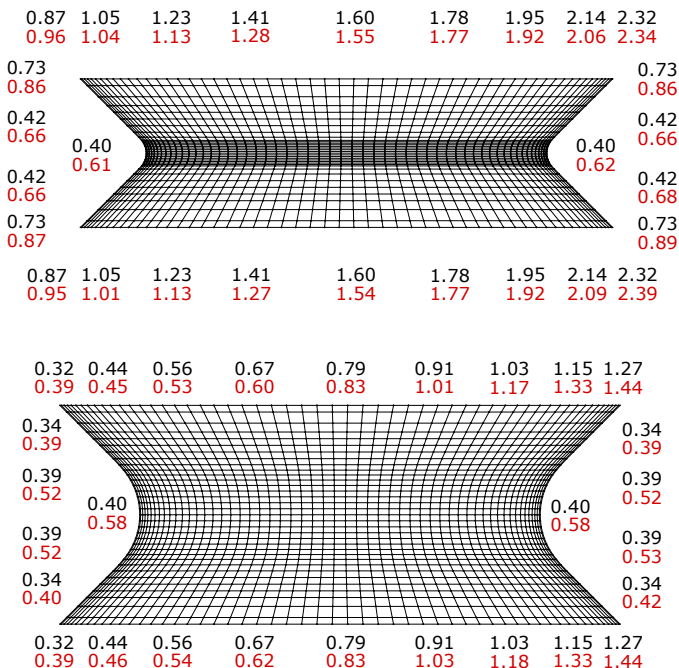

Fig. 11. Measurements on the local thickness of the two prototypes (red) is compared to the local thickness of the optimized modelled geometry (black). Measurements are only performed on the accessible perimeter of the shells.

V. DISCUSSION

A. Numerical results

The typical behavior during deformation of a compliant shell is a result of complex interplay between all parts of its structure. However, an intuitive approach, whereby several sub-functions are attributed to separate parts, turned out to be effective during investigation of this particular type of struc-

ture. The optimization procedure resulted in behavior similar to the intuitive prediction (figure 4), whereby a distinctive loading phase could be identified and the energy increase of the crease region during transition indeed approximates the expected linear course. To compensate, the flanges provide the opposite characteristic, whereby superposition results in a constant energy level, indicating neutral stability. From this perspective, the crease and the flanges can be considered as the load-carrying and compensating elements respectively, similar to the approach taken in most of the previously mentioned existing examples of neutrally stable shell structures [12].

A remarkable outcome is the apparent simplicity of the required optimization parameters, i.e. the linearly varying flange thickness, in order to produce results that approach this unique state of neutral stability very closely. A constant thickness gradient might initially sound as a sensible guess, but close inspection of equation 14 reveals a cubic relationship between the material thickness and associated deformation energy. So far, no profound explanation for this phenomenon has been thought of.

Most of the energy deviations within the optimization window occur around the window's borders, while the majority of the transition features a close-to-constant energy level. This could be explained by edge-effects and the inability of the constant thickness gradient to compensate for it.

Another notable feature of the resulting neutrally stable behavior is the energy level whereat it takes place. The objective function is designed to reduce the sum of the constraining forces to zero, creating an energy course with a derivative that approaches zero. No bounds were set to control the energy magnitude: this value is arbitrary. However, in both cases, this energy level matches the energy level of the inverted state closely, suggesting even a smooth transformation between the transition phase and the inverted state. This can indeed be experienced while handling the physical models. A possible explanation is continuity, which states that an abrupt behavioral change is unlikely to occur.

The shell in this investigation is considered to be 'free floating in space', i.e. no constraints are imposed on the structure's boundaries. However, when one would look at this structure as to have a clamped base and free end-effector, it can be regarded as a beam element that exhibits neutral stability in its bending degree of freedom. This lays the foundation for compliant building blocks with beam-like appearance and -kinematic behavior that are internally statically balanced.

B. Experimental results

Although the material thickness of the manufactured prototypes did not match the optimized results, neutrally stable behavior was experienced during the experiments. In figure 12, various stable configurations during transition from undeformed (1) to inverted (6) state are depicted. A possible explanation is internal friction of the material, responsible for the hysteresis loop in figure 10. Energy dissipation within the material enables no reaction force to be measured if the hysteresis band crosses the zero-force line. Although hardly noticeable, visco-elastic deformation towards a near stable
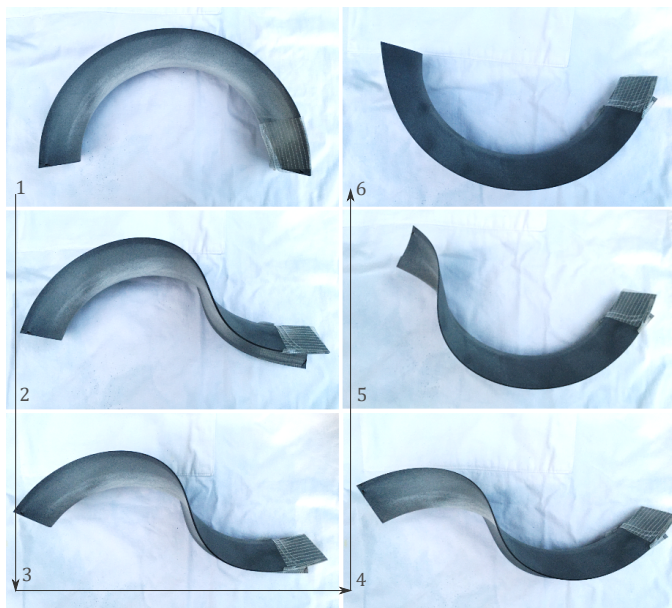
Fig. 12. Several stable configurations during transition from the undeformed (1) to the inverted (6) state. Although the modelled results do not predict stability, a continuous equilibrium was observed.

configuration presumably does occur, but on a different, imperceptible timescale. Dynamic analysis that takes into account the material visco-elasticity would capture this phenomenon.

Hysteresis loss is more notably present in the design that requires higher reaction forces, corresponding to $r_{t,0} = 0.01$m. Apart from a larger average thickness, this shell features higher stains during transition (figure 9) as a possible cause for higher energetic losses. Finally, gravity was not taken into account in the numerical analysis and, although the experimental setup avoids measuring weight, the presence of a gravitational field does effect the structure's geometry. However, this effect is assumed to be negligible compared to the effects caused by the elastic forces.

C. Future work

Development of the optimization process towards more accessible manufacturing methods is desired to increase its applicability. Prior research by the authors [18] has shown promising results in the optimization of geometric properties, e.g. local flange width and local longitudinal curvature, to influence the energetic path during transition. This allows for a structure with a uniform thickness that is not solely bound to a 3D-printing manufacturing process.

VI. CONCLUSION

In this investigation, the transition between the undeformed and inverted equilibrium configurations of a double-curved shell structure is analysed. The approach, that involved functional separation of the parts within this distributed compliant shell, turned out to be useful for the creation of a neutrally stable deformation mode. Optimization of the design parameters resulted in a constant energy level within a significant portion of transition. Therefore, we present a new type of

neutrally stable shell structure that, in contrast to examples in literature, does not rely on pre-stress obtained during the manufacturing process or boundary conditions to be imposed. Instead, it features neutral stability as part of a continuous deformation process, allowing a stress-free configuration to exist.

Successful optimization runs, based on a variable material thickness, resulted in shell structures with a significant near-constant-energy region as part of their transition. Ultimately, physical realization of 3D-printed prototypes validate the modelled results by featuring infinitely many equilibrium configurations along the deformation path. Remarkably, a constant thickness gradient of the flange sections over the length of the structure is sufficient for this unique behavior to occur. An explanation thereof is not yet given.

This shell structure can be considered as a beam element with a neutrally stable bending degree of freedom, laying the foundation for statically balanced compliant building blocks with a beam-like appearance and - kinematic behavior. However, despite the progress made, the variable material thickness throughout the structure limits the manufacturing method to 3D-printing. Other tactics to tune the behavior that allow for a uniform material thickness [18] could be investigated to facilitate manufacturing and applicability.

REFERENCES

[1] G. Radaelli and J. L. Herder, "Gravity balanced compliant shell mechanisms," *International Journal of Solids and Structures*, vol. 118-119, pp. 1339–1351, 2017. [Online]. Available: http://dx.doi.org/10.1016/j.ijsolstr.2017.04.021

[2] J. Herder and F. Van Den Berg, "Statically balanced compliant mechanisms (sbcmâs), an example and prospects," in *Proceedings of the 26th ASME DETC biennial, mechanisms and robotics conference*, 2000.

[3] J. A. Gallego, *Statically Balanced Compliant Mechanisms: Theory and Synthesis*, 2013. [Online]. Available: http://repository.tudelft.nl/view/ir/uuid:081e3d0e-173b-4a36-b8d6-c29c70eb7ae3/

[4] H. Alkisaei, "Statically Balanced Compliant Walls," Tech. Rep.

[5] G. Radaelli and J. L. Herder, "A monolithic compliant large-range gravity balancer," *2015 IFToMM World Congress Proceedings, IFToMM 2015*, 2015.

[6] M. R. Schultz, M. J. Hulse, P. N. Keller, and D. Turse, "Neutrally stable behavior in fiber-reinforced composite tape springs," *Composites Part A: Applied Science and Manufacturing*, vol. 39, no. 6, pp. 1012–1017, 2008.

[7] T. W. Murphey and S. Pellegrino, "A novel actuated composite tape-spring for deployable structures," *Collection of Technical Papers - AIAA/ASME/ASCE/AHS/ASC Structures, Structural Dynamics and Materials Conference*, vol. 1, pp. 260–270, 2004.

[8] X. Lachenal, P. M. Weaver, and S. Daynes, "Multi-stable composite twisting structure for morphing applications," *Proceedings of the Royal Society A: Mathematical, Physical and Engineering Sciences*, vol. 468, no. 2141, pp. 1230–1251, 2012.

[9] S. Daynes and P. M. Weaver, "Stiffness tailoring using prestress in adaptive composite structures," *Composite Structures*, vol. 106, pp. 282–287, 2013. [Online]. Available: http://dx.doi.org/10.1016/j.compstruct.2013.05.059

[10] X. Lachenal, S. Daynes, and P. M. Weaver, "A zero torsional stiffness twist morphing blade as a wind turbine load alleviation device," *Smart Materials and Structures*, vol. 22, no. 6, 2013.

[11] S. Daynes, X. Lachenal, and P. M. Weaver, "Concept for morphing airfoil with zero torsional stiffness," *Thin-Walled Structures*, vol. 94, pp. 129–134, 2015. [Online]. Available: http://dx.doi.org/10.1016/j.tws.2015.04.017

[12] S. Kok, "Literature review of occurrences and working principles of elastic neutral stability," Tech. Rep., 2020.

[13] S. Guest, "Zero stiffness elastic shell structures," vol. 6, no. 7, 2011.

[14] B. Doornenbal, "Zero stiffness composite shells: Using thermal pre-stress," Delft University of Technology, Tech. Rep. September, 2018.

[15] J. P. Stacey, M. P. O'Donnell, and M. Schenk, "Thermal Prestress in Composite Compliant Shell Mechanisms," *Journal of Mechanisms and Robotics*, vol. 11, no. 2, pp. 1–10, 2019.

[16] C. Vehar, S. Kota, and R. Dennis, "Closed-loop tape springs as fully compliant mechanisms -preliminary investigations," in *Proceedings of the ASME Design Engineering Technical Conference*, vol. 2 B, 2004, pp. 1023–1032.

[17] L. L. Howell, Ed., *Handbook of Compliant Mechanisms*. John Wiley & Sons Inc.

[18] S. Kok, G. Radaelli, and A. A. Nobaveh, "Neutrally stable transition of a multi-stable curved crease compliant shell structure," 2020.

[19] D. A. Galletly and S. D. Guest, "Bistable composite slit tubes. II. A shell model," *International Journal of Solids and Structures*, vol. 41, no. 16-17, pp. 4503–4516, 2004.

[20] G. P. Knott and A. Viquerat, "Modeling the Bistability of Laminated Composite Toroidal Slit Tubes," no. June, 2016.

[21] G. Knott and A. Viquerat, "Curved bistable composite slit tubes with positive Gaussian curvature," *AIAA Journal*, vol. 56, no. 4, pp. 1679–1688, 2018.

[22] G. Knott, "Helical bistable composite slit tubes," *Composite Structures*, vol. 207, no. May 2018, pp. 711–726, 2019. [Online]. Available: https://doi.org/10.1016/j.compstruct.2018.09.045

[23] C. Calladine, *Theory of shell structures*.

[24] T. J. Hughes, J. A. Cottrell, and Y. Bazilevs, "Isogeometric analysis: CAD, finite elements, NURBS, exact geometry and mesh refinement," *Computer Methods in Applied Mechanics and Engineering*, vol. 194, no. 39-41, pp. 4135–4195, 2005.

5

Paper IV: A constant-force curved-crease shell mechanism

Towards constant-force curved-crease compliant shell mechanisms

Sjaak Kok

Abstract—**Curved creases are characterized by the coupled facet deformation upon actuation. The forces exerted by the facets can be used to oppose the effects of crease stiffness during actuation to achieve an overall stiffness decrease. In this paper, a non-developable bi-stable shell structure with a torus-shaped curved crease and connected facets is investigated. An analytical approach, based on a combination of a pseudo-rigid-body model (PRBM) and plate theory, predicts the potential for constant-force actuation around its second stable, or 'inverted' state. The accuracy of the model is validated by numerical simulations. However, due to prototype inaccuracies, the experimental results do not feature the desired constant-force behavior. Nevertheless, a stiffness decrease, or 'softening' is experienced, verifying the concept and marking a first step towards statically balanced curved creases.**

I. INTRODUCTION

Constant-force generators are used for a variety of applications, but are arguably best recognised in the form of gravity balancers, where gravitational energy is exchanged with elastic energy and stored in spring elements. Herein, conventional rigid-link mechanisms [1], [2] and compliant mechanisms [3]–[5] can be distinguished, following the categorization of [6]. Compliant shell mechanisms form a group within the compliant mechanisms and are characterized by their potential for large deformations and highly non-linear behavior. This increases their applicability but simultaneously requires more challenging design methods [4].

Structures featuring a curved crease can also be considered compliant shell mechanisms [7]. Curved creases are widely discussed in the field of origami and enable the creation of more complex designs [8]. Where the classical art of origami typically focuses solely on the geometrical aspects, the field of origami engineering adds the interest into motion and forces. The kinematics of a curved-crease structure are especially interesting, since actuation of a curved crease requires deformation of the adjacent facets [9]. When the creases are a result of folding, i.e. plastic deformation, actuation of which is accompanied by a stiffness that prevents the deformed facets from flattening and, instead, equilibrium is settled and structural stiffness is obtained [10]. Other applications require crease actuation [9] and deploying [11], [12] and would potentially benefit from internally balanced creases to minimize actuation effort.

The goal of this paper is to develop a constant-force curved-crease shell mechanism by taking advantage of the facet deformation that occurs as a result of crease actuation. Literature exists wherein the interplay between crease stiffness and compliant facets is discussed [13], but only straight crease lines are assumed and facet deformation is a result of the boundary conditions applied. This study focuses on a non-developable compliant shell structure, featuring a torus-shaped curved crease and two extended cone-shaped facets (figure 1). An inverted configuration exists wherein the stiffness during crease actuation is decreased by the deformed facets, from hereon referred to as the 'flanges'. The study contains preliminary investigations to characterize this behavior and verify its potential for use as a constant force mechanism.

The methods section is subdivided into three parts, wherein an analytical, numerical and experimental approach are discussed. The results of all three approaches are presented in the results section and compared in the discussion, where an attempt is made to explain disparities between the outcomes.

II. METHODS

A. An analytical approach

1) Inextensional idealisation: The mechanical behavior of thin shells can be approximated by a inextensibility assumptions [14]. It states that stretching of the midsurface is unlikely to occur because the energy required overshadows the energy associated with bending of thin shells. As a result, the local *Gaussian curvature* of the shell surface, defined as the product of the two principal curvatures, remains invariant. Deformation of this type of shells can be approximated by bending only, but the result becomes less accurate when the applied boundary conditions require midsurface stretching, e.g. by the application of a 'twist'. The structure presented here only involves the conical bending deformation of developable surfaces that maintain zero Gaussian curvature throughout their deformation, justifying the inextensional approach.
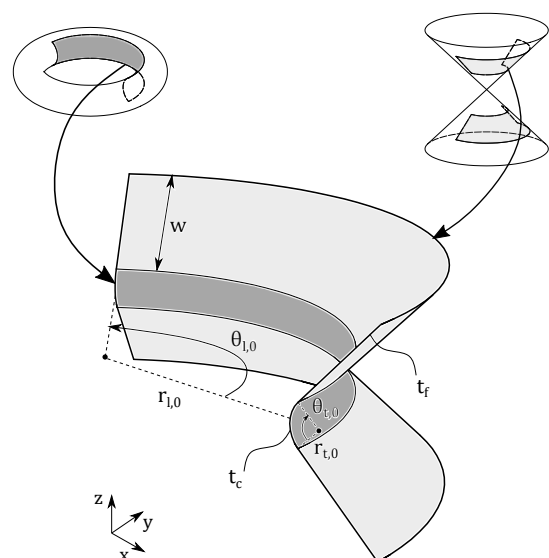

Fig. 1. The geometry of the investigated shell structure is composed of a torus surface section and two cone-shaped flanges. The design parameters that define the undeformed geometry are depicted.

2) Elastokinematic behavior: Kinematic coupling between the (curved) crease and the flanges enables this structure to be considered as a single-degree-of-freedom (1 DOF) mechanism, whereby actuation of the crease automatically results in deformation of the connected flanges. The angle between the flanges φ is chosen as generalized coordinate. The initial geometry is defined by the initial inclination angle between the flanges φ_0, the flange width w, the longitudinal radius $r_{l,0}$ and the transverse (crease) radius $r_{t,0}$. The overall size of the structure is determined by the longitudinal subtended angle $\theta_{l,0}$ (figure 1). In this investigation, a structure of unit length, i.e. $\theta_{l,0} = 1\mathrm{rad}$, is assumed and edge effects are excluded. The subtended crease angle $\theta_{t,0}$ is directly coupled to the initial inclination angle of the flanges, according to:

$$\varphi_0 = \frac{\pi - \theta_{t,0}}{2}. \tag{1}$$

A hybrid pseudo-rigid-body model (h-PRBM) is used to analytically approach the mechanical behavior. Therefore, the torus-shaped crease section, assumed to be of circular cross-section, is replaced by idealized, 1 DOF torsional springs with a stiffness k_c per unit crease length (figure 2). The longitudinal curvature change of the original crease section is hereby omitted and the inner perimeters of the flanges are assumed to coincide as a result of this approach.

Gaussian curvature of the flanges is assumed to remain zero throughout the deformation process as a result of the inextensibility condition, requiring one of the two principal curvatures to equal zero. This enables a geometric interpretation whereby the flanges are formed by surface segments of a cone of variable pitch (figure 3). The variable longitudinal radius r_l follows from crease actuation and can be approximated via the invariant distance vector r_i by:

$$r_i = \frac{r_{l,0}}{\cos\left(\frac{\pi - \theta_{t,0}}{2}\right)} \tag{2}$$

$$r_l = r_i \cos(\varphi). \tag{3}$$

The surface curvature, defined by the non-zero principal curvature, varies along the width, but can be approximated by the average curvature κ_m, that follows from the inner - and outer radius projections r_l' and r_o', as:

$$r_l' = \frac{r_l}{\sin(\varphi)} \tag{4}$$

$$r_o' = r_l' + \frac{w}{\tan(\varphi)} \tag{5}$$

$$r_m = \frac{r_l' + r_o'}{2} \tag{6}$$

$$\kappa_m = \frac{1}{r_m}. \tag{7}$$

The elastic energy associated with crease actuation is composed of two elements: (1) the energy required for the curvature change of the flanges and (2) the energy absorbed by the crease, represented by a torsional spring. Deformation
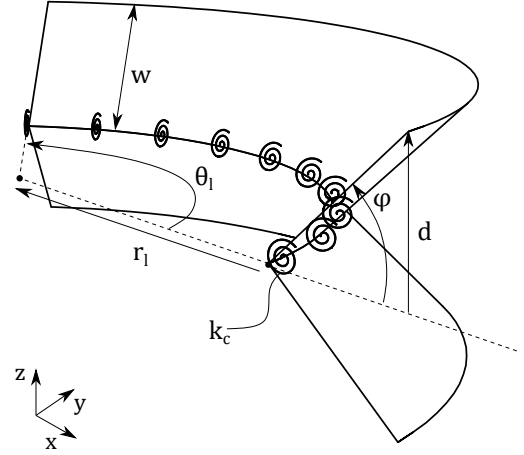

Fig. 2. The hybrid PRBM model with generalized coordinate φ and dependent dimensions.
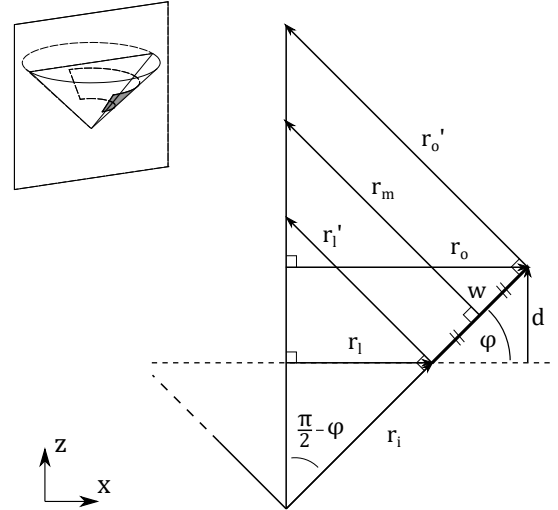

Fig. 3. The surface curvature of the cone segments can be estimated based on its cross-section dimensions.

of the flanges can be approximated by plate theory and a linear material law, where the associated energy is given by [14]:

$$\mathcal{E} = \frac{1}{2} \int_A \left[\begin{array}{c} \boldsymbol{\gamma} \\ \Delta\boldsymbol{\kappa} \end{array} \right]^{\mathrm{T}} \left[\begin{array}{cc} \mathbf{A} & \mathbf{B} \\ \mathbf{B} & \mathbf{D} \end{array} \right] \left[\begin{array}{c} \boldsymbol{\gamma} \\ \Delta\boldsymbol{\kappa} \end{array} \right] dA, \tag{8}$$

where $\boldsymbol{\gamma}$ and $\Delta\boldsymbol{\kappa}$ denote the membrane stretch and curvature *change* vectors respectively that are related to the energy $\mathcal{E}$ via the ABD-matrix and surface area A. With no midsurface stretching assumed, i.e. $\boldsymbol{\gamma} = 0$, this simplifies to:

$$\frac{\mathcal{E}}{\theta_{l,0}} = \mathcal{E}' = \frac{1}{2} \int_S \Delta\boldsymbol{\kappa}^{\mathrm{T}} \mathbf{D} \Delta\boldsymbol{\kappa} \, dS, \tag{9}$$

with variable S denoting the radial dimension and matrix D containing the material properties, according to:

$$\boldsymbol{D} = \frac{E t_f^3}{12\left(1 - v^2\right)} \left[\begin{array}{ccc} 1 & v & 0 \\ v & 1 & 0 \\ 0 & 0 & \frac{1-v}{2} \end{array} \right], \tag{10}$$

where E, ν and t_f denote the modulus of elasticity, the Poisson factor and material thickness of the flanges respectively. Variable vector $\Delta\kappa$ represents the curvature *change*, given by:

$$\Delta\boldsymbol{\kappa} = \begin{bmatrix} \Delta\kappa_\mathrm{m} \\ 0 \\ 0 \end{bmatrix} = \begin{bmatrix} \kappa_\mathrm{m}(\varphi) - \kappa_\mathrm{m}(\varphi_0) \\ 0 \\ 0 \end{bmatrix}. \quad (11)$$

This results in an expression for the energy of the two flanges per longitudinal radial unit length:

$$\mathcal{E}_\mathrm{f}' = 2 \cdot \frac{1}{2}\mathbf{D}_{(1,1)}\,\Delta\kappa_\mathrm{m}{}^2\,(w r_{\mathrm{l},0} + \frac{1}{2}w^2). \quad (12)$$

The torsional stiffness per radial unit length of the surrogate crease can be estimated by the properties of the original crease of circular cross-section, according to:

$$k_\mathrm{c} = \frac{E t_\mathrm{c}^3\,r_{\mathrm{l},0}}{12\,(1 - v^2)\,r_{\mathrm{t},0}}, \quad (13)$$

where t_c denotes crease thickness. This results in the following expression for the crease energy, expressed as function of the generalized coordinate φ:

$$\mathcal{E}_\mathrm{c}' = \frac{1}{2}\,k_\mathrm{c}\,(\Delta\varphi)^2. \quad (14)$$

3) Constant force: Equation 12 is of the form $\tan(\varphi)^2$ and shows asymptotic behavior around $\varphi = \pi/2 + k\,\pi$. The energy in the crease section is of order $O\left(\varphi^2\right)$ according to equation 14. Figure 4(a) shows the energy path for an arbitrary geometry with initially parallel flanges, i.e. $\varphi_0 = 0$. It predicts the theoretical existence of a second stable, though non-zero energy state, corresponding to the local energy minimum. In this stable 'inverted state', the tendency of the flanges to flatten opposes the tendency of the crease towards its as-fabricated state, resulting in static balance.

A translation of the angular generalized coordinate φ to the vertical distance d between the flange edge and the symmetry plane reveals approximately linear behavior in the energy domain. The derivative translates this into constant-force behavior within a specific region of the range of motion (figure 4(b) and 4(c)).

Several design parameters of the structure can be tuned to optimize the region of constant force. A change of initial inclination angle φ_0 or pre-stressed assembly cause a relative shift between the contributing elements. A change of $r_{\mathrm{t},0}$, w or material thickness t_c controls scaling of the contributing elements (further discussed in supplementary material section C.2). These design parameters are manually varied to create the desired constant-force behavior.

B. A numerical approach

1) Model setup: The shell is modelled in accordance with the Kirchhoff-Love plate theorem whereby a linear isotropic elastic constitutive law is applied. The numerical analysis is based on an isogeometric framework that makes use of B-splines to describe the geometry [15] and a Newton-Raphson numerical integration approach to solve for the equilibrium configurations. The control points that define the B-splines
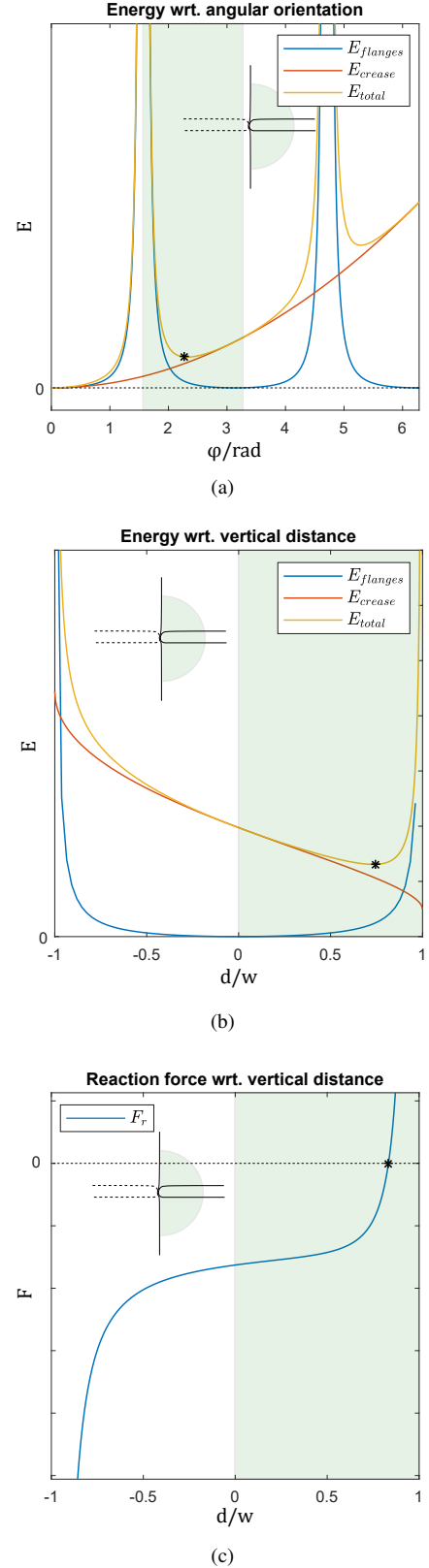

Fig. 4. A schematic representation of the energy path during actuation of the inverted curved-crease shell as a function of angular deflection (a) or vertical distance (b) where the local minimum corresponds to the inverted stable configuration. The reaction force (c) is equal to zero there, but also shows a region of near-constant force. The marker denotes the inverted equilibrium.

create a two-dimensional grid. For these simulations, a model with $m = 35$ control points in the transverse (u) direction and $n = 56$ control points in the longitudinal (v) direction of the shell structure is used.

2) Constraint application: An effective method for obtaining the inverted equilibrium of the shell structure is by estimating its inverted geometry and solving for its closest equilibrium configuration. Figure 5 depicts the initial (a) and the inverted (b) equilibrium configurations. To achieve crease actuation, all control points that describe the longitudinal edges are aligned parallel to the xy-plane. The distance between the sets of control points to the xy-plane, d, is incrementally decreased with a step size of $\Delta d = 1e^{-3}$m (c). The associated reaction forces are obtained.

3) Design optimization: Manual variation of the design parameters $\theta_{t,0}$, $r_{t,0}$, w and t_f resulted in a geometry with close-to-constant force behavior. Design parameters $\theta_{l,0}$, $r_{l,0}$ and t_c are fixed to bound the overall dimensions of the structure. Table I contains the values of the design parameters used for evaluation.

C. An experimental approach

1) Prototype fabrication: Due to the requirements on the material thickness, 3D-printing is chosen as a method for the fabrication of prototypes. Multi jet fusion is a 3D-printing technique that allows for small wall thicknesses while providing reasonable accuracy. The method provides sufficient material homogeneity and the printing material (PA-12) provides sufficient elasticity (i.e. high yield strength with respect to E-modulus). Prototypes are made on a $1:1$ scale, based on the optimized geometry discussed in section II-B.

2) Experimental setup: The modelled conditions are mimicked in an experimental environment, where a vertical distance is imposed between the shell edges (figure 6). Two identical shells (5) are brought into their inverted stable state and positioned between two parallel plates (1,2), such that the setup is axially symmetric. The top plate is connected via a force transducer (4), located in the axis of symmetry, to an end-effector (3), of which the vertical position can be controlled. Because of symmetry, no moments will be exerted on the plates, ensuring their parallel configuration to be maintained throughout vertical displacement.
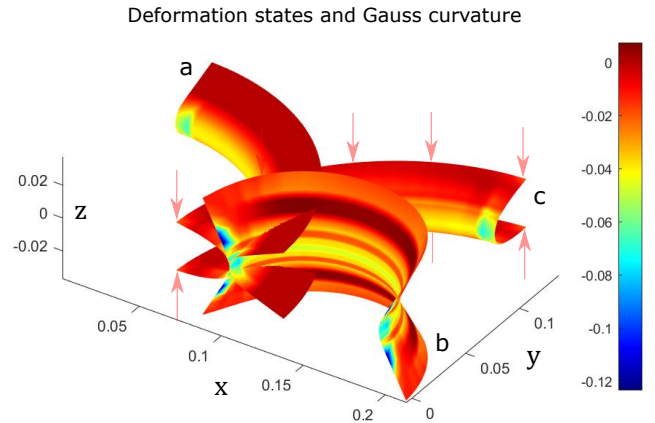

Fig. 5. Visualisation of the Gaussian curvature associated with the undeformed (a) and deformed (b,c) configurations. Note that the vertically compressed configuration (c) does not belong to the equilibrium configurations. Colors suggest little to no Gaussian curvature change during deformation, supporting the inextensibility assumption.

The signal from force transducer ($9N$ miniature S-beam load cell, Futek LSB200) is processed by a signal conditioner (Scaime CPJ2S) before fed into a acquisition module (NI USB-6008). Data is acquired with a sampling rate of 10Hz.

3) Measurement procedure: Prior to positioning in the test setup, the shell is brought into its inverted state. A method that involves the initiation of a transition region (elaborated in prior research by the authors [16]) allows the inverted state to be obtained while circumventing the infinite-energy configuration, depicted in figure 4(a). The measurement procedure starts after the two plates are brought in contact with the entire edges at a distance of $d = 60$mm. From there, vertical displacement is applied in the range 10mm $< d < 60$mm with a velocity of 400mm/min where the unloading phase directly succeeded the loading phase.

III. RESULTS

The reaction forces, estimated with the analytical model, are presented together with the numerical and experimental results in figure 7. Also depicted are the modelled results, corrected for the actual dimensions of the 3D-printed prototypes. Figure 5 simultaneously shows the Gaussian curvature of the undeformed (a), inverted stable (b) and maximally actuated (c) configurations.

IV. DISCUSSION

A. On the modelled results

Both the analytical and the numerical model predict the existence of a near-constant-force region. The required actuation forces are higher according to the numerical analysis, which could be explained by the longitudinal curvature change of the crease section, not accounted for in the analytical model. Also, the simplification of the flange curvature, i.e. approximate average instead of an exact integral, could contribute to this disparity.

TABLE I
DESIGN PARAMETERS USED FOR NUMERICAL EVALUATION

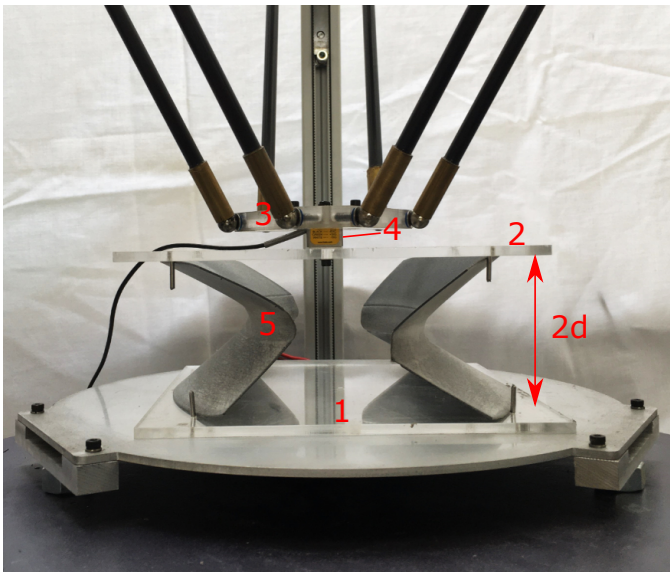| Parameter	Value	Unit
$\theta_{t,0}$	$\frac{\pi}{2}$	rad
$r_{t,0}$	0.01	m
$\theta_{l,0}$	1	rad
$r_{l,0}$	0.1	m
w	0.03	m
t_c	$4e^{-4}$	m
t_f	$8.5e^{-4}$	m
E	$1.8e^9$	$\frac{\text{N}}{\text{m}^2}$
ν	0.4	-

Fig. 6. The experimental setup used to apply vertical displacement on the shell edges. The top- and bottom plates (1,2), the vertically moving end-effector (3), the force transducer (4) and the prototypes are shown. Axial symmetry of the setup ensures a parallel configuration of the plates.
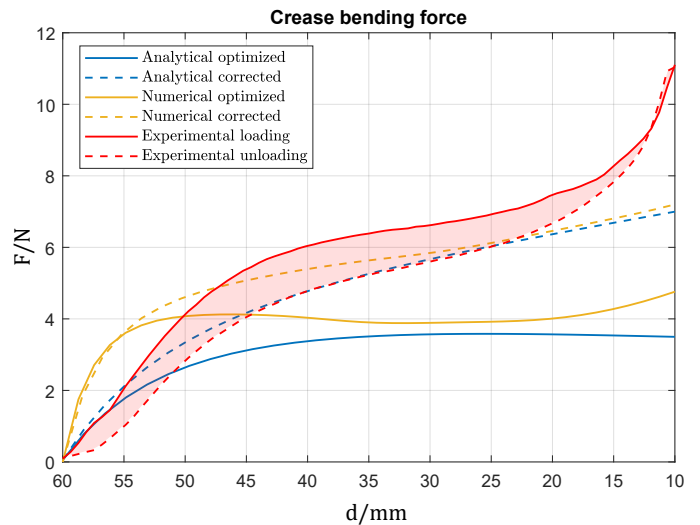

Fig. 7. Reaction force of a curved crease shell structure, compressed in its inverted state. The blue and yellow curves represent the results of the analytical and numerical model respectively. The dashed lines represent the corrected results for prototype dimensions. The experimental loading and unloading are presented as the red solid and - dashed lines respectively.

Figure 5 indicates an invariant Gaussian curvature throughout the deformation process. This validates the inextensional assumptions and approves the approach, which involved kinematic coupling between the constitutive elements.

A situation wherein the flange energy curve completely opposes the crease energy curve would result in static balance during crease actuation. This state of 'neutral stability' is not obtained with the investigated design parameters. Energy associated with crease bending dwarfs the decreasing flange energy in most cases. This energy difference can be reduced orders of magnitude by combining multiple materials with diverse E-moduli. The results of preliminary multi-material investigations are described in supplementary material section C.5.

B. On the experimental results

The prototypes used in the experimental validation featured multiple deviations from the ideal modelled geometry. Dimensions on the thickness, having a significant influence on the behavior, were off by up to 40%. Moreover, the printing orientation caused a thickness variability in the crease region and a loss of material homogeneity (figure 8(a)), with a non-circular crease cross-section and high localized stress as a result (figure 8(b)). A correction for these geometric deviations is made to the analytical and numerical model to represent the real prototype as good as possible and resulted in significantly different force curves and loss of the constant-force behavior. However, 'softening' of the crease stiffness did occur and the corrected results match the experimental data acceptably well.

Discrepancies between the experimental setup and the simulated environment also involved the constraint application. The parallel plates in the experimental setup represent a contact constraint, i.e. a constraint that can transfer forces in one direction only. In the modelled environment, also negative forces could be applied, which indeed turned out to be present.

Energy loss within the loading-unloading cycle emerge from material visco-elasticity (*internal friction*) and Coulomb friction (*external friction*). The surface area of the so-called hysteresis band (shaded red in figure 7) is a quantitative measure for the energetic losses and is of expected appearance. External friction, caused by edge-sliding is minimized by reducing the coefficient of friction between the prototype and contact plate material to approximately $\mu \approx 0.15$ (Nylon - PMMA, with a thin layer of PTFE lubricant).

V. CONCLUSION

In this study, a method is proposed to reduce the stiffness of a curved crease shell structure by coupled deformation of the connected facets. Both an analytical and a numerical approach predict constant-force behavior, i.e. zero-stiffness, within a significant range of motion. However, experimental validation of this phenomenon is obstructed by prototype inaccuracies. Despite the inequalities between the models and physical prototype, a significant stiffness reduction, or 'softening', was experimentally observed.

Analytical and numerical results are similar for both the near-constant-force - and the corrected case, supporting the choices for the simplifications used in the analytical model. The approach, that involved a hybrid-PRBM model in combination with the inextensiblity assumptions, shows promising results. It gives an indication of the mechanical behavior, which is comparable to the results of the numerical analysis.

Neutral stability of a curved crease, wherein crease forces are entirely balanced out by facet forces, is not yet achieved with the current design parameters. Nevertheless, this study can be considered as a first step towards statically balanced curved creases, with applications in e.g. origami engineering.
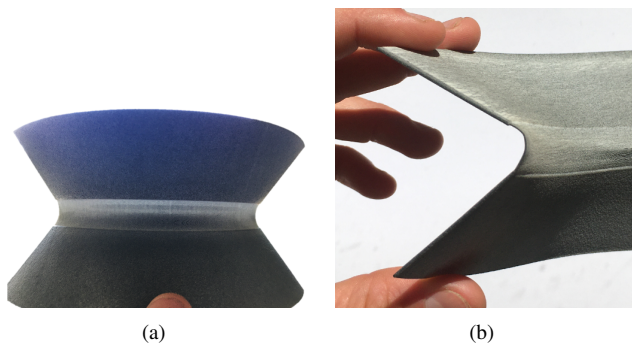
Fig. 8. Translucency of the shell material reveals a thickness variation in the crease region (a) which causes a non-circular cross-section when deformed.

VI. SUPPLEMENTARY MATERIAL

A. The influence of design parameters (Appendix C.2)

B. Video of experimental setup (digital versions only)

REFERENCES

[1] R. H. Nathan, "A constant force generation mechanism," *Journal of Mechanical Design, Transactions of the ASME*, vol. 107, no. 4, pp. 508–512, 1985.

[2] J. L. Herder, "Energy-free Systems. Theory, conception and design of statically," Ph.D. dissertation, 2001.

[3] R. Cadman, "Rolamite-Geometry and Force analysis," 1969.

[4] G. Radaelli and J. L. Herder, "Gravity balanced compliant shell mechanisms," *International Journal of Solids and Structures*, vol. 118-119, pp. 1339–1351, 2017. [Online]. Available: http://dx.doi.org/10.1016/j.ijsolstr.2017.04.021

[5] M. de Jong, "Synthesis of a Force Generator using Two-Fold Tape Loops," Ph.D. dissertation, Delft University of Technology, 2018.

[6] P. Wang and Q. Xu, "Design and modeling of constant-force mechanisms: A survey," *Mechanism and Machine Theory*, 2018.

[7] N. P. Bende, A. A. Evans, S. Innes-Gold, L. A. Marin, I. Cohen, R. C. Hayward, and C. D. Santangelo, "Geometrically controlled snapping transitions in shells with curved creases," *Proceedings of the National Academy of Sciences of the United States of America*, vol. 112, no. 36, pp. 11 175–11 180, 2015.

[8] M. A. Dias, L. H. Dudte, L. Mahadevan, and C. D. Santangelo, "Geometric mechanics of curved crease origami," *Physical Review Letters*, vol. 109, no. 11, pp. 1–5, 2012.

[9] F. Van Elteren, "Challenge the future Department of Precision and Microsystems Engineering Actuation of an origami inspired curved-crease gripper with a planar bending actuator," Ph.D. dissertation, Delft University of Technology.

[10] S. R. Woodruff and E. T. Filipov, "Curved creases redistribute global bending stiffness in corrugations: theory and experimentation," *Meccanica*, vol. 7, 2020. [Online]. Available: https://doi.org/10.1007/s11012-020-01200-7

[11] T.-u. Lee, "Elastic Energy Behaviours of Curved-crease Origami," Ph.D. dissertation, The University of Queensland, 2019.

[12] M. Kilian, A. Monszpart, and N. J. Mitra, "String Actuated Curved Folded Surfaces," *ACM Transactions on Graphics*, vol. 36, no. 4, p. 1, 2017.

[13] J. Rommers, G. Radaelli, and J. Herder, "A Pseudo Rigid Body model of a Single Vertex Compliant-Facet Origami Mechanism (SV-COFOM)," *Proceedings of the ASME Design Engineering Technical Conference*, vol. 5B-2016, pp. 1–10, 2016.

[14] C. Calladine, *Theory of shell structures*.

[15] T. J. Hughes, J. A. Cottrell, and Y. Bazilevs, "Isogeometric analysis: CAD, finite elements, NURBS, exact geometry and mesh refinement," *Computer Methods in Applied Mechanics and Engineering*, vol. 194, no. 39-41, pp. 4135–4195, 2005.

[16] S. Kok, G. Radaelli, A. Amoozandeh Nobaveh, and J. Herder, "Neutrally stable transition of a multi-stable curved crease compliant shell structure," 2020.

6
Conclusion

This section serves to highlight the main contributions per chapter and discuss the challenges that are still to be addressed.

6.1. Main contributions

In this thesis, a new type of neutrally stable shell structure is introduced. In contrast to existing examples, it does not require any pre-stressing actions during the manufacturing process or external constraints to be applied during operation. Instead, it features neutral stability as part of a continuous, unconstrained deformation process, which allows a stress-free configuration to exist.

In chapter two, an attempt is made to give an overview of the occurrences of elastic neutral stability, categorize examples and find methods for creating neutral stability in compliant shell mechanisms. Examples of neutrally stable elastic systems have been found in both mechanical and biological disciplines, where they share a common purpose: reducing operating effort. Moreover, a categorization is established wherein pre-stress obtained by the manufacturing process or externally applied boundary conditions are considered as the working principles of neutrally stable operation.

In chapter three, a new type of structure is introduced that features a curved crease, but distinguishes itself from origami mechanisms because of its non-developable nature. It also features a unique deformation mode that, by tuning of basic design parameters, is neutrally stable. Moreover, it requires neither of the aforementioned conditions found in literature to be applied.

Chapter four describes the extension towards a monolithic structure that shows similar behavior. The approach, that involved functional separation of the parts within this continuous shell, turned out to be useful to gain insight into the mechanical behavior. A new modelling method is proposed that enables equilibrium configurations to be found by estimating their approximate geometry. This is used effectively and enabled numerical analysis of the transition and structural optimization towards neutral stability. Herein, a linear thickness variation of the flange sections was introduced to compensate for crease stiffness and resulted in a constant energy level within a significant portion of transition. This shell structure can be considered as a beam element with a neutrally stable bending degree of freedom, laying the foundation for statically balanced compliant building blocks with a beam-like appearance and - kinematic behavior.

In chapter five, a method is proposed to reduce the stiffness of a curved-crease shell mechanism by utilizing the coupled deformation of the compliant facets. The inverted stable configuration of the same structure served as a starting point, but the deformation mode of interest differs from prior investigations. The 'softening' effect was indeed observed and constant-force behavior was predicted by both an analytical model and numerical simulations. The analytical model, that involved a hybrid pseudo-rigid-body approach, shows quantitative agreement with the simulations. This study can be considered as a first step towards statically balanced curved creases, with applications in e.g. origami engineering.

6.2. Future work

This section serves to sum up the open ends left at the end of this project. It contains improvements on the already established results and additional areas that can be explored in future research. A more elaborate description is given in the 'future work' sections of appendices A, B and C.

Future studies on the curved-crease structure, described in chapter three, could address aspects as support stiffness. Structural compositions might be developed to increase stiffness in desired directions, while maintaining a neutrally stable degree of freedom. Also, the potential for optimizing the neutrally stable equilibrium *path*, custom force generation and multi-stability could be investigated.

More research is required on the equilibrium paths of the neutrally stable continuous shell, discussed in chapter four. A tendency towards a parasitic 'twisting' motion with negative stiffness behavior is observed, which impairs the stability of the inverted configuration. Other recommendations apply to the physical realisation of prototypes, currently bound to 3D-printing. Alternative strategies, e.g. varying local flange width or local curvature, could be investigated and potentially enable other manufacturing methods, thereby facilitating applicability.

In order to obtain more accurate analytical predictions, the analytical model presented in chapter five could be expanded. Cone curvature and longitudinal curvature of the crease section could be incorporated in the form of an exact integral, without adding significant computational effort. Neutral stability of the curved crease is obstructed by relatively high crease stiffness, but multi-material structures could be used to solve this (preliminary investigations in Appendix C). In the context of (developable) origami mechanisms, the required pre-stress could be obtained by plastic deformation of the fold lines as a first step towards the creation of statically balanced actuated origami mechanisms.

A
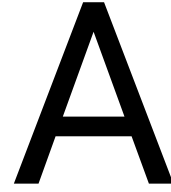
Supplementary material - Paper II

A.1. Details on modelling

All modelling involved static analysis using a modified version of the isogeometric analysis (IGA) framework, developed at the Delft University of Technology. Some adaptations to the code were made for this specific application. This section serves to provide background information on the modelling environment and elucidate the choices made in the modelling procedure regarding the pre-loading step prior to propagation and the geometry updating in between the analysis of varying geometries.

A.1.1. IGA framework

The Isogeometric Analysis method makes use of B-splines, defined by a grid of control points, to determine the geometry of the structure. A big advantage compared to conventional FEA analysis is that the geometry of the structure to be analysed is preserved, instead of being approximated by meshing. Comprehensive details of this method are given by Hughes et al. [10].

Force equilibrium is found with a non-linear solver using a standard Newton-Raphson iteration scheme by finding the solutions of the system of equations:

$$\left[\begin{array}{cc} \mathbf{K} & \mathbf{R}' \\ \mathbf{R} & \mathbf{0} \end{array} \right] \left[\begin{array}{c} d_{\mathrm{i}} \\ F_{\mathrm{c}} \end{array} \right] = \left[\begin{array}{c} F_{\mathrm{i}} \\ d_{\mathrm{c}} \end{array} \right], \tag{A.1}$$

where matrix K and R denote the stiffness and constraint matrix respectively, d_{i} and F_{i} denote the node displacements and internal node forces respectively and F_{c} and d_{c} represent the constraint forces and - displacements at the nodes where constraints are applied.

An adaptation made to the standard code effects the boundary conditions during static analysis. The 'beams' and 'sliders', normally used to define the clamped base and clamped end-effector, are removed so displacements and external forces need to be applied to the individual control points. This adaptation makes modelling a more comprehensive exercise, but simultaneously allows for more modelling freedom, which is not superfluous as will become clear in the following sections.

A.1.2. Pre-loading

In order to obtain a deformed state that features a transition region, the structure is pre-loaded. This pre-loading action is no part of the primary analysis (i.e. transition region propagation) and requires different boundary conditions to be applied. The initially undeformed flat shell is fixed in space at an arbitrary control point, where also rigid body rotation is prevented by an angular constraint with a neighbouring control point. Next to that, the structure is constrained along its inner perimeter such that the corresponding control points are free to move in the xy(symmetry)-plane. A rotation is applied to the radially oriented control points at one end of the structure and forces the transition towards the second flat zero-energy configuration (figure A.1). However, certain adaptations to the initial geometry cause a third stable configuration to exist. Figure A.2 shows the energetic paths resulting from the loading phase, where the local width of the structure is altered (i.e. narrower middle) and the local curvature of the initially circular geometry is varied (i.e. ellipse with lower curvature towards the middle) respectively. Rotation is interrupted when the corresponding local

energy minimum is reached (marked in figure A.2) and the rotational constraint is relaxed, leaving behind the structure in a (stable) state of self-stress.

In this configuration, the material around the inflection point is directed normal to the xy(symmetry) -plane. Propagation of the transition region is accomplished by imposing this constraint consecutively on control points in the longitudinal direction, as discussed in chapter 3.
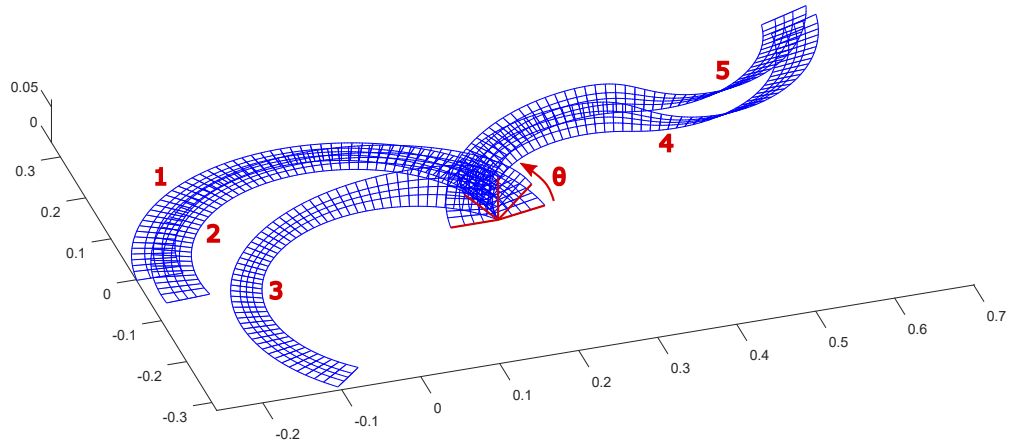

Figure A.1: The deformation steps required during the pre-loading step. One of the short edges is rotated πrad while the inner perimeter of the structure is constrained to the xy(symmetry) -plane. This allows only one half to be modelled. Starting from configuration (4), a transition region is formed.
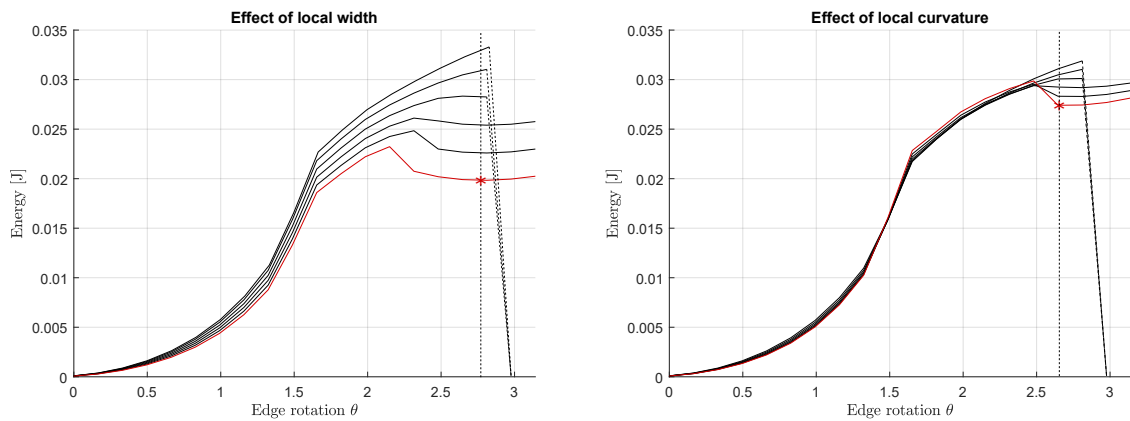
Figure A.2: The effect of a local width (left) or local curvature (right) variation on the energy curves during to the pre-loading step is shown. The red curves correspond to geometries with the most notable local energy minimum (indicated with the marker) and are used as the initial geometries for the geometry updating procedure. The down-sloping lines indicate snap-back behavior, not captured with the current displacement-controlled modelling approach.

A.1.3. Geometry updating

Many geometric variants of the basic circular geometry are investigated. To prevent the labor intensive and situation specific pre-loading step to be executed for every geometric variation, an alternative strategy is

chosen. The result of an initial (arbitrary) pre-loaded geometry is stored and used as a starting point for all following simulations. The description of the initial geometry is changed by variation of a certain design parameter and solved together with the previously known deformed geometry. When geometric changes to the undeformed geometry are kept sufficiently small, the resulting displacements with respect to the current deformed geometry are also sufficiently small and allow the solver to converge within a acceptable amount of iterations. This way, a loop can be programmed that imports the initial pre-loaded workspace, changes the undeformed geometry by variation of a desired design parameter and propagates the transition region. The workflow is schematically presented in figure A.3. This method also allows for the transition modelling of structures that do not naturally show local energy minima and do not feature a transition region naturally.
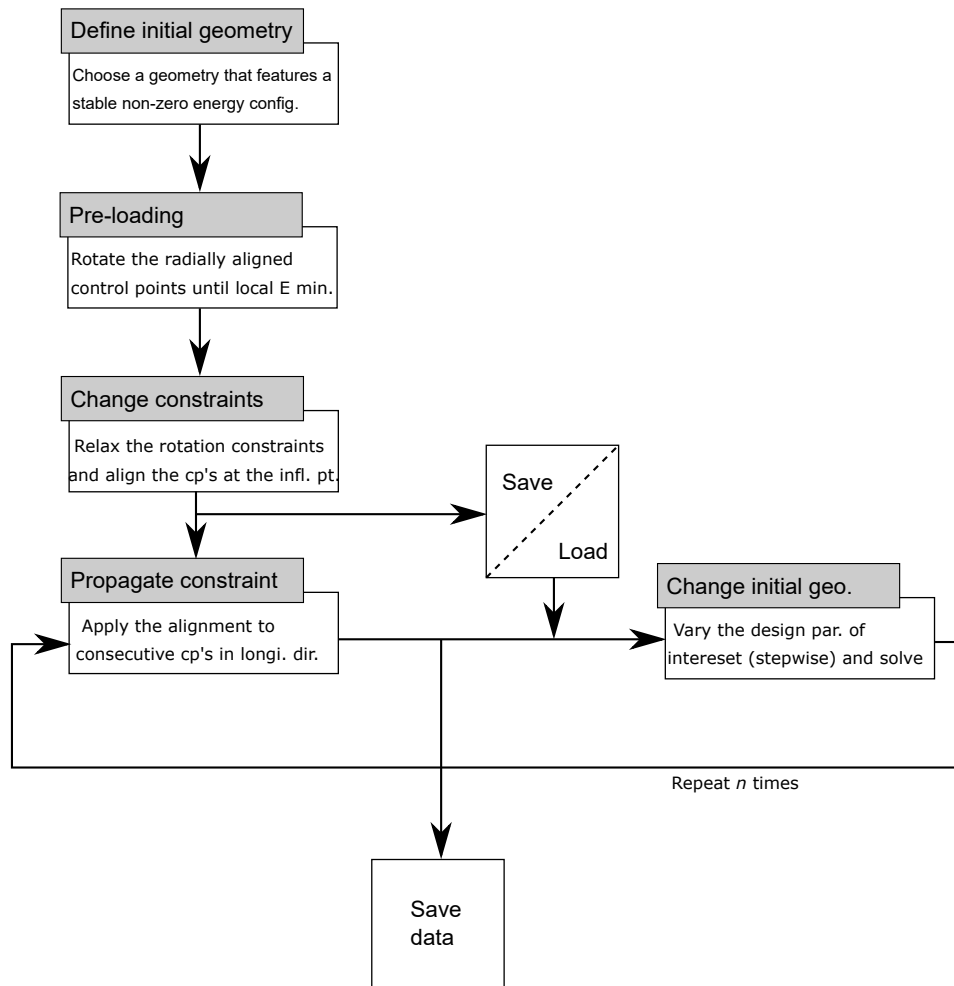
Figure A.3: The workflow regarding the geometry-updating process for a stepwise approach in evaluating the behavior of a geometrically similar series of structures. The pre-loading step is only required once, after which the deformed geometry is updated in a loop.

A.1.4. Validity of inextensibility assumptions
The intuitive approach in chapter 3 required the shell structure to be assumed inextensible. However, surface analysis of the deformed geometry reveals non-zero Gaussian curvature, suggesting mid-plane stretch around the inflection point (figure A.4, left). This energy-costly deformation could also contribute to the relatively high energy storage within the transition region, as can be seen from figure A.4 (right), where the energy distribution within the shell is shown during transition. This renders analytical approximation (e.g. by PRBM) of the deformation during transition with inextensibility assumptions not suitable for capturing the behavior.
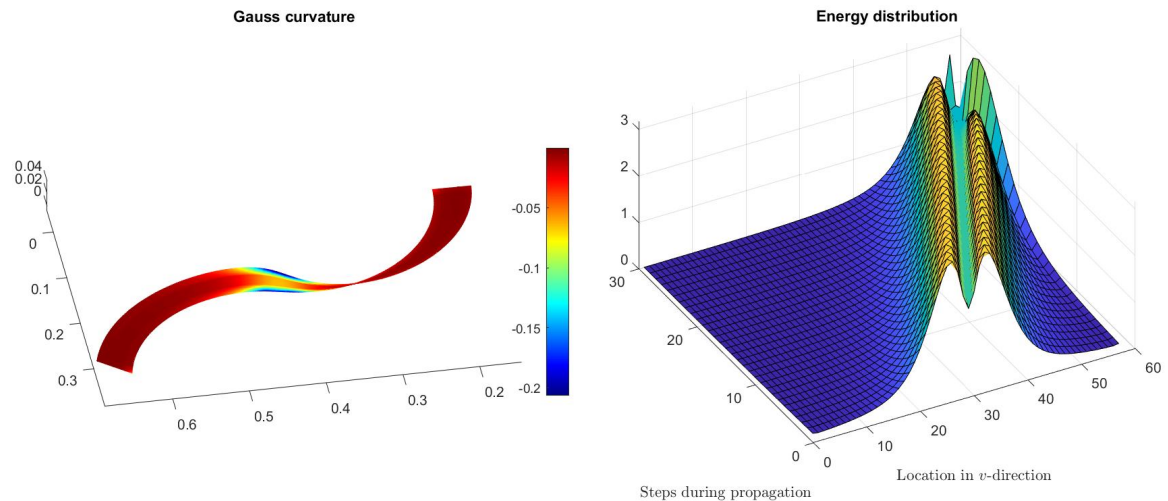
Figure A.4: The Gaussian curvature of the initially flat geometry is depicted (left) and indicates the presence of membrane stretch around the transition region. This could be the explanation for the high localized energy storage during transition (right) and invalidates the inextensibility assumptions.

A.2. Manufacturing methods

Prototype fabrication has played an important role during research. Apart from enabling the experimental validation of the modelled results, it facilitated idea generation throughout the project. In this section, the evolution of manufacturing methods for prototypes is described and the performance and limitations of every method are discussed.

A.2.1. Performance requirements

The requirements depend on their role within the project. Early prototypes, used for idea generation and proof of concept verification, benefit most from easy manufacturing and can compromise on performance. However, the ideal prototypes for experimental validation mimic the modelled conditions as close as possible, which sets the focus on material properties. The guidelines for ideal performance can be separated into material properties of the flanges and the crease respectively, as follows:

- The flange material should deform according to a linear elastic material law, should not show visco-elastic behavior and have a high yield strength and low hysteresis.

- The crease should behave as an ideal crease, i.e. has no stiffness and does not add any volume to the structure.

A.2.2. Early prototypes

First prototype were made of laminated paper, cut by hand, and connected at intervals with duct-tape. Because of the availability of the materials, many prototypes could be made to explore the design space. In later versions, laminated paper was replaced by PET sheet material ($t = 0.5$mm), enabling a better insight into the elastic behavior.

A.2.3. Prototypes for experimental validation

Material choice   For prototypes are fabricated to verify the modelled results, with the emphasis on performance. Materials are chosen to match the modelled conditions as close as possible. Polycarbonate (PC) is a thermoplastic polymer known for its toughness and relatively low internal friction. Apart from that, it is an available easy-to-work material, creating favorable conditions for manufacturing. A 0.5mm thick sheet is used.

The crease is formed by glass fiber reinforced adhesive tape (3M 8959). It features excellent tensile strength and high tensile stiffness while being very compliant in bending. It is sufficiently thin and has good adhering properties, required to transfer the internal forces.
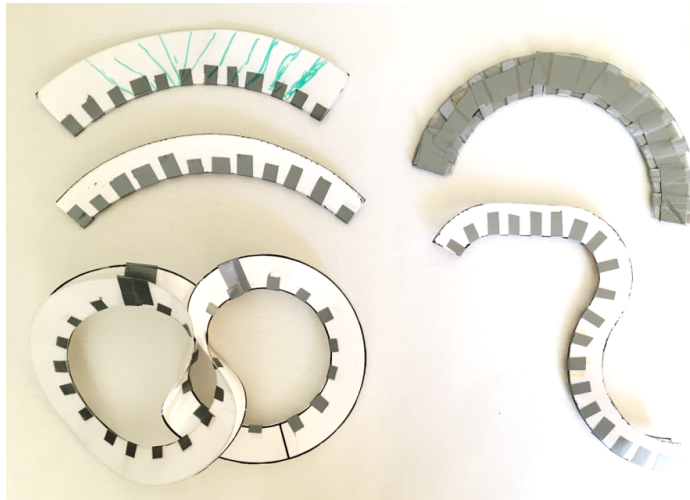
Figure A.5: A few examples of early prototypes are shown. Top-left showing two standard geometries with varying width. Bottom left showing a infinite variant of the structure to mitigate the edge effects. Bottom right shows a variant with concave, convex and straight portions of crease. Top right illustrates a different attempt to a manufacturing method, where PET sheeting is used as flange material and the tape is replaced by a wound cross-over ribbon.

From computer to physical model   The investigated geometries are modelled by B-splines and are defined by a grid of control points. Translation between the B-spline surfaces and volumetric models is achieved using the *igesout* function in Matlab®. The resulting surface part with '.*iges*' extension is suitable for post processing in most of the regular CAD packages. The step between computer model and physical prototype is bridged by a CNC drag knife plotter. Standard milling toolpaths are created and post processed using the *Dragknife* extension in Autodesk ®Fusion to compensate for the lagging contact point with respect to the spindle axis. The resulting toolpaths (G-code) are tuned for a specific drag knife setup and sent to a CNC machine.
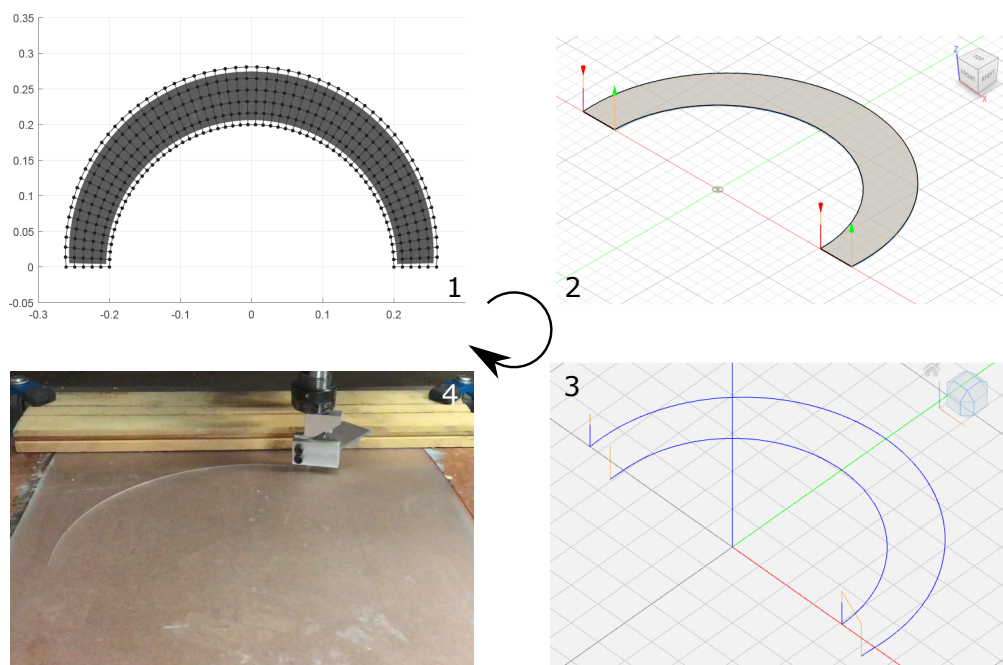

Figure A.6: The manufacturing process of the modelled flanges is shown in four consecutive steps: The control points that define the B-spline surface are exported from Matlab (1), made into a solid part in a CAD program where toolpaths are created (2), the toolpaths are modified for drag knife applications (3), and are sent to a CNC-machine with a drag knife extension that cuts the geometries out of sheet plastic (4).

Assembly   Two matching flange sections are clamped together to maintain alignment during assembly. A cardboard dummy between the sections ensures a spacing equal to twice the tape thickness. A narrow strip (20mm) of tape is placed along the head-end perimeter and slits are cut every 10mm to accommodate for the radial length increase upon folding. When the tape is folded and adhered properly, the structure is flipped inside out and the process is repeated on the other side. The cardboard strip ensured equal spacing between the flanges in both stable configurations.
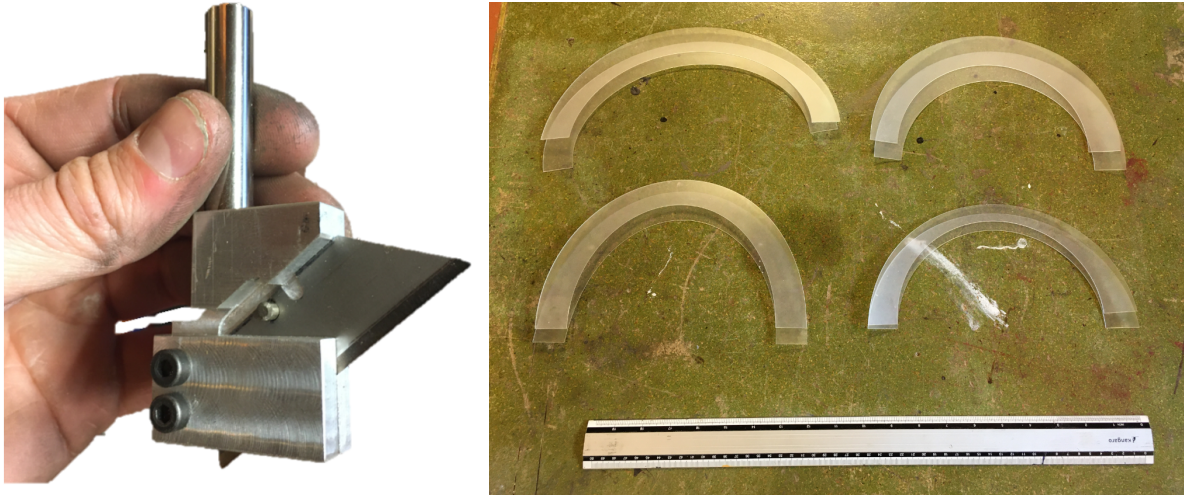
Figure A.7: The drag knife tool (left) used to cut the desired flange geometry out of plastic sheeting. And a series of prototypes created with this manufacturing method (right).
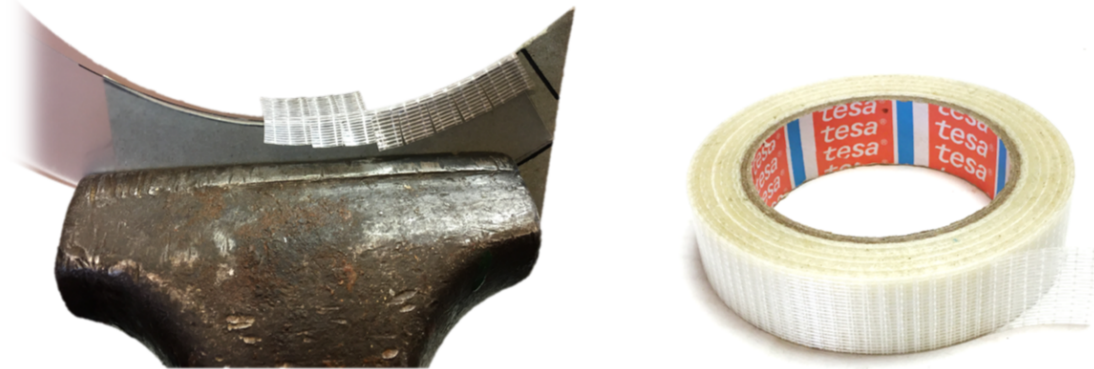
Figure A.8: The assembly process (left), where two flanges are connected by a taped crease is shown. A cardboard sheet is inserted between the flanges prior to taping the first side to ensure equal spacing in both configurations. Incisions are made in the tape to allow for a smooth curved crease when folded over. The tape used (right) features longitudinal and transverse glass fibers, of which the last is responsible for the load bearing capacities of this structure.

A.3. Multi-stable shells

Multi-stability can be obtained by projecting a sine-wave with a higher period waveform onto the width of the initially circular geometry. Figure A.9 shows the energetic paths during transition for increasing amplitude at a period of $\pi/5$ rad. Additional local energy minima arise with a sufficiently high amplitude. The undeformed geometry corresponding to the red curve is shown below on the left, together with one of its additional stable configurations on the right.
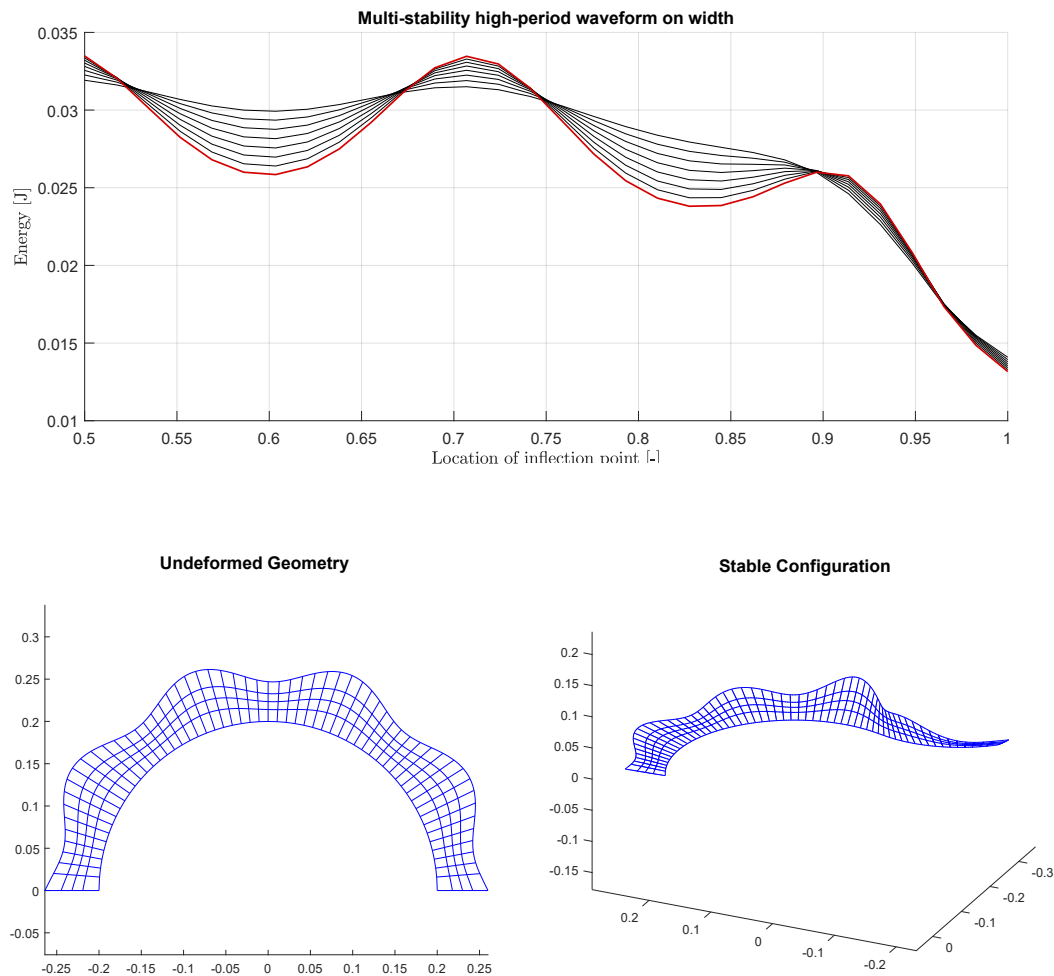
Figure A.9: The energetic paths (top) correspond to a geometry with oscillating width and variable amplitude. The undeformed configuration (bottom left) as well as one of the additional stable configurations (bottom right) is shown.

A.4. Towards a non-zero stiffness crease: a model extension

The idealized assumption of a zero-stiffness crease contradicts the practical feasibility and causes a discrepancy between the modelled and experimental results. An attempt to investigate the influence of a non-zero stiffness crease is made by extending the numerical model. The goal of this exercise is to explain the differences between the modelled and experimental results and to work towards a continuous, monolithic shell.

Addition of a torsional stiffness is achieved by imposing a configuration-dependent moment on each of the control points that make up the crease line. A constant stiffness is assumed that scales the moment linearly with the angle between the material segment spanned by two radially adjacent control points and the xy (symmetry)-plane (figure A.10). The moment is applied in the form of a force F_i on the radially adjacent control point and decomposed into its x- y- and z- components. Because these forces are configuration dependent and at the same time considered *external*, convergence of the solver, that uses the *internal* stiffness matrix to approach equilibrium, is impeded. Therefore, only relatively low stiffness values are allowed to enable convergence. A torsional stiffness of $0.15e^{-4}$Nm/rad is applied to every of the $n = 60$ control points that form the crease line. This value is estimated to match the stiffness of the double tape layer. The results are depicted in figure A.11, where the zero-stiffness crease results (red) are compared with the added torsional stiffness (blue). The energy curve during a half transition is shown for the total energy (top) as well as the separate flange (middle) and crease (bottom) contributions. The energy distribution at the beginning and the end is shown above each of the aforementioned plots.
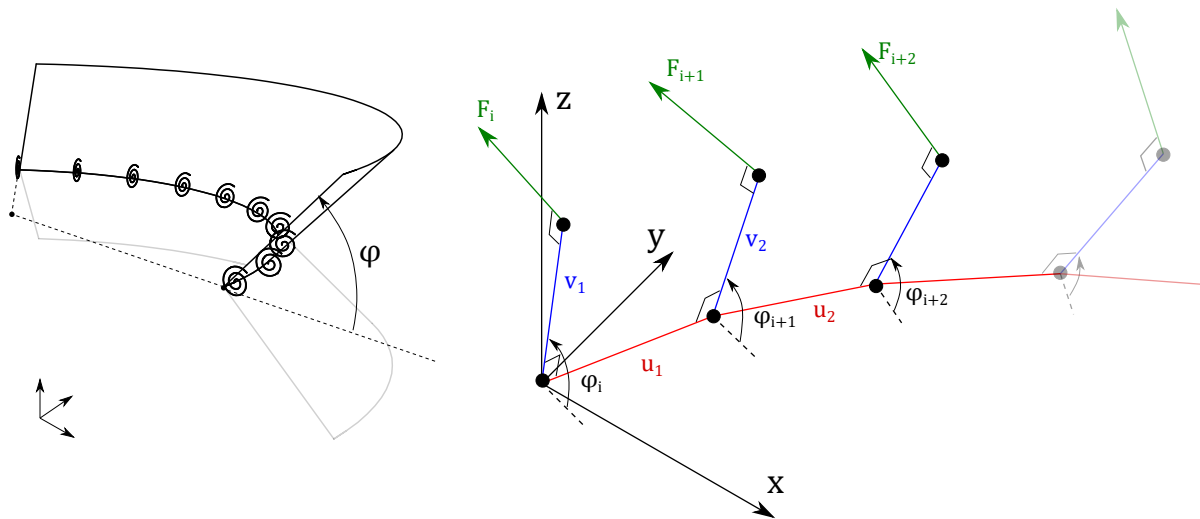
Figure A.10: A schematic representation of the model wherein the idealized crease is replaced by torsional springs, located at every control point along the inner perimeter(left). The configuration-dependent moments are applied as external forces on the neighboring control points (right).

Three important observations on the torsional crease results are: (1) The addition of the torsional crease constant mainly affects the geometry on the side of the structure where the crease is most actuated. (2) The contribution of the energy change in the crease is linear over the complete range of motion. (3) The slope of the energy curve changes from close-to-zero to non-zero.

The first two observations serve to gain insight into the behavior of a monolithic structure. The last observation could explain the difference between the modelled and measured results, in which case the torsional crease counteracted the forces applied by the flanges.

A.5. Future work

Succeeding studies could address the issue of support stiffness in order to increase the stiffness ratio. Stiffness can be evaluated by decomposition of the stiffness matrix at the end-effector, and visualized using stiffness - and compliance ellipsoids. Degrees of freedom (DOFs) can be identified and, following the theory of 'Freedom and constraint systems', compositions with a single (neutrally stable) DOF can be developed based on this neutrally stable element.

The relative motion within the structure can potentially be tuned to match a desired characteristic. Two design parameters have been shown to be effective for neutrally-stable optimization. Both the 'path of primary compliance' and the associated (infinite) compliance can theoretically be optimized simultaneously.

Other properties that can be investigated are: its effectiveness as a custom force generator (e.g. gravity balancing), multi-stability and energy-free wave propagation. Finally, crease realisation should be improved in order to avoid the current labour-intensive and cumbersome procedure and extend the durability and performance of the structure.
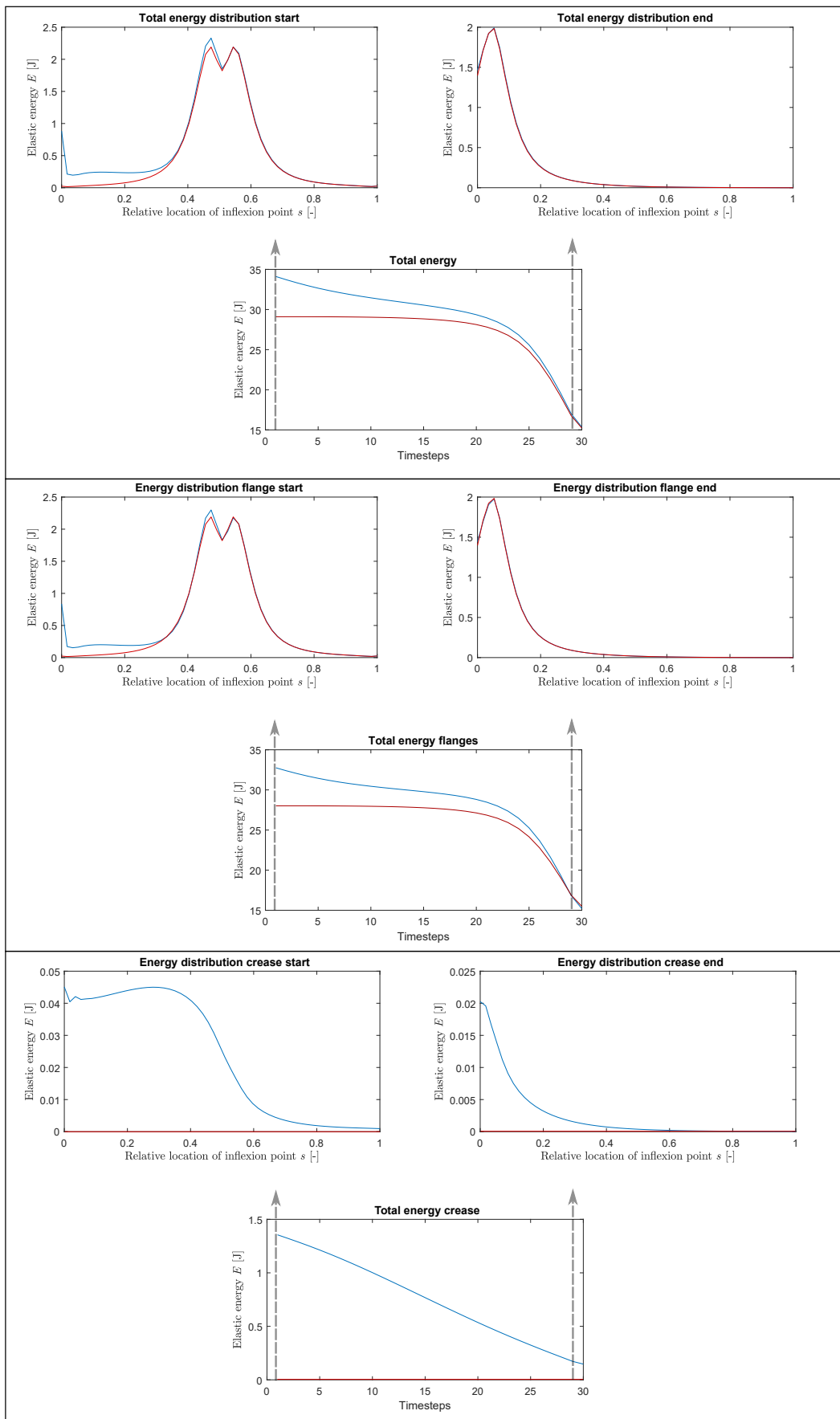
Figure A.11: The results of a simulation with a zero-stiffness crease (red) and additional torsional crease stiffness (blue). The top, middle and bottom block correspond to the total, flange and crease energy respectively. The top two plots in each block depict the *energy distribution* as a function of the length of the structure.

B

Supplementary material - Paper III

B.1. Details on modelling

All modelling involved static analysis using the IGA framework, developed at the Delft University of Technology. For more details, the reader is referred to section A1.1. This section serves to provide background information on the modelling procedure by going into the details of the geometry definition, the pre-loading phase and the choices made regarding the optimization procedure. Also, the effect of these considerations on the obtained results will be discussed.

B.1.1. Geometry definition

The geometry is defined in a cylindrical coordinate system (ρ ϕ z), whereby the constant cross-section is defined in the ρ z-plane. This cross-section consists of the crease section, defined by a circular curve and two tangent straight line segments. This cross-section is revolved around the z-axis, expressed by the coordinate ϕ, with $\phi_{\max}$ equal to the longitudinal subtended angle.

B.1.2. Pre-loading and constraint choice

For transition to occur in the continuous shell, an inflection point along the crease line must be created. This first deformation step is unrelated to the succeeding propagation of the transition region, since it requires a number of steps during which the applied constraints are constantly varied. The following procedure, consisting of a number of steps, describes a successful attempt for transition initiation.

A selective portion of the structure is brought into its inverted state by first inverting the structure in its entirety. This inverted equilibrium configuration is found using a method here referred to as 'geometry estimation', introduced in chapter 5 and discussed extensively in section C. From this pre-stressed state, half of the structure's edges is constrained to move in vertical direction (i.e. clamped between two virtual parallel plates) while the flanges on the opposite end are rotated back. All but one mirrored set of vertical constraints on the edges are relaxed, leaving a partially inverted structure that is in static equilibrium by 'pinching' of two control points close to the inflection point (figure B.1). By application of this constraint to neighboring sets of control points, the transition region can be propagated in both directions.

The location of the transition region can be controlled as long as there is a potential energy increase while propagating in the direction with the constraint lagging behind, or potential energy decrease while propagating with the constraint leading. The constraint distance affects the energetic path to a certain extent. As a general guideline, the 'pinching' distance should be sufficient for transition region propagation without exceeding the distance between opposing edge control points in the inverted stable state. The effect of different constraint distances on the propagation of a close-to-neutrally stable structure is shown in figure B.2.

It can be seen that, although the potential energy level remains close-to constant, the required reaction forces increase with consequences for the optimization procedure, as will be discussed in section B.1.3. This phenomenon can be explained by a simplified example of a rain gutter being pinched in its transverse direction (figure B.3). Translation of this pinching constraint will not result in an energetic change, translating into zero reaction force and neutrally stable deformation. However, when the constraint distance is increased, neutral stability is not impeded, but occurs at another energy level. An additional effect is that the transition region becomes separated from the constraint location, causing the complete transition to occur in a
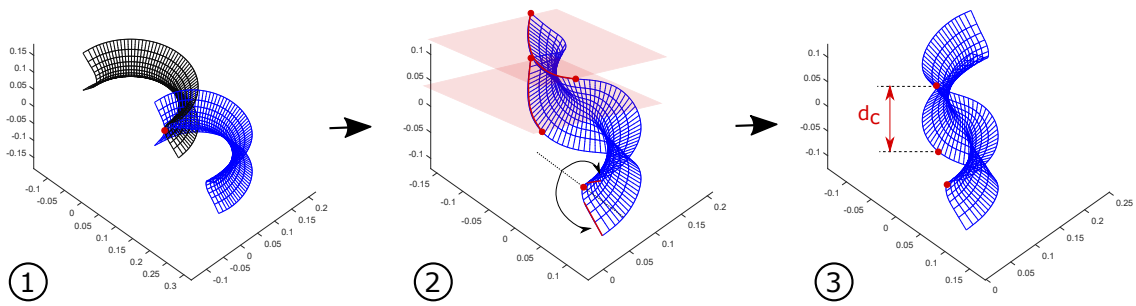
Figure B.1: The process of pre-loading the continuous shell structure involves finding the inverted equilibrium (1), back-rotation of the flanges while constraining a significant part of the edges in height (2) and relaxing all but two of the edge-constraints to locally 'pinch' the structure.
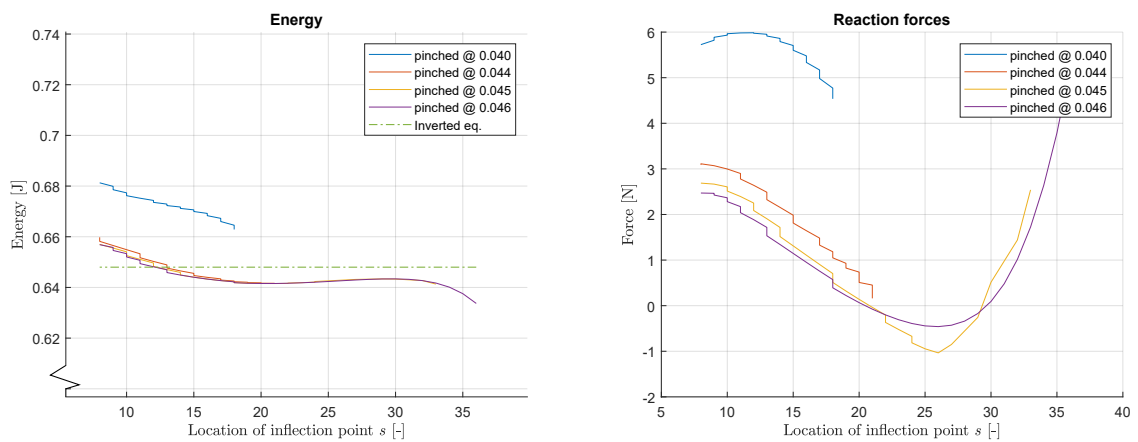

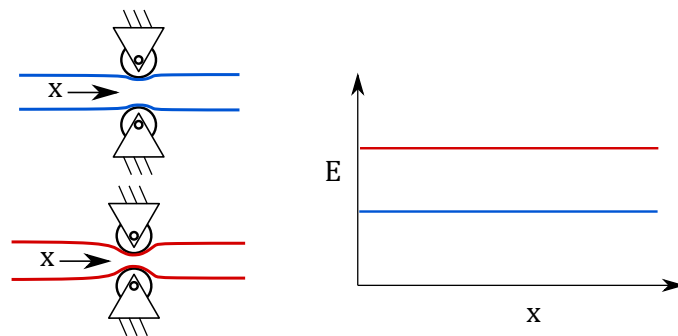Figure B.2: The effect of different constraining distances on the energy - and force paths.

Figure B.3: A schematic representation of the effect of varying the 'pinching' distance, illustrated by varying the compression distance on a rain gutter. When the constraint is moved along the (infinite) structure, the energy remains constant (i.e. implying neutral stability) but its magnitude depends on the compression distance.

small distance travelled by the constraint. Because of these reasons, a distance is chosen during analysis that resulted in the lowest energy level.

For visualisation of the results, the location of the pinching constraint is translated into the location of the inflection point s, defined as the location where the spine of the structure changes curvature sign. This way, the potential energy curve becomes independent of the constraint location and properties as linearity can be coupled to the location of the inflection point.

B.1.3. Optimization procedure

Neutrally stable transition is achieved when the reaction forces during transition are zero. Local adaptations to the geometry can be made to reach this goal. Out of several tactics, including local width and local curvature variation and local material thickness variation, the later was chosen because of its acceptance of the constraint choice. Local width and curvature adaptations would potentially obstruct proper constraint behavior, with convergence issues as a consequence.

During the optimization process, a varying linear thickness gradient was applied on a fixed net of control points that defines the mid-surface of the shell structure. Updates on the thickness of the structure were executed on the pre-loaded geometry, allowing the pre-loading steps to be excluded from the optimization structure in a similar way as discussed in section A. This procedure requires the geometric changes to be small in order to converge towards a solution. Therefore, the new set of objective parameters chosen by the optimization algorithm is compared to the initial set. The difference is then split up in multiple steps with a known step size and processed in a loop that solves for each of the variable number of intermediate steps prior to transition (figure B.4).
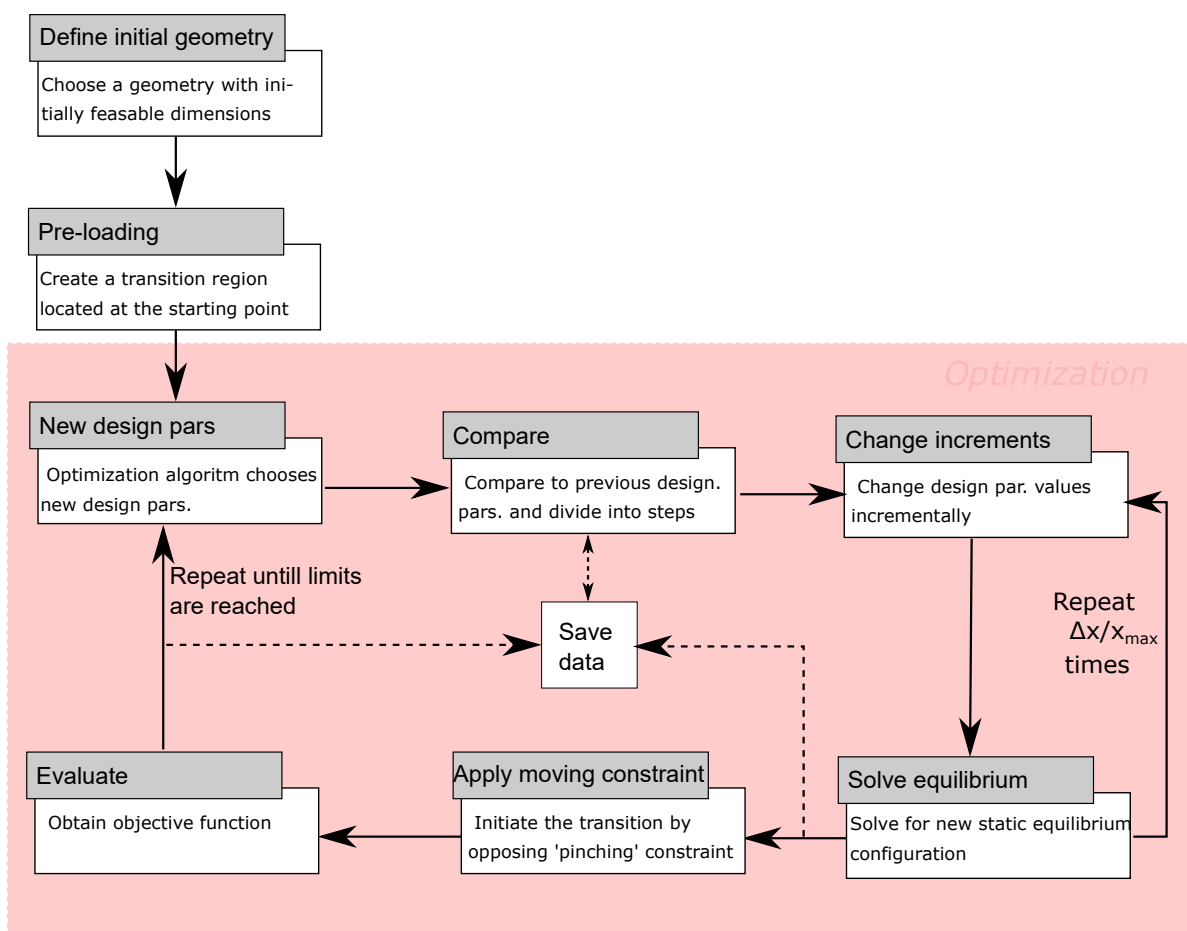

Figure B.4: The workflow during the optimization procedure of a thickness variation of the flanges of the continuous shell.

B.2. Manufacturing methods and early prototypes

The construction of prototypes early in the process facilitated the generation of new ideas en validated early concepts. Later in the process, prototypes were made to exactly match the modelled geometries, requiring more advanced techniques. In the first part of this section, the findings and lessons learned from the fabrication of early prototypes are described, after which some considerations regarding 'high-performance' manufacturing methods are discussed.

B.2.1. Fabrication of early prototypes

First efforts towards a continuous shell resulted in a very rough prototype whereby the flat flanges are connected by curved strips, acting as torsional crease elements discussed in section A (figure B.5, left). In accordance with the modelled results, a second stable non-zero energy configuration existed (figure B.5, right).

Further attempts for creating a continuous toroidal crease involved a fiberglass lamination process with a bicycle inner tube (approximate torus) acting as the mould (figure B.6). The method seemed promising, but the curved crease sections on themselves did not show bi-stable behavior. A new mould was created including a toroidal section and two adjacent parallel planes. The resulting fiberglass shells featured an inverted stable configuration (shown in figure B.7, bottom right). Also, transition between the initial and inverted state was practically achievable, laying the foundation for neutrally stable transition. At the same time, a pitfall was discovered: a twisting degree of freedom renders the inverted state not inherently stable.

Fabrication was impeded by the use of directional fiber mats. To facilitate production of prototypes with smaller radii, a variant was constructed out of chopped strand mat (CSM fibers with random direction). Three variants of the structure are depicted in figure B.8 (from left to right): CSM with small transverse and longitudinal radius and wide flanges, cross-ply directional fiber mat with small transverse and longitudinal radius but limited flange width, cross-ply directional fiber mat with two large radii and wide flanges. The behavior of these prototypes suggested that a small transverse and longitudinal radius and wide flanges promote stability of the inverted state.
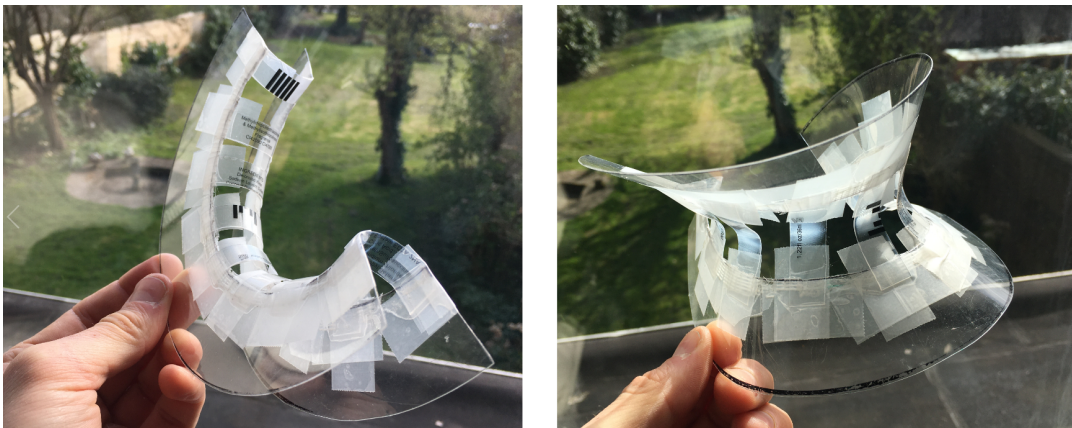

Figure B.5: A connection between the two flat flanges is realized by taping curved sections of elastic material in the very early prototypes. It featured an inverted stable state, presumably also present in a continuous structure.

Figure B.6: An attempt to fabricate double curved shell sections, representing the crease sections of the shell. On their own, no stable inverted state was noticed.

Figure B.7: The manufacturing process for creating the first bi-stable shell prototypes required a mould (top left) and a fiberglass lamination process (top right). The undeformed and inverted state are depicted in the bottom left and bottom right pictures respectively.

Figure B.8: Three prototypes that resulted from the lamination process: (from left to right) CSM with small transverse and longitudinal radius and wide flanges, cross-ply directional fiber mat with small transverse and longitudinal radius but limited flange width, cross-ply directional fiber mat with two large radii and wide flanges.

B.2.2. Fabrication of 'high-performance' prototypes

Prototypes for situations that demand accurate dimensioning control and material homogenity, require other types of manufacturing methods. Little manufacturing methods for shells enable accurate control over local material thickness: the driving force behind the optimized neutrally stable shell geometries. Multi jet fusion is a 3D-printing strategy that provides respectable material homogeneity, enables material thickness down to the tenth-of-a-millimeter scale and allows for processing of materials with sufficient elasticity (i.e. high yield strength with respect to E-modulus), rendering it suitable for this application. The 3D-printed optimized prototypes are shown in figure B.9.

Printing accuracy below 0.5mm is not guaranteed by the supplier and prototypes indeed showed some deviation from the computer model (discussed in chapter 4). Also, visco-elastic behavior of the printing material (PA-12) resulted in internal friction and relatively wide hysteresis bands (chapter 4), which in this case enabled neutral stability of the prototype.
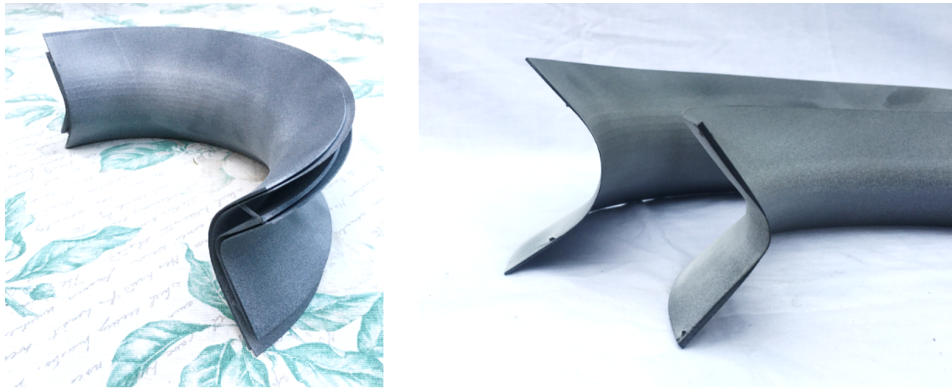
Figure B.9: The 3D-printed prototypes used for experimental validation of the modelled results, fabricated with multi jet fusion, are depicted in their as-fabricated (left) and separated states (right).

B.3. Future work

More research is required on the existence of near equilibrium paths. A tendency towards a parasitic 'twisting' DOF is observed whereby the structure's spine forms an out-of-plane helical shape. This equilibrium path features negative stiffness (when a clamped condition is assumed) towards its undeformed zero-energy state. The stability of the configurations encountered during neutrally stable operation can then be related to how close this negative stiffness path is approached. Solutions could be found in the form of compositions that follow from the theory of 'freedom and constraint systems', whereby this structure is considered as a kinematic building block.

Advances towards a neutrally stable shell with constant thickness include some ideas, but as of today, these are not yet implemented with success. Two promising tactics involve the application of a width variation of the flanges or a longitudinal curvature variation over the length of the structure. Preliminary investigations have shown that the energy increase as a result of crease bending, dwarfs the energy decrease that can be realised by feasible flange width variation. This also applies to local curvature variation. Possible solutions are geometries with a localized steep decrease in flange width (and thereby compromising the range of motion) and spiral curves with sufficient curvature change (figure B.10).
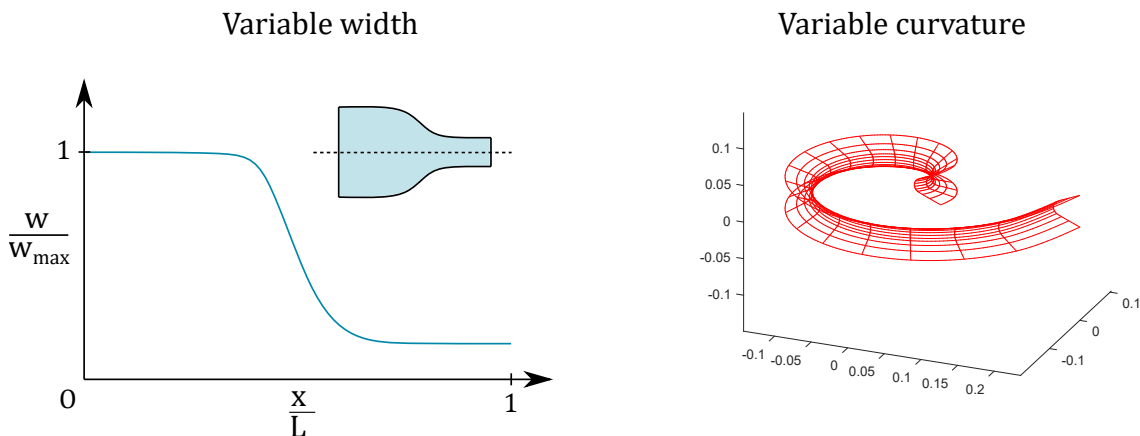

Figure B.10: A steep decrease of flange width (left) and variable decreasing curvature by a spiral geometry (right) are both tactics to achieve neutral stability with constant material thickness.

C

Supplementary material - Paper IV

C.1. Details on modelling

C.1.1. Finding second equilibrium

The inverted stable configuration is found using the method discussed in section B. Here, the process is described of estimating a deformed geometry before feeding it into the non-linear solver. When the estimation is sufficiently close to actual equilibrium, the solver experiences no trouble converging. This method enables the inverted state to be reached without a continuous deformation process and bypasses the infinite-energy configuration. A downside is that is it hard to predict which equilibrium configuration is found: the solver may find other equilibria (e.g. the undeformed configuration) during iteration. Figure C.1 illustrates the steps required to obtain the inverted configuration.
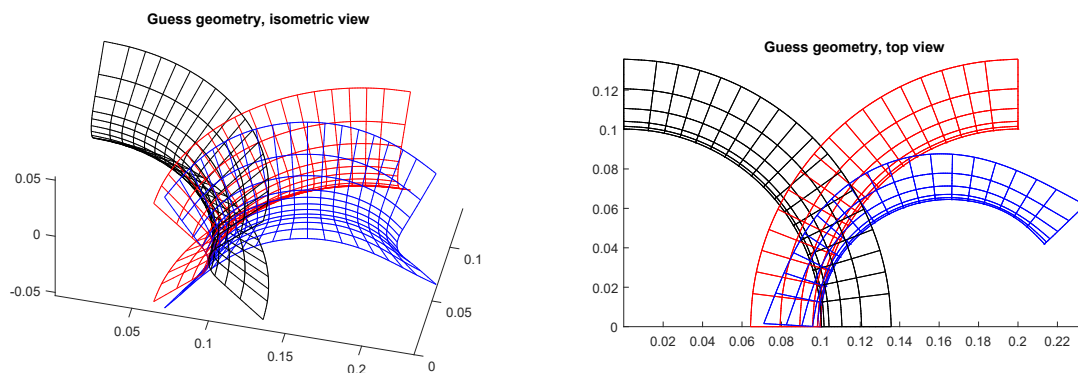

Figure C.1: The procedure to find inverted equilibrium (blue) involves guessing the geometry (red) after which the non-linear solver converges towards its closest equilibrium. The undeformed geometry (black) is shown for comparison.

C.1.2. Constraint application

All control points that describe the edges of the shell are vertically aligned by the application constraints in z-direction. Edge effects cause the vertical location of the edge in the inverted configuration to slightly differ from point to point. An insurmountable consequence is that the reaction force direction can differ from point to point, actually 'pulling' some parts while the sum of the forces suggest a 'compressive' force. This effect is difficult to mimic in the experimental procedure, where a contact constraint is introduced.

C.2. The influence of design parameters

The analytical model provides insight into the effect of variation of the design parameters. This knowledge can be used to intuitively iterate the geometry towards zero-stiffness behavior. Two contributors to the energetic path are investigated: the flange energy due to conical deformation and the crease energy, approximated by single-axis torsional springs. Parameters that are discussed are: (1) initial inclination angle, (2)
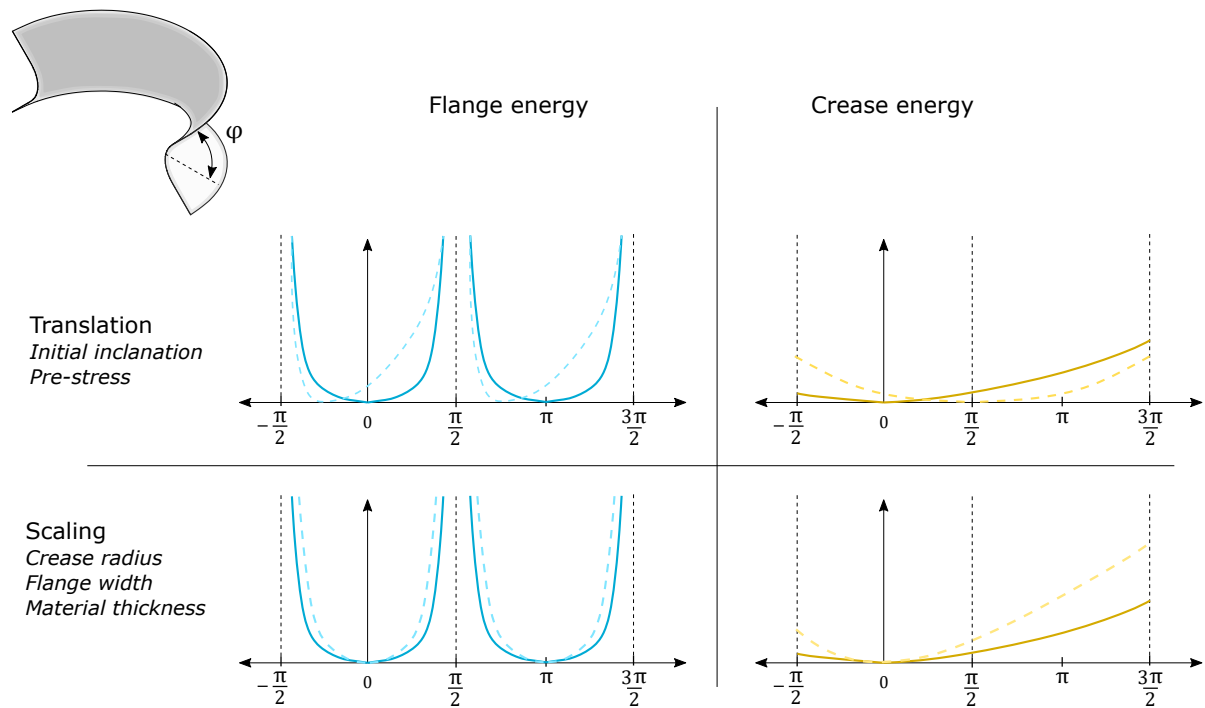
Figure C.2: The influence of the design parameters on the energy contributors is shown. Relative translation and scaling can be used as an intuitive method for creating the desired energy profile.

pre-stressed assembly, (3) crease radius, (4) flange width and (5) relative material thickness. The first two mainly result in a relative shift of the energy curves and the latter three cause relative scaling. The effects are schematically illustrated in figure C.2.

C.3. Considerations on the experimental setup

Given the current (May 2020) circumstances (COVID 19), accessibility to the measurement lab is impeded and a (sub-optimal) home-brew version of a linear actuating measurement platform is created. Adaptations are made to a 3D-printer with delta configuration where a load cell is connected to the end-effector (figure C.3). Commands on position are given via Simplify-3D software *without* a feedback loop. Meaning that the actual position is estimated based on commands given and knowledge of the mechanics of the system. The measurement hardware and a schematic overview of the internal connections of the setup is shown in figure C.3 (right).

Visco-elasticity is a velocity-dependant resistance. As a result, actuation speed does have an effect on the internal losses. With the goal to reduce hysteresis in the measurement results, a relatively high vertical actuation speed is chosen. Moreover, no pause is inserted in between the 'loading' and 'unloading' phase. Slower actuation did seem to cause a wider hysteresis band (graphs not included).

C.4. Alternative optimization results

For different results, an optimization procedure using the Matlab® *Optimization toolbox* is performed. The function *fmincon* is used to minimize the following *objective function*:

$$f(x) = \sum_{i=i}^{n} |F_i| \tag{C.1}$$

Whereby the force F_i is composed of the sum of the reaction forces along the upper perimeter at a specific configuration during vertical compression of the flanges. n denotes the number of steps required for the full deformation process. The *objective parameters* used to define the geometry of the shell in this optimization procedure were the crease (transverse) radius, crease thickness and crease and flange material thickness, given by:
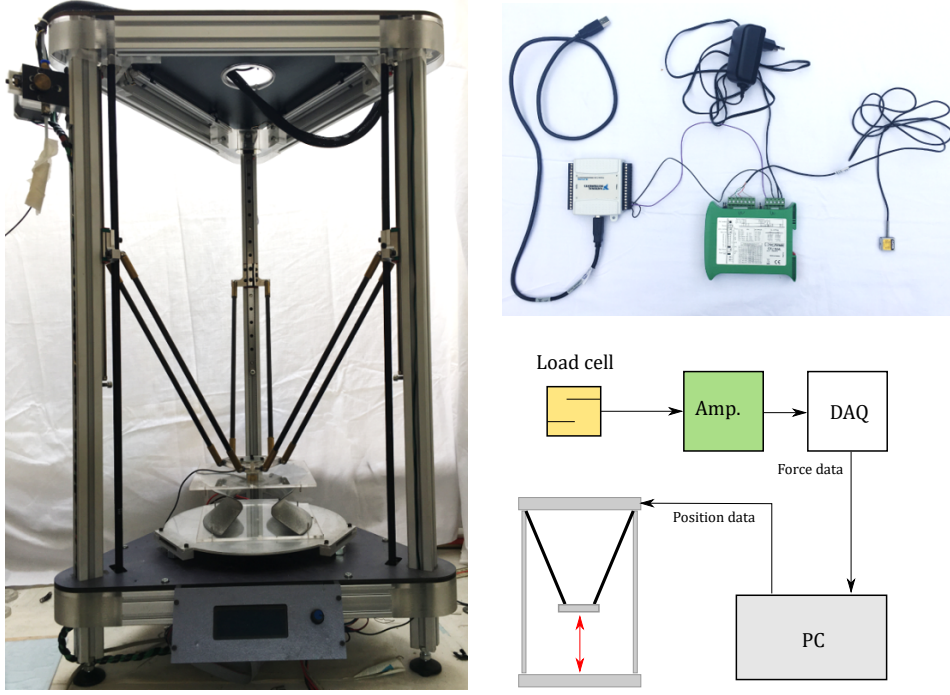
Figure C.3: The modified 3D-printer used to apply a vertical displacement (left) together with the measurement hardware (top right) are shown. A schematic overview displays the connections between the individual parts.

$$\boldsymbol{x} = [r_{t,0} \quad t_c \quad t_f] \tag{C.2}$$

The boundaries were set to feasible fabrication limits, as follows:

$$\boldsymbol{x}_{min} = [2e^{-3} \quad 4e^{-4} \quad 4e^{-4}] \tag{C.3}$$

$$\boldsymbol{x}_{max} = [2e^{-2} \quad 2e^{-3} \quad 4e^{-3}] \tag{C.4}$$

And initial values set by:

$$\boldsymbol{x}_0 = [1e^{-2} \quad 4e^{-4} \quad 1e^{-3}] \tag{C.5}$$

During the optimization procedure, the geometry is defined, the inverted equilibrium is found using the method described in B, constraints on the vertical edge displacement are defined dependent on the design variables, the deformation steps are performed and results on the reaction forces are stored. A fixed optimization window of $0.025\text{m} < d < 0.05\text{m}$ is used to evaluate the performance and to determine the succeeding set of objective variables.

The optimization procedure is interrupted when the maximum number of iterations ($n = 60$) was reached, with the following optimized objective variables:

$$\boldsymbol{x}_{opt} = [1.95e^{-2} \quad 4e^{-4} \quad 7e^{-4}] \tag{C.6}$$

Yet, a satisfying result featuring a near-constant force region resulted (figure C.4). The negative force resulted from a displacement in the opposite direction of the stable inverted configuration and zero force was measured exactly at the stable inverted configuration. Figure C.4 shows the underformed geometry (black) and two configurations encountered during deformation: inverted equilibrium (blue) and maximum displacement (red). Other design parameters were chosen as described in chapter 5.
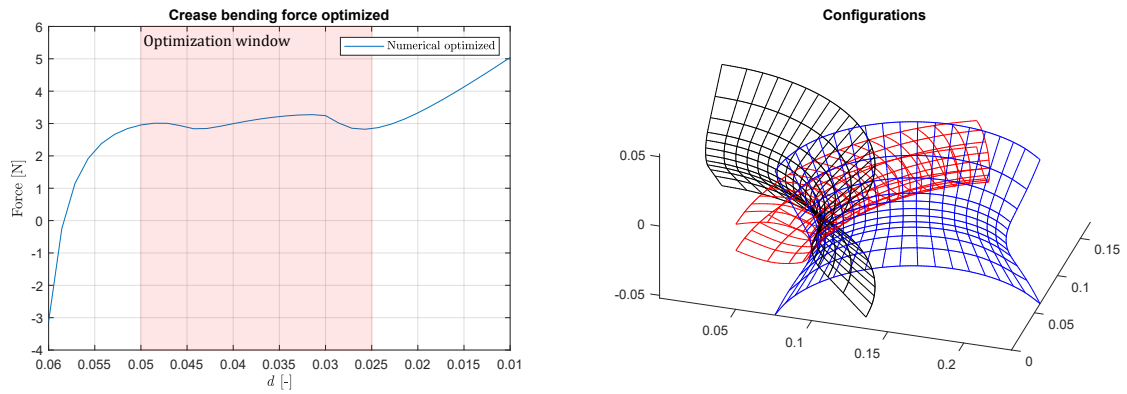
Figure C.4: The left figure shows the reaction forces during displacement of the optimized geometry. Forces are near-constant in the optimization window, zero in the stable inverted configuration and negative during displacement opposite from the inverted configuration. Two configurations encountered during edge displacement are shown on the right: the inverted stable state (blue) and the maximum displacement (red). Also the underformed geometry is depicted (black).

C.5. Towards a neutrally stable curved crease: multi-material structures

C.5.1. Optimization procedure

In order for the decreasing flange energy to compensate for the increasing crease energy, one of the two energy contributors should scale several orders of magnitude. The approach taken here is the application of a dual material structure, whereby the crease is made from a material with a much lower material stiffness. Material properties of silicone ($E = 50$MPa, $v = 0.49$) are used and locally replace the polycarbonate properties. A geometry is assumed whereby the crease material thickness, crease radius and flange width variable and all other design parameters are fixed. Manual optimization of these three parameters resulted in modelled neutrally stable behavior during a significant part of crease actuation.

C.5.2. Prototype manufacturing

A method for combining stiff flanges with a relatively compliant silicone crease section involves a moulding process of liquid dual-component chemically curing silicone. A mould, made up of two parts, featuring a pocket with the desired crease dimensions was 3D-printed, while reserving some space to account for the
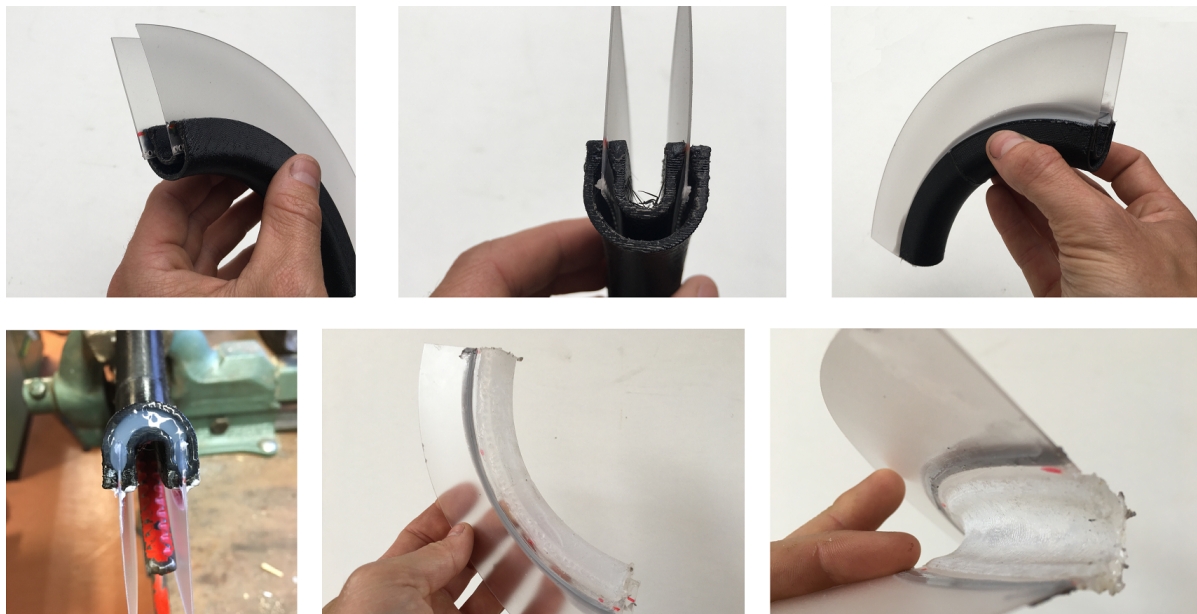

Figure C.5: The steps during the fabrication of a prototype with a silicone crease. Numerical analysis predicts neutral stability in the bending direction.

flange thickness. Flanges (polycarbonate, 0.5mm) where cut out using a drag knife (described in section A) with a slight extension of the inside perimeter where holes ($d = 1.5$mm) are drilled at small intervals (figure C.5). The flanges are then inserted into the mould and all gaps are sealed. The mould is filled with liquid silicone (Smooth On Dragon Skin 10 Fast) and set to cure before releasing from the mould. The resulting structure interlocks, reinforcing the bond between the two materials.

C.5.3. Results discussion

No neutrally stable behavior was observed with this prototype. Possible explanations are the air pockets within the silicone that resulted from a tedious filling procedure of the mould and the far-from-ideal material coupling between the crease and flanges. Future efforts could benefit from silicone with a lower uncured viscosity and bonding (i.e. gluing) capabilities.

C.6. Future work

The analytical model, used to describe the kinematic of the structure, is simplified a number of occasions. Cone curvature and longitudinal curvature of the crease section could be incorporated in the form of a continuous integral, without adding significant computational effort. The accuracy of the analytical model could potentially be increased such that numerical modelling becomes superfluous.

Subsequent investigations could be directed towards statically balancing crease forces by facet deformation. In the current setup, crease forces account for most of the experienced stiffness. Multi-material structures (section C.5) could solve this problem by designing a crease with a relatively low modulus of elasticity.

In the context of origami mechanisms, plastic deformation of crease material results in pre-stress. When designed properly, (curved) crease stiffness can potentially balance out facet deformation, thereby working towards the creation of statically balanced actuated origami mechanisms.

Bibliography

[1] Hoessein Alkisaei. Statically Balanced Compliant Walls. Technical report.

[2] Arthur Baumann, Antoni Sánchez-Ferrer, Leandro Jacomine, Philippe Martinoty, Vincent Le Houerou, Falko Ziebert, and Igor M. Kulić. Motorizing fibres with geometric zero-energy modes. *Nature Materials*, 17(6):523–527, 2018. ISSN 14764660. doi: 10.1038/s41563-018-0062-0.

[3] Juan A Gallego. *Statically Balanced Compliant Mechanisms: Theory and Synthesis.* 2013. ISBN 9789461862150. doi: 10.4233/uuid:081e3d0e-173b-4a36-b8d6-c29c70eb7ae3. URL http://repository.tudelft.nl/view/ir/uuid:081e3d0e-173b-4a36-b8d6-c29c70eb7ae3/.

[4] S Guest. Zero stiffness elastic shell structures. 6(7), 2011.

[5] W. Hamouche, C. Maurini, S. Vidoli, and A. Vincenti. Multi-parameter actuation of a neutrally stable shell: A flexible gear-less motor. *Proceedings of the Royal Society A: Mathematical, Physical and Engineering Sciences*, 473(2204), 2017. ISSN 14712946. doi: 10.1098/rspa.2017.0364.

[6] JL Herder and FPA Van Den Berg. Statically balanced compliant mechanisms (sbcm's), an example and prospects. In *Proceedings of the 26th ASME DETC biennial, mechanisms and robotics conference*, 2000.

[7] Justus Laurens Herder. *Energy-free Systems. Theory, conception and design of statically.* PhD thesis, 2001.

[8] H. W. R. Houwers. Closed-loop two-fold tape spring transmissions. Technical report, Delft University of Technology, 2016.

[9] Larry L. Howell, editor. *Handbook of Compliant Mechanisms.* John Wiley & Sons Inc. ISBN 1118516516.

[10] T. J.R. Hughes, J. A. Cottrell, and Y. Bazilevs. Isogeometric analysis: CAD, finite elements, NURBS, exact geometry and mesh refinement. *Computer Methods in Applied Mechanics and Engineering*, 194(39-41): 4135–4195, 2005. ISSN 00457825. doi: 10.1016/j.cma.2004.10.008.

[11] William Thomson Baron Kelvin and Peter Guthrie Tait. *Treatise on natural philosophy*, volume 1. Claredon Press, 1867.

[12] E. Lamacchia, A. Pirrera, I. V. Chenchiah, and P. M. Weaver. Non-axisymmetric bending of thin annular plates due to circumferentially distributed moments. *International Journal of Solids and Structures*, 51 (3-4):622–632, 2014. ISSN 00207683. doi: 10.1016/j.ijsolstr.2013.10.028.

[13] Yang Liuyi, Tan Huifeng, and Cao Zongsheng. Thin-Walled Neutrally Stable Deployable Composite. (July):19–24, 2015.

[14] Thomas W. Murphey and Sergio Pellegrino. A novel actuated composite tape-spring for deployable structures. *Collection of Technical Papers - AIAA/ASME/ASCE/AHS/ASC Structures, Structural Dynamics and Materials Conference*, 1:260–270, 2004. ISSN 02734508. doi: 10.2514/6.2004-1528.

[15] G. Radaelli and J. L. Herder. A monolithic compliant large-range gravity balancer. *2015 IFToMM World Congress Proceedings, IFToMM 2015*, 2015. doi: 10.6567/IFToMM.14TH.WC.OS20.018.

[16] G. Radaelli and J. L. Herder. Gravity balanced compliant shell mechanisms. *International Journal of Solids and Structures*, 118-119:1339–1351, 2017. ISSN 00207683. doi: 10.1016/j.ijsolstr.2017.04.021. URL http://dx.doi.org/10.1016/j.ijsolstr.2017.04.021.

[17] Marc R. Schultz, Michael J. Hulse, Philip N. Keller, and Dana Turse. Neutrally stable behavior in fiber-reinforced composite tape springs. *Composites Part A: Applied Science and Manufacturing*, 39(6):1012–1017, 2008. ISSN 1359835X. doi: 10.1016/j.compositesa.2008.03.004.

[18] K. A. Seffen and R. A. McMahon. Heating of a uniform wafer disk. *International Journal of Mechanical Sciences*, 49(2):230–238, 2007. ISSN 00207403. doi: 10.1016/j.ijmecsci.2006.08.003.

[19] Jonathan P. Stacey, Matthew P. O'Donnell, and Mark Schenk. Thermal Prestress in Composite Compliant Shell Mechanisms. *Journal of Mechanisms and Robotics*, 11(2):1–10, 2019. ISSN 19424310. doi: 10.1115/1.4042476.

[20] Christine Vehar, Sridhar Kota, and Robert Dennis. Closed-loop tape springs as fully compliant mechanisms -preliminary investigations. In *Proceedings of the ASME Design Engineering Technical Conference*, volume 2 B, pages 1023–1032, 2004. doi: 10.1115/detc2004-57403.

[21] Doran F Wilkes. Rolamite-a new mechanical design concept. 1967.

[22] W. H. Wittrick, W. H. Wittrick, D. M. Myers, and W. R. Blunden. Stability of a bimetallic disk. *Quarterly Journal of Mechanics and Applied Mathematics*, 6(1):15–31, 1953. ISSN 00335614. doi: 10.1093/qjmam/6.1.15.